Abstract

Title of Document:	FATIGUE DAMAGE ACCUMULATION DUE TO COMPLEX RANDOM VIBRATION ENVIRONMENTS: APPLICATION TO SINGLE-AXIS AND MULTI-AXIS VIBRATION
	Mark Edward Paulus, Doctor of Philosophy, 2011
Directed By:	Professor Abhijit Dasgupta, Department of Mechanical Engineering

A combination of experiments and modeling are used to address the vibration durability of structures subjected to different random vibration environments. Presented in this work are a set of experimental data comparing the rate of change of the first natural frequency and the measured time to failure, of simple structural members under repetitive shock (RS) vibration, single-axis electrodynamic (ED) vibration and multi-axis ED vibration. It was found that multi-axis testing is more severe than single-axis testing at the same level. In addition the RS system low frequency amplitude is often too weak to efficiently propagate the crack. Smoothing of the input power spectral density (PSD) or poor line resolution was also shown to change the time to failure of a test. A poor correlation was shown between the PSD and the rate of natural frequency change (RFC) over a wide frequency shift. The change in natural frequency caused the initial PSD to be

ineffective in determining the total time to failure. A predictive, analytic methodology to quantify the RFC was developed to predict the fatigue life of a structure experiencing random vibration excitation. This method allows the estimation of fatigue life using the frequency domain, where only the input power spectral density, damping factor and structural information are required. The methodology uses linear elastic fracture mechanics for fatigue crack propagation and accounts for the frequency shifting that occurs due to fatigue crack evolution. The analytic model has been shown to compare favorably to both finite element analysis (FEA) and experimental results, for mild-steel cantilever beams. Monte Carlo simulations have been conducted to assess the sensitivity of the model predictions to uncertainties in the input parameters. In addition a semi-empirical model was developed whereby the input PSD and damping factor are measured from life tests, and the resulting time to failure and the acceleration factors between different vibration environments can be determined. The improved modeling methodology developed by this work are of value not only to structural designers who wish to design for dynamic environments, but also to test engineers who wish to qualify products through accelerated life testing, and to vibration engineers who wish to compare the relative severity of different random vibration environments, in terms of their potential to cause fatigue damage accumulation.

FATIGUE DAMAGE ACCUMULATION DUE TO COMPLEX RANDOM VIBRATION ENVIRONMENTS: APPLICATION TO SINGLE-AXIS AND MULTI-AXIS VIBRATION

By

Mark Edward Paulus

Dissertation submitted to the Faculty of the Graduate School of the
University of Maryland, College Park, in partial fulfillment
of the requirements for the degree of
Doctor of Philosophy
2011

Advisory Committee:
Professor Abhijit Dasgupta, Chair
Professor Donald Barker
Professor Amr Baz
Professor Mohammad Modarres
Professor Norman M. Wereley

Acknowledgements

First of all I would like to thank my advisor Abhijit Dasgupta for taking the time to work with me on this project. I am grateful for his guidance and suggestions in pursuing my PhD. I would also like to thank my committee members Donald Barker, Amr Baz, Mohammad Modarres and Norman M. Wereley for their valuable suggestions.

I also would like to thank my management Kerry Flint, Ron Herr, Gary Zook, and John Burwell for their support throughout this project. Their support was instrumental in my ability to complete this project. I would also like to thank Kirk Doughty for being a great sounding board. He was a great help in formulating my ideas.

The FEA contained in this dissertation was done primarily by Ed Habtour from AMSAA. I am very grateful for his help on this project, and would not have been able to accomplish this without him.

Table of Contents

List of Tables

List of Figures

Chapter 1 Introduction

Within industry random vibration environments have long been the cause of many fatigue induced failures. As such, vibration has long been an area of study. This work will extend on the available knowledge base for analyzing complex random vibration environments

1.1 Background and Motivation

Random vibration environments have long been specified in terms of the power spectral density (PSD). This method of specification is widely accepted as a convenient way to compare different vibration environments. It's very beneficial to designers and engineers therefore, if the PSD can be successfully used in predictive models to assess vibration durability. However, as this study demonstrates, there are several limitations in traditional approaches for using the PSD for life prediction. This study aims to develop a methodology to overcome these limitations and present a viable methodology for accurate life prediction.

Historically most random vibration testing has been done on single-axis vibration systems. For requirements where the frequency range is up to 2000 Hz, this is almost exclusively done on electrodynamic shakers. In recent years the capability to perform simultaneous multi-axis testing has increased. Multi-axis testing is becoming common place in labs around the country in the form of both repetitive shock (RS) vibration and electrodynamic (ED) vibration [1] (note hydraulic vibration systems generally do not test up to 2000 hz). Each vibration system uses different methods to excite the test item. RS vibration systems use pneumatic hammers that impact a specially engineered plate that the test specimen is mounted on. This plate then resonates, introducing vibration into the

test specimen. Although the vibration is multi-axis in nature and can excite all 6 degrees of freedom (DOF), the amplitude between 20 and 500 Hz is too low. In the case of ED vibration, an internal driver coil is powered by an electronic amplifier. One characteristic difference is that RS vibration has many peaks and valleys at adjoining frequencies due to the resonances of the table [1]. This is unlike ED vibration, which can have very smooth profiles. Another characteristic difference is that ED vibration systems can control the shape and the amplitude of the PSD. For an RS vibration system, only the amplitude can be controlled.

With multiple environments available for testing, methods to compare these environments have become important. Many different methods have been proposed in engineering communities. Many of these methods focus on the 1st mode response [2,3] of the test specimen. This comes from an underlying assumption that damage occurs in a narrow band around the 1st resonant frequency [4]. Stress at the failure site is estimated by calculating the response amplitude of the 1st mode and accounting for item geometry. As failure occurs, however, the propagation of fatigue induced cracks causes a decrease in the natural frequency of vibration. Recent work in manufacturing practices and equipment reliability has focused on using resonant mode shifting to detect possible failure points before catastrophic failure occurs [5-9]. Despite these advances, the shifting of the natural frequency is not taken into account in traditional durability analysis. In addition, when analyzing random vibration input profiles, peaks and valleys that are "far" from the resonant frequency are often ignored. Analysis of vibration failures are further complicated by plasticity near final fracture and large scatter in available fatigue data. Often times material properties and geometry limitations make the

development of analytic life models cost prohibitive. In this case, engineers often turn to semi-empirical life models. In a semi-empirical model, a physics of failure model is identified, and then a set of experimental variables are determined by an accelerated life test. The validity of the accelerated life test is highly dependent on the underlying physics of failure model. The purpose of this investigation was to develop a frequency domain physics of failure based predictive model, as well as a semi-empirical model, to predict time to failure of a simple structural member for different vibration environments. Although the model developed here will be for single-axis vibration environments that have the characteristics of RS and ED vibration, the experimental data that is presented and ongoing research should allow a predictive model to be developed for multi-axis vibration.

1.2 Research Objectives

The objectives of this research are as follows:

- Experimentally investigate the effect of notches in the power spectral density profile, on time to failure for a simple structural member under random vibration excitation.
- Experimentally investigate the effectiveness of using the PSD as an indicator of test severity, where time-to-failure is used as a severity metric.
- Develop a predictive, frequency domain, physics of failure, analytic model, which accounts for frequency shifting during vibration fatigue.
- Analyze the effects of different methods for determining and modeling damping, on the accuracy of the model predictions.

- Develop a semi-empirical life model that accounts for frequency shifting and can be calibrated with accelerated test data for life prediction under different vibration conditions.

1.3 Dissertation Overview

This dissertation is structured into individual chapters, with each chapter comprising a stand-alone publication. Consequently, there is some amount of necessary redundancy across the chapters, in the interest of completeness, to make each chapter self-contained. Chapter 2 is a paper that was published in the *Journal of the Institute of Environmental Sciences and Technology (IEST)*, and it describes an experimental investigation into the effect of notches in the input PSD on the fatigue durability of structures subjected to random vibration excitation. Chapter 3 is an article which has been submitted for review to *the Journal of Shock and Vibration*. This article presents an experimental data set which compares repetitive shock vibration, 3-axis electrodynamic vibration and single-axis electrodynamic vibration, in terms of their relative effectiveness in causing fatigue damage accumulation. Chapter 4 is an article formatted for publication which develops a physics of failure (PoF) model to predict time to failure in the frequency domain using linear elastic fracture mechanics (LEFM). The goodness of the model is tested against the experimental results presented in Chapter 3. Chapter 5 is an article formatted for publication which explores the uncertainties associated with the model developed in Chapter 4, because of the variabilities of the input parameters. Chapter 6 is an article formatted for publication which simplifies the model of Chapter 4 to a 2 parameter semi-empirical life model where the 2 parameters can be determined experimentally. Chapter 7 presents the

overall conclusions and contributions of this dissertation, discusses its limitations and suggests relevant future work. Appendix A provides a detailed flow of the calculation method used in Chapter 4.

Chapter 2 Effect of Resonant Frequency Shifting on Time to Failure of a Cantilevered Beam under Vibration

Published in the Journal of the IEST, V. 53. No. 1 2010.

2.1 Background

With increasing recognition of the value of highly accelerated life testing/highly accelerated stress screen (HALT/HASS), the use of repetitive shock (RS) vibration has greatly increased. RS vibration uses pneumatic hammers that impact a plate. This plate then resonates, introducing vibration into the test specimen. In the case of electrodynamic (ED) vibration, an internal driver coil is powered by an electronic amplifier. One characteristic difference is that RS vibration has many peaks and valleys at adjoining frequencies [1]. This is unlike ED vibration, which can have very smooth profiles. The existence of the peaks and valleys in RS raises a question as to their effect on the severity of the vibration environment.

2.2 Purpose

During equipment design, many methods focus on the 1st mode of vibration [2,3]. This comes from an underlying assumption that damage occurs in a narrow band around the 1st resonant frequency [4]. Stress is computed by calculating the response of the 1st mode and accounting for item geometry. Shifting of the natural frequency is never taken into account.

In comparing vibration environments, the power spectral density (PSD) values at the resonant frequency are often used to express equivalence. Sine testing goes so far as to find the resonant modes, and then dwell at those resonance points during testing. In

addition, many random tests ignore peaks and valleys that are “far” from the resonant frequency. Recent work in manufacturing practice and equipment reliability studies has focused on using resonant mode shifting to detect possible failure points before catastrophic failure has occurred [5–9]. Resonant mode shifting has also been used to capture manufacturing problems in sheet material [10]. The resonant shifting during failure challenges the fundamental assumption of examining a single frequency for computing damage due to a vibration spectrum. This study will show the effect of resonant frequency shifting on the time to failure of a cantilevered beam. In addition, it will demonstrate cautions that should be considered when performing testing where the PSD has large valleys and peaks, sine-on-random testing is used, or sine dwells are used.

2.3 Experiment

To evaluate the effect of the peaks and valleys, a cantilevered beam was subjected to five vibration profiles while measuring the time to failure. In addition, the natural frequency was monitored during the crack growth. The cantilevered beam was manufactured from 4.763 mm × 15.88 mm (.1875 in. × .625 in.) 1018 bar stock. A notch was cut, as illustrated in Fig. 1.

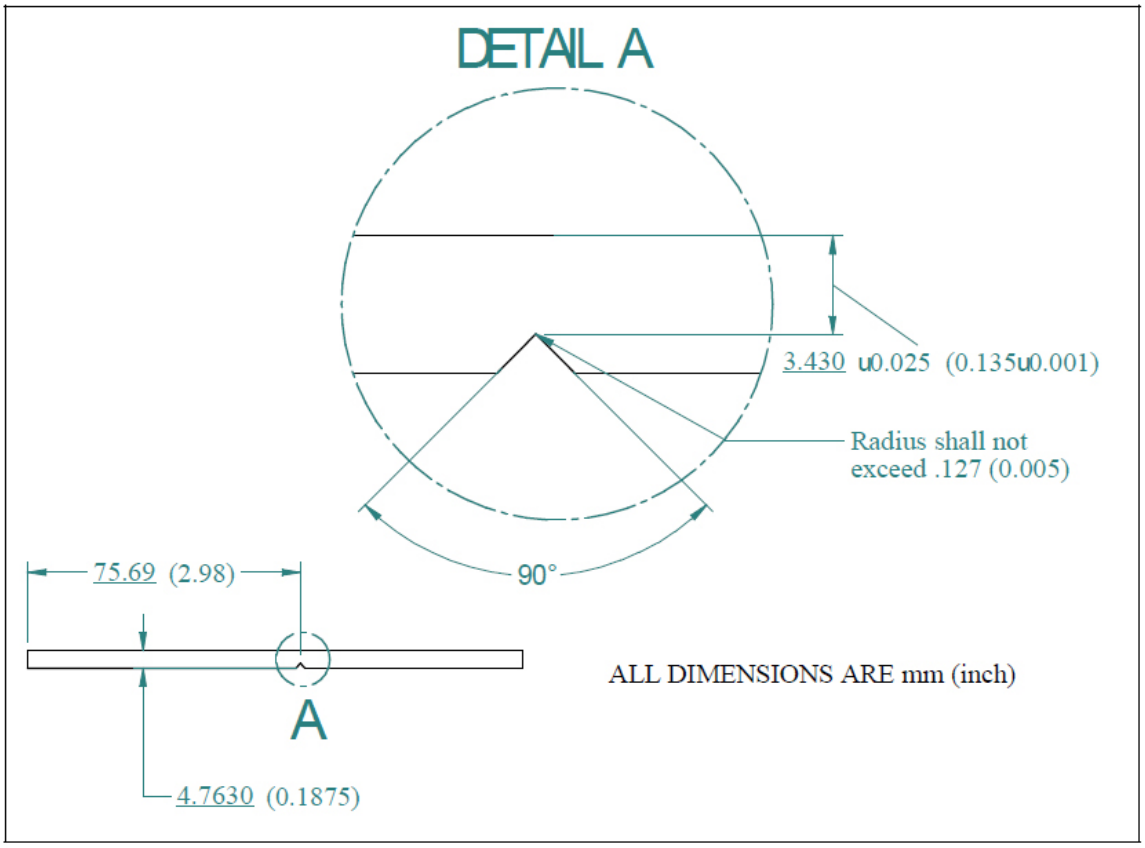

Fig. 1. Cantilevered beam dimensions.

On the end of the beam, a 430-g (.95-lb) mass was secured. Fig. 2 shows the beam attached to the exciter.

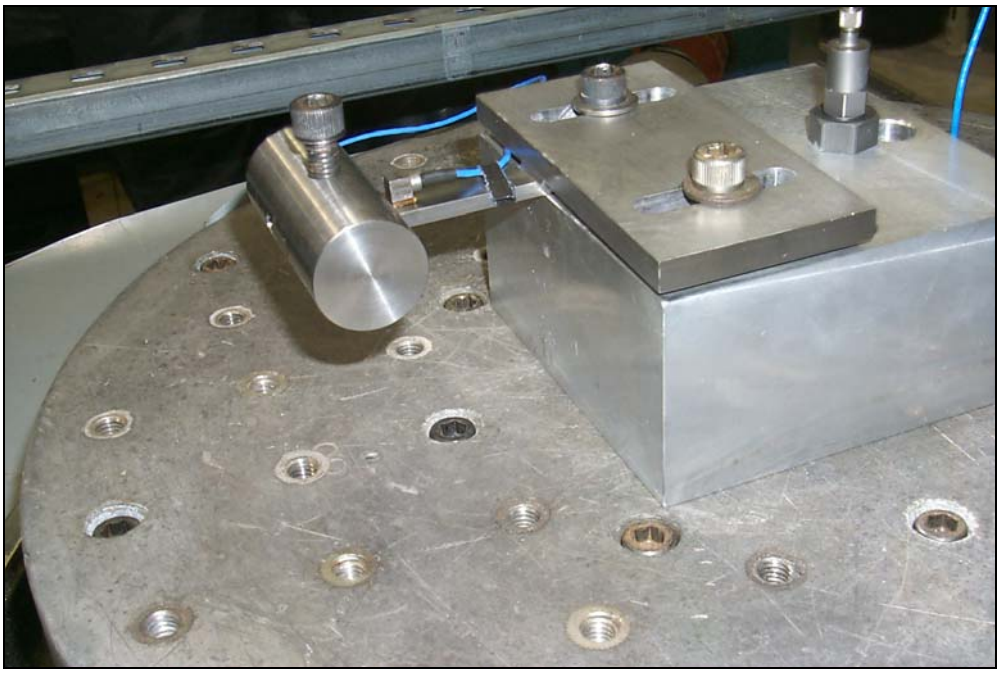

Fig. 2. Experimental setup of resonant beam with end mass.

A control accelerometer was mounted on the fixture as illustrated in Fig. 2. In addition, a response accelerometer was attached as close as possible to the end. The response accelerometer was used to measure the natural frequency of the beam. A sine sweep was performed to measure the resonant modes, as illustrated in Fig. 3.

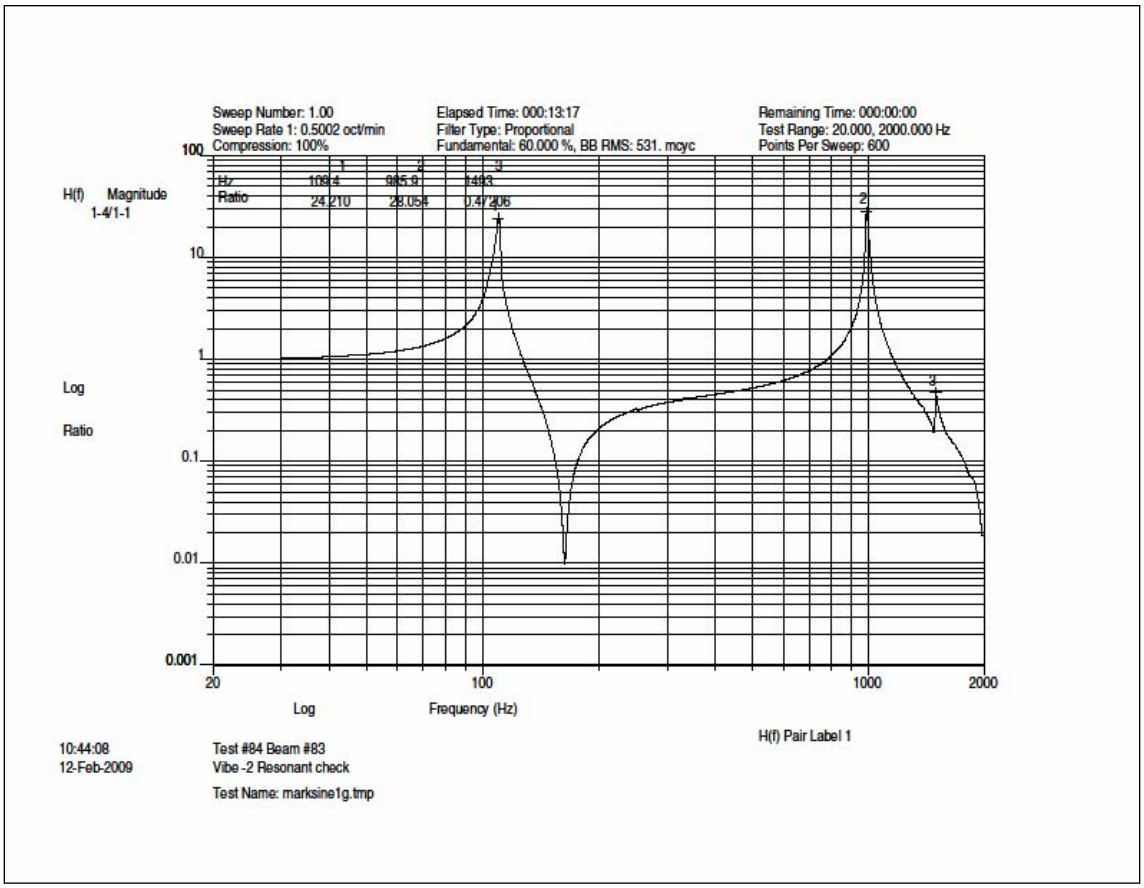

Fig. 3. Resonant frequency search.

The resonant frequencies were 110 Hz and 985 Hz. These were the 1st and 2nd bending modes of a cantilevered beam.

Each vibration profile was developed based on the resonant frequencies. The profiles are illustrated in Fig. 4 and described in Table 1.

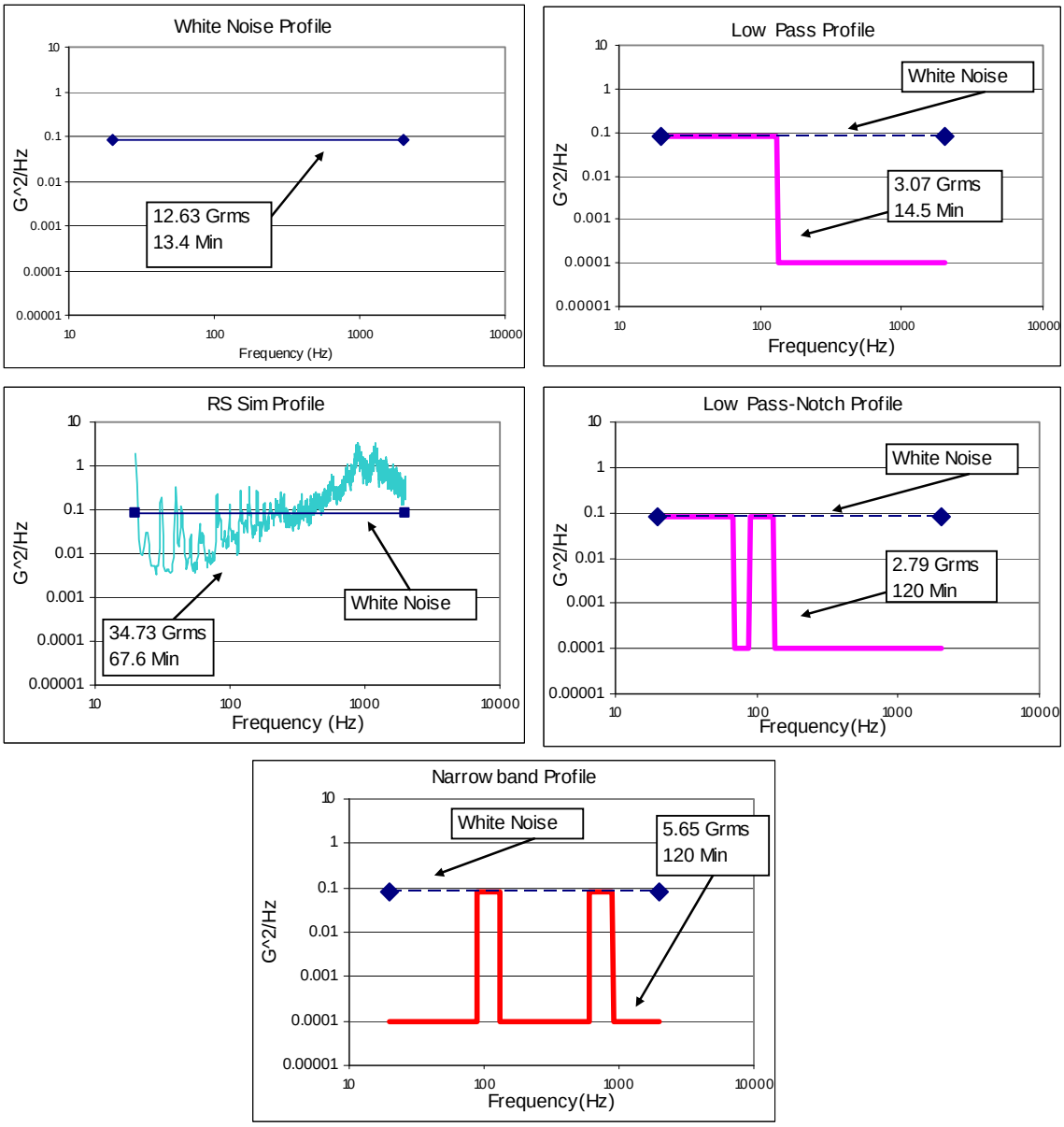

Fig. 4. Input profiles with G_{rms} and average time to failure.

Profile	Description
White noise profile	This white noise profile will be used as a baseline.
Low pass profile	There was concern as to whether the energy input (G^2/Hz) at the 2nd mode (985 Hz) would affect the time to failure. This profile was run to demonstrate the difference in time to failure between exciting the 1st mode and exciting the 1st and 2nd mode simultaneously.
RS sim profile	This profile incorporates data that was measured on an RS system and simulated on an ED system.
Low pass-notch profile	This profile was used to examine the effects of a 20-Hz notch starting 20 Hz below the natural frequency of 110 Hz.
Narrowband profile	This profile was used to examine the effect of not having any input outside of a 40-Hz bandwidth of the 1st natural frequency. The energy around the 2nd mode was shown to be insignificant by the low pass profile.

Table 1. Description and purpose of each profile

A minimum of four trials were used for each profile, with the exception of the RS sim and the narrowband profile. Due to the nature of the frequency shift, fewer trials were necessary for those profiles. All of the profiles were run using a Jaguar controller from Spectral Dynamics with the σ clipping set to "off." The random signal-generation algorithm, however, only allows peaks of 4σ. The profiles were controlled from 20–2000 Hz using 120 DOF. All of the profiles except the RS sim profile had a frequency resolution of 2.5 Hz. For the RS sim profile, a frequency resolution of 0.625 Hz was used. These profiles were run using breakpoints to develop a PSD. The abort limits were ±3 db, although in most cases the controller was more accurate.

2.4 Results

Fig. 5 illustrates the time to failure for each of the various profiles. The time to failure values are indicative of the damage potential for each of the input profiles. Confidence levels (CL) of 90% were also calculated and plotted.

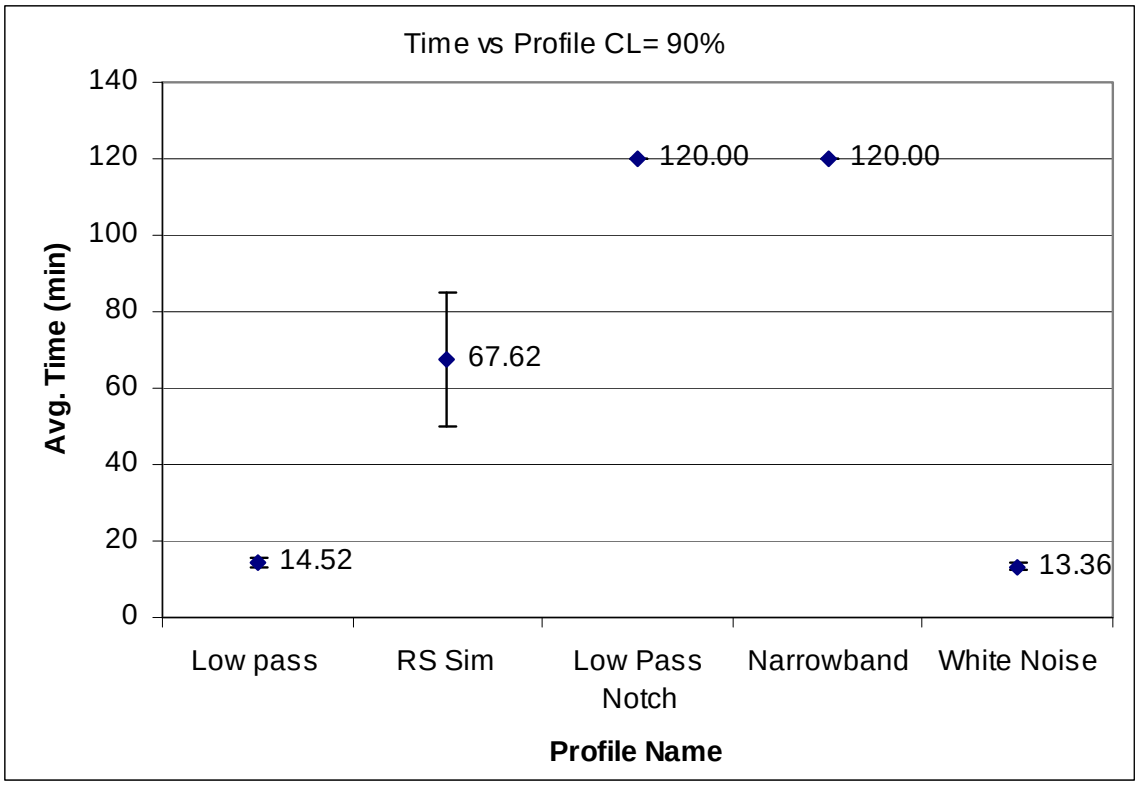

Fig. 5. Time to failure for various profiles.

Fig. 5 illustrates that despite having PSD values that are the same (within a 10-Hz bandwidth around natural frequency) the time to failure was statistically different for each profile. For those profiles where the time to failure was 120 minutes, the time indicated termination of the test, not failure. The low pass profile and the white noise profile showed statistically equivalent times to failure. Since the low pass profile only excited the 1st mode, it was demonstrated that the 2nd vibration mode effect was smaller than the experimental error and fatigue scatter. The RS sim profile showed a longer time to failure than the white noise profile and the low pass profile. As fatigue cracks propagated through the material, the 1st mode resonant frequency of the beam shifted. As the shift occurred, it aligned with the peaks and valleys of the input profile. When the 1st mode aligned with the valleys of the input, the natural frequency shift would slow

down, indicating a reduced crack propagation speed. When the 1st mode aligned with the peaks of the input, the natural frequency shift would speed up, indicating an increase in crack propagation speed.

An extreme case of this was demonstrated by the narrowband profile. The narrowband profile did not fail, despite having an initial PSD input at the 1st mode that was equivalent to the low pass profile and the white noise profile, and higher than the RS sim profile. The resonant frequency shifted at the same rate as the low pass profile and the RS sim profile, but stopped once the natural frequency got to an area of low energy input. At this point, the 1st mode frequency remained constant, and no failure occurred. The low pass-notch profile behaved similarly to the narrowband profile. The frequency of the 1st mode shifted up to the valley and then stayed there until about 90 minutes. At this point, some of the test samples began to experience a shift in the natural frequency. One item failed at 1 hr 56 min, which shows that an item may get stuck in a valley for a significant amount of time, but still is able to move through that area if there is enough energy below the natural frequency. Fig. 6 depicts the 1st mode frequency shifting as a function of time. The natural frequency was determined in real time and no sine sweeps were performed during the random excitation. Furthermore, data for all of the samples were averaged.

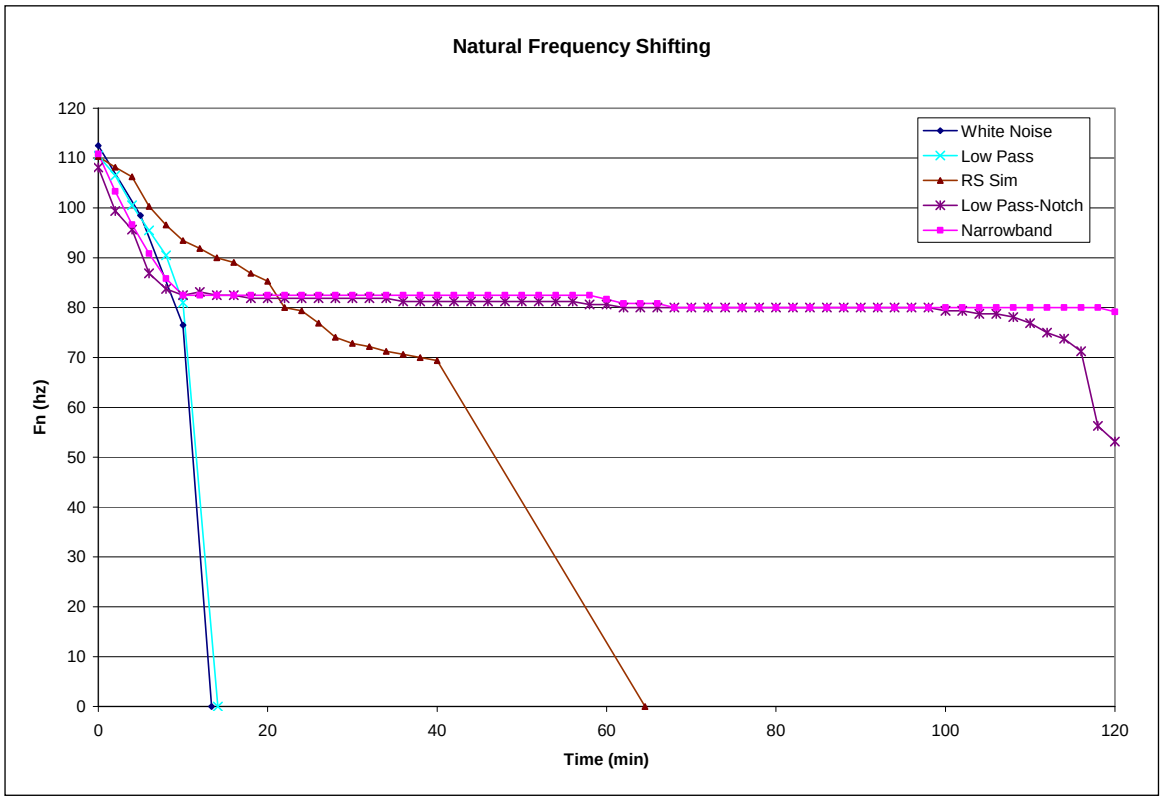

Fig. 6. Shifting of the natural frequency.

Fig. 6 shows that both the slope of the 1st mode frequency shift and the frequency of the 1st mode vary with time. This change in slope illustrates the changing crack propagation speed. This is evident as the natural frequency goes through the peaks and valleys of the RS sim, low pass-notch and narrowband profiles. Although not recorded, it was noted that as the natural frequency shifted, the damping value increased.

The change in natural frequency is problematic for evaluation of damage potential. Using methods such as those discussed in Ref. 2, 3, and 11 requires knowledge of the rate at which the natural frequency is shifting. This may not be known *a priori*, but must be determined experimentally. These results lead to some startling conclusions.

2.5 Conclusions

Due to resonant frequency shifting during crack propagation, the frequency band of excitation below the natural frequency becomes important. In this particular case, the initial resonance was 110 Hz. The amount of input excitation at frequencies between 50 Hz and 110 Hz was statistically significant to the time to failure of the component. Secondly, this data shows that crack propagation will be accompanied by a change in the natural frequency. This analysis could be extended to testing of items where a natural frequency shift during vibration has occurred. The natural frequency shift may be indicating that fatigue failure has started and should be addressed. In more complex systems, it is possible that the change in natural frequency could be due to other factors, but crack propagation should be considered. This would be particularly important in a HALT/HASS or design test. A resonant frequency change may indicate that a failure is starting to occur that would be propagated to a patent defect if testing was allowed to continue.

Finally, some test methods may be called into question. Tests where there are large valleys and peaks might not propagate a defect to failure. The crack would grow until the frequency shift made the natural frequency coincident with a valley. At this point, the crack would stop growing, or would slow significantly, and the failure would not occur. However, this same test, when subjected to a smoother profile, would propagate the defect to failure. This is of particular concern in RS testing, especially at frequencies below 1000 Hz. Sine dwells would also be suspect as the natural frequency may simply shift out of the sine dwell range, and no further damage would occur. Sine-on-random vibration profiles would also be suspect if the test environment was not an

exact replication of a field environment. The sine peaks could cause a crack initiation that would go undetected as the natural frequency shifted into a random-only section. It may be advantageous to use random-on-random instead.

2.6 References

[1] Jawaid, S. and P. Rogers. 2000. Accelerated reliability test results: Importance of input vibration spectrum and mechanical response of test article. *Proceedings of the Annual Reliability and Maintainability Symposium*, 248–53. Piscataway, NJ: IEEE.

[2] Harris, Cyril and Allan Piersol. 2002. *Harris' shock and vibration handbook,* 5th ed. New York: McGraw-Hill.

[3] Steinberg, Dave S. 2001. *Preventing thermal cycling and vibration failures in electronic equipment*. Hoboken, NJ: John Wiley & Sons.

[4] Fackler, Warren C. 1972. *Equivalence techniques for vibration testing*. Shock and Vibration Information Center. Washington, DC: US Department of Defense.

[5] Giannoccaro, N. I., A. Messina, et al. 2006. Fatigue damage evaluation of notched specimens through resonance and anti-resonance data. *Engineering Failure Analysis* 12:340–52.

[6] Al-Najjar, B. 2000. Accuracy, effectiveness and improvement of vibration-base maintenance in paper mills: case studies. *Journal of Sound and Vibration* 229 (2): 389–410.

[7] Maynard, K. P., M. W. Trethewey, et al. 2001. Application of torsional vibration measurements to shaft prevention technology. *Proceedings of the 55th Meeting of the Society for Machinery Failure Prevention Technology* 55:217–26.

[8] Trethewey, Martin, Joshua Friell, et al. 2008. A spectral simulation approach to evaluate probabilistic measurement precision of a reactor coolant pump torsional vibration shaft crack monitoring system. *Journal of Sound and Vibration* 310:1036–56.

[9] Wang, Rui-Jie, De-Guang Shang, et al. 2008. Fatigue damage model based on the natural frequency changes for spot welded joints. *International Journal of Fatigue* 30:1047–55.

[10] Mfoumou, Etienne, Oleg V. Rudenko, et al. 2006. Acoustical measurement accompanying tensile test: New modality for nondestructive testing and

characterization of sheet materials. Paper presented at the 13th International Congress on Sound and Vibration, Vienna, Austria.

[11] Henderson, G. and Piersol, A. G. 1995. Fatigue damage related descriptor for random vibration test environments. Special dynamic testing reference issue, *Shock and Vibration*, 20–24.

Chapter 3 Limitations of the Power Spectral Density as an Indicator of Test Severity

In the previous chapter notches below the initial natural frequency were shown to drastically effect the time to failure. This effect was linked to the change in natural frequency that occurred during failure. This next chapter will directly compare RS vibration systems and ED vibration systems and their ability to cause fatigue related damage

3.1 Introduction

Random vibration environments have long been specified in terms of the power spectral density (PSD). This method of specification is widely accepted as a way to compare vibration levels. Historically most testing has been done on single-axis vibration systems. For requirements where the frequency range is up to 2000 Hz, this is almost exclusively done on electrodynamic shakers. In recent years the capability to perform simultaneous multi-axis testing has increased. Multi-axis testing is becoming common place in labs around the country in the form of both repetitive shock (RS) vibration and electrodynamic (ED) vibration [1,2]. With multiple environments available for testing, methods to compare these environments have become important. Many different methods have been proposed in engineering communities. Many of these methods focus on the 1st mode of vibration [2,3]. This comes from an underlying assumption that damage occurs in a narrow band around the 1st resonant frequency [4]. Stress is computed by calculating the response of the 1st mode and accounting for item geometry. Recent work in the manufacturing practices and equipment reliability studies

has focused on using resonant mode shifting to detect possible failure points before catastrophic failure has occurred [5-9]. The shifting of the natural frequency is not taken into account in traditional analysis. In addition many random tests ignore peaks and valleys that are "far" from the resonant frequency. Analysis of vibration failures is further complicated by plasticity near final fracture and large scatter in available fatigue data. The purpose of this investigation was to analyze the effectiveness of using the power spectral density in combination with the G_{rms} level to compare vibration environments. This investigation will focus on single-axis ED, multi-axis ED and RS vibration. In addition an experimental data set will be generated that will allow comparison of the effectiveness of various analytic models at predicting vibration severity, as indicated by time to failure.

3.2 Background

Repetitive Shock Vibration is generated by pneumatically driven hammers that impact a plate. This plate responds according to its modal properties, imparting a vibration to the unit under test (UUT) mounted on the plate. The vibration is generally found to contain energy in all 6 degrees of freedom (3 rotation and 3 translation motions). The vibration generated by these types of machines produces a significantly nonuniform response on the mounting plate, thus making the test condition vary significantly between different locations on the mounting plate. In addition, there is large variation between different sizes of machines as well as between manufacturers. The only control parameter is the G_{rms} in the out-of-plane direction, over the entire frequency spectrum that is being excited. In general that is about 500-10,000 Hz. The shape of the PSD profile cannot be controlled and is driven by the table and hammer

dynamics. Many of the RS machines also experience high energy peaks during the impact of each hammer, followed by low levels in between impacts [10]. As such for any RS test it is unique to the particular table, at a particular location and at a particular G-Level. ED vibration on the other hand is very controllable. Nearly any PSD can be run on nearly any ED vibration system (assuming it can handle the load). This controllability is the only way to simulate real world environments. ED vibration is generally limited to 5-2000 Hz, although some systems can provide vibration excitation at higher frequencies. In recent years multi-axis ED vibration systems have become available. It is now possible to procure an off-the-shelf 6 degree of freedom (DOF) multi-axis vibration system. Testing has been conducted to compare single-axis ED vibration and multi-axis ED vibration [11,12]. These tests have found that multi-axis testing will cause a test specimen to fail in a shorter time compared to single-axis testing. In addition Himelblau and Gregory performed separate investigations regarding the response of a test item to multi-axis vibration [13,14]. They outfitted a test item with accelerometers or strain gages and measured the strain or acceleration response.

3.3 Experimental Development

In order to compare the vibration environments two test specimens were built. The first test specimen was primarily sensitive in the Z-axis (See Fig. 3) and is depicted in Fig. 1 (all dimensions in inches).

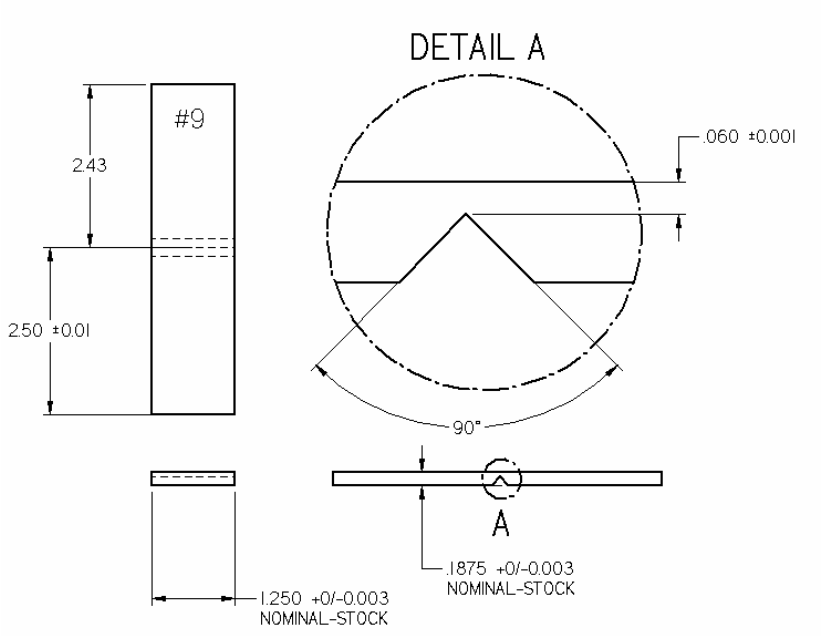

Fig. 1. Test Beam 1.

The second test specimen was sensitive in two directions, although it had a primary sensitivity in the Z-direction. This is illustrated in Fig. 2 (all dimensions in inches).

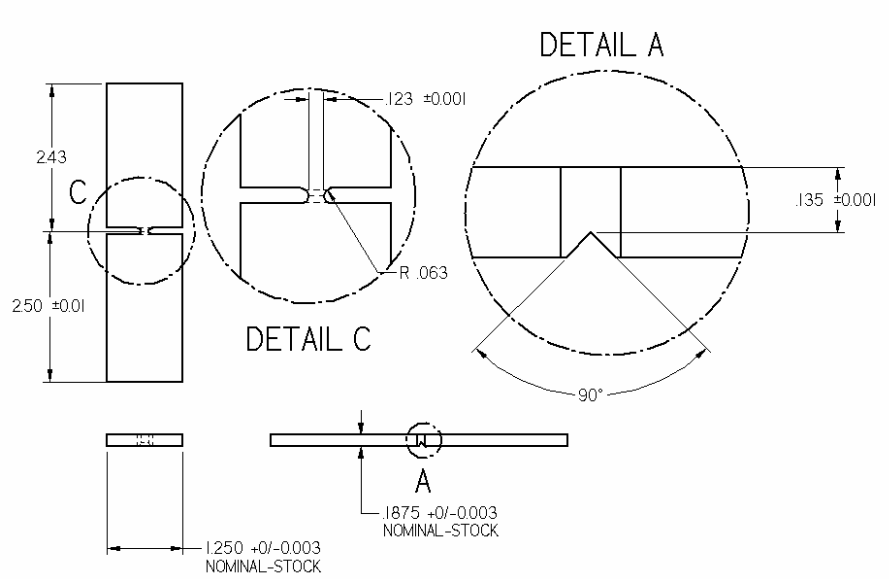

Fig. 2. Test Beam 2

The first bending mode of Beam 1 in the vertical direction was 415 Hz. In the transverse direction the first bending mode was 3520 Hz. For Beam 2 the first bending mode in the

vertical direction was 330 Hz. In the transverse direction the 1st bending mode was also 330 Hz. The beam was mounted for vibration as follows.

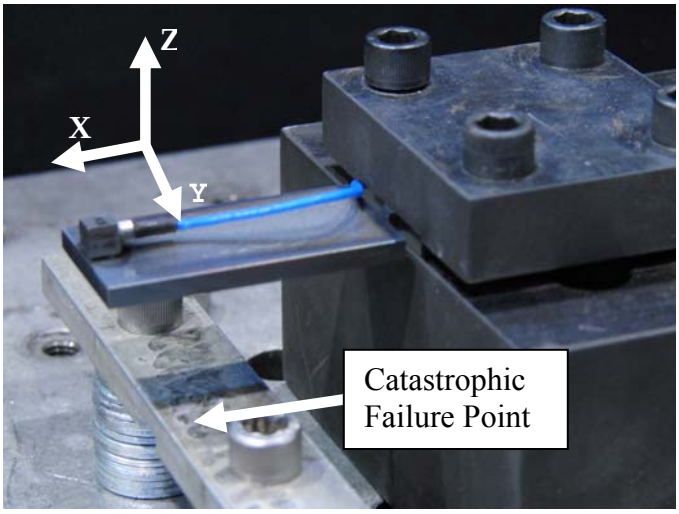

Fig. 3. Beam mounted on shaker

It should be noted that the test was continued until catastrophic failure of the beam. Catastrophic failure was determined to occur when the test specimen interacted with the member located just below the beam. The beam was made of cold rolled 1018 steel. As a result of the cold roll process the grain structure was different between production runs. In order to minimize the difference between lots the beams were annealed. After machining, the beams were heated to 1650 F for 2 hours and then allowed to slowly cool. This allowed recrystallization within the material and made the samples more uniform. In order to ensure that the data was unbiased the profiles were ran in random order, the machined beams were randomized for testing, and all test were run on the same vibration system in the same location. Each profile was tested using 5 samples.

The beams were subjected to 10 different profiles. To determine the profiles, the repetitive shock chamber PSD level was measured in the Z-Axis. All profiles in the RS system were designated by RS-XX, where the XX was the G_{rms} level that was indicated on the controller. In the case of the particular controller that was used it measured from

10-8,000 Hz in the z-axis only, near the center of the table. ED SIM RS-40 was created for the ED system by matching the PSD of the RS-40 Profile. The simulation profile used 3200 lines from 0-2000 Hz to describe the PSD. ED SMOOTH RS-40 was created by smoothing ED SIM RS-40. This was done by simply taking the time history and sampling it at 5120 Hz with 200 Lines. These profiles are depicted in Fig. 4.

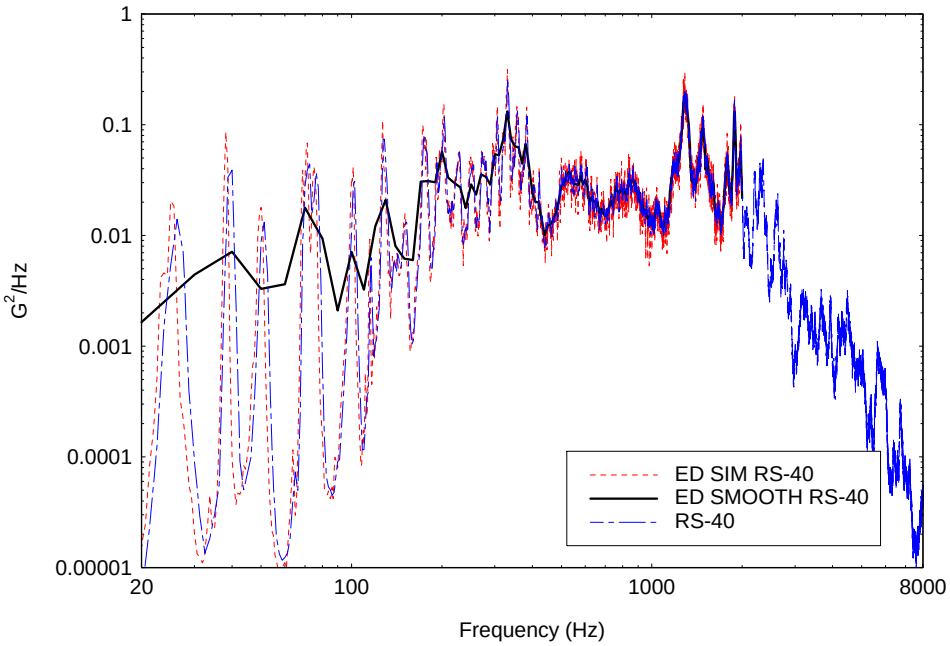

Fig. 4. RS-40 and electrodynamic simulation

WHITE-HIGH was developed by using a flat line profile to match the G_{rms} level of the RS-40 profile from 20-2000 Hz. These profiles are depicted in Fig. 5.

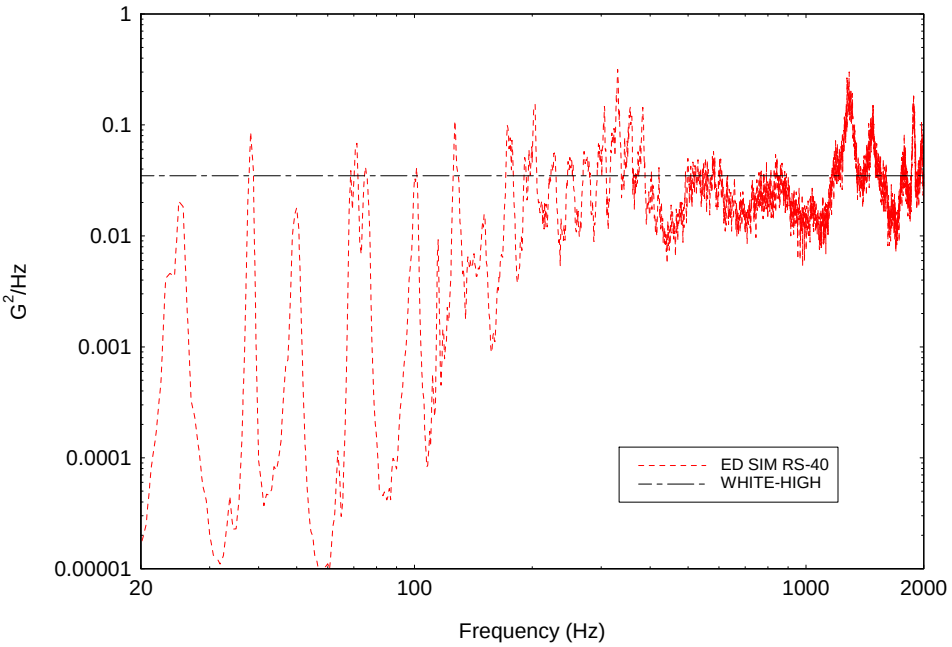

Fig. 5. Electrodynamic simulation and flat line profiles

The RS-60, ED SIM RS-60 and ED SMOOTH RS-60 were developed in the same manner as RS-40, ED SIM RS-40 and ED SMOOTH RS-40 respectively. These profiles allowed a comparison of each type of profile at two different levels. These profiles are depicted in Fig. 6.

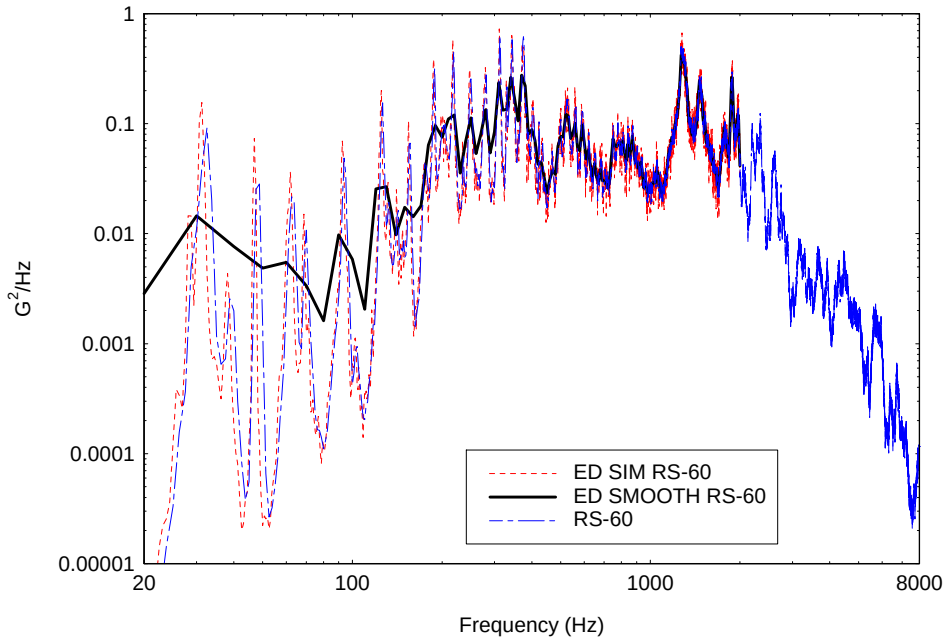

Fig. 6. RS-60 and electrodynamic simulation

A comparison was also made between ED single-axis vibration and ED multi-axis vibration. Due to limitations in the controllability of the 3 axis ED system at frequencies above 1000 Hz, the profiles were only run out to 1000 Hz. Two single-axis ED profiles were developed that were also tested in 3-axes They were WHITE-LOW which was -6db down from WHITE-HIGH and WHITE-MED which was -3db down from WHITE-HIGH. This allowed two levels to be tested on the 3 axis ED system. The corresponding 3-axis profile 3ED WHITE-LOW and WHITE-MED were also developed. For the 3-axis ED test all of the axes had the same PSD, with a low control coherence of .05. These profiles are depicted in Fig. 7.

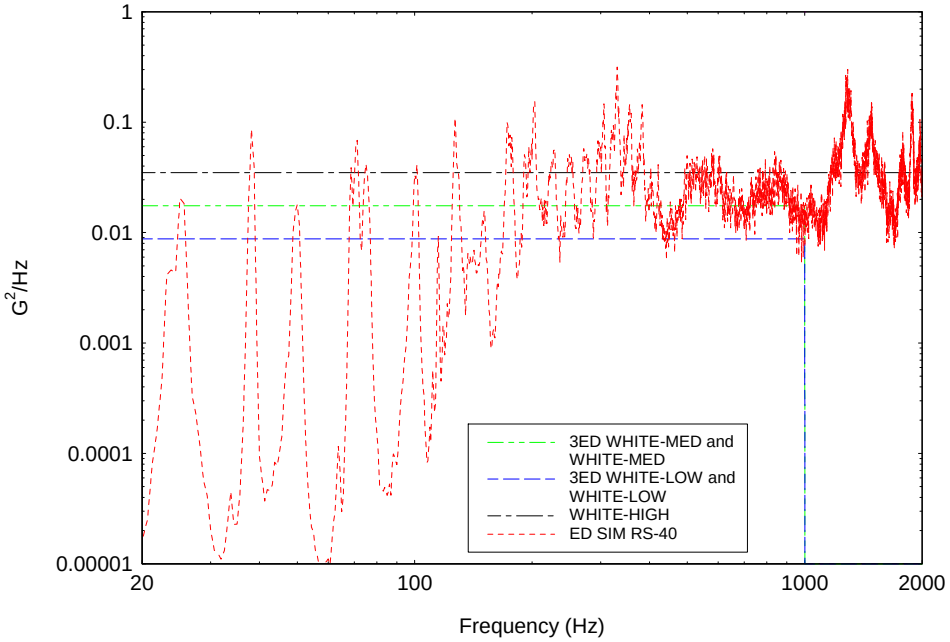

Fig. 7. Single-axis and 3-axis ED

A Summary of the profiles is included in Table 1.

Profile Name	Profile Description
ED SIM RS-40	Single-axis ED simulation of RS-40 Z-axis
ED SIM RS-60	Single-axis ED simulation of RS-60 Z-axis
ED SMOOTH RS-40	Smoothed version of ED SIM RS-40
ED SMOOTH RS-60	Smoothed version of ED SIM RS-60
WHITE-HIGH	Match the Grms level of the RS-40 profile from 20-2000 Hz
RS-40	Z-axis of repetitive Shock System set to 40 Grms
RS-60	Z-axis of repetitive Shock System set to 60 Grms
3ED WHITE-LOW	3-axis ED at White Low level in all axes
WHITE-LOW	Single-axis ED -6db of WHITE-HIGH ran from 20-1000 Hz
3ED WHITE-MED	3-axis ED at WHITE MED level in all axes
WHITE-MED	Single-axis ED -3db of WHITE-HIGH ran from 20-1000 Hz

Table 1. Summary description of profiles

The repetitive shock system that was used did not display the peaks and valleys in the time history that is typical for a RS system. In addition the kurtosis of this signal was 3.4 compared with a pure Gaussian signal which has a kurtosis of 3 [15]. Due to the small discrepancy, the signal is assumed to be Gaussian. Furthermore the Y axis component, although uncontrolled, had a PSD that was nearly identical to the z-axis.

3.4 Results

Typical evaluation of the severity of a test profile is undertaken by analyzing the PSD value at the natural frequency [2]. A simple comparison of three of the profiles is depicted in Fig. 8.

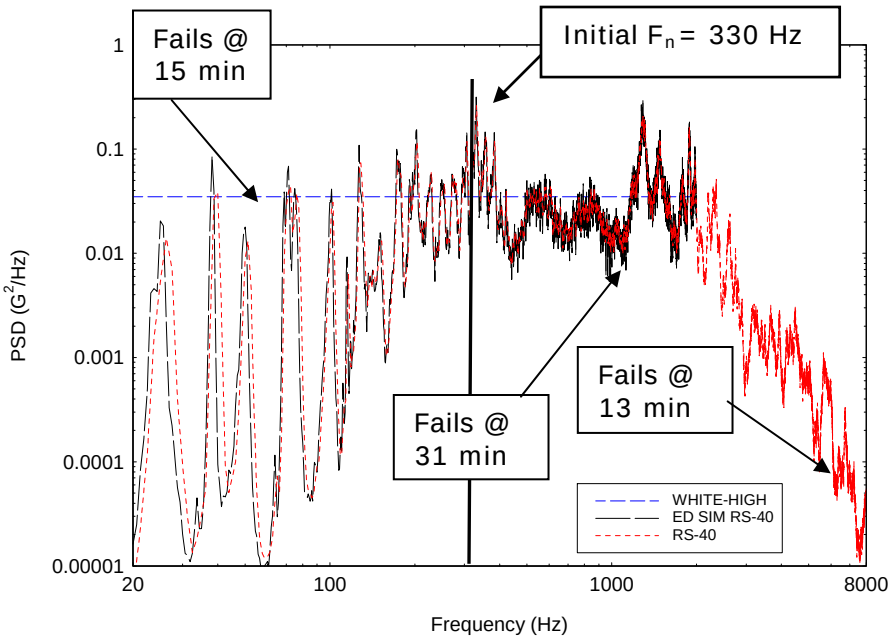

Fig. 8. Time to failure for different profiles

From Fig. 8 ED SIM RS-40 has a higher initial PSD level than WHITE-HIGH, yet takes approximately 2 times as long to fail. This discrepancy was due to a change in natural frequency (first bending mode) as the beam under went failure. This change in natural frequency has been reported by other researchers [4,5]. In their particular cases the natural frequency shift was not as important because they were comparing the same profile for multi-axis vs. single-axis testing. The frequency shifting becomes much more important when trying to compare different profiles. A sample of the frequency shift data is depicted in Fig. 9.

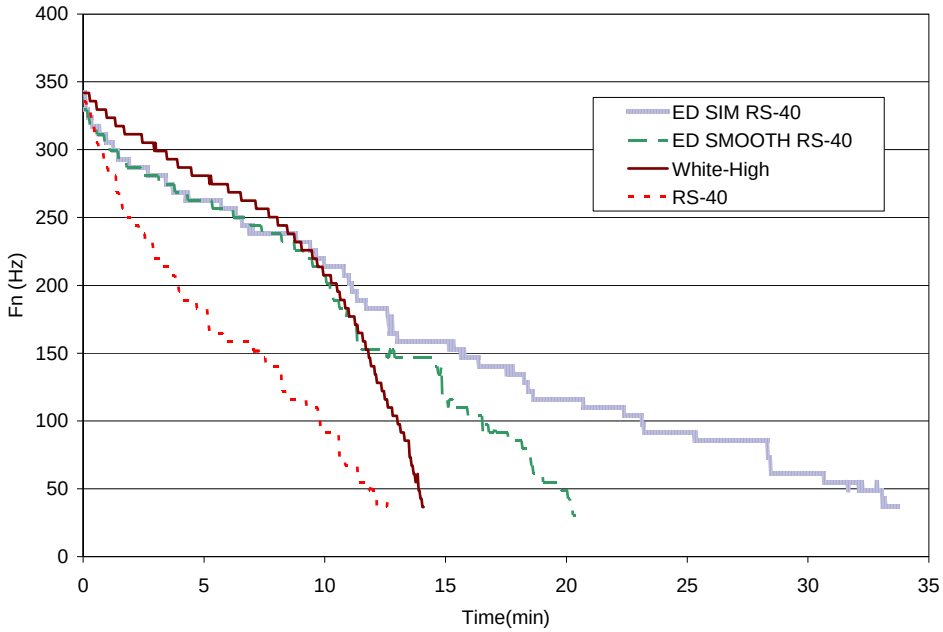

Fig. 9. Example of natural frequency shift during failure

From Fig. 9 it can be seen that the slope of natural frequency vs. time changes as the beams go through failure. It can also be seen that the slope changes from profile to profile. Characterization of this effect is done by calculating the rate of natural frequency change (RFC) in accordance with the following,

$$RFC_i = \frac{fn_i - fn_{i-1}}{t_i - t_{i-1}} \text{ [Hz/min]} \tag{1}$$

where Eq. 1 allows examination of the RFC at a given natural frequency. The RFC can be combined with the frequency spacing to yield the total time to failure as,

$$TTF = \int_{f_{nc\_fail}}^{f_{nc\_start}} \frac{1}{RFC} df_{nc} \text{ [min]} \tag{2}$$

where f_{nc_start} is the starting cracked natural frequency, f_{nc_fail} is the natural frequency at failure and TTF is total time to failure. As the frequency changes, the excitation level may go up or down depending on the local trend of the nonuniform PSD profile. This change in excitation level changes the RFC. This concept is illustrated in Fig. 10.

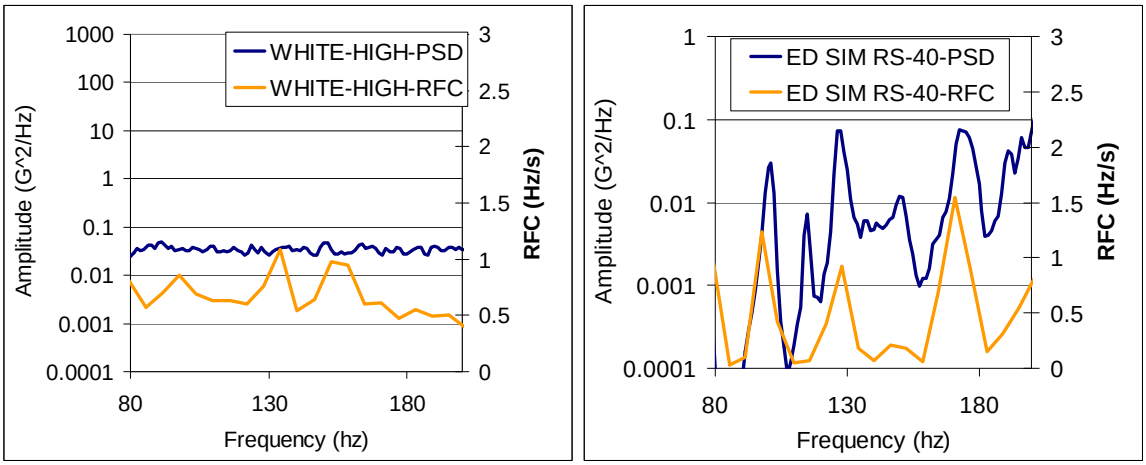

Fig. 10. Comparison of slope change

Over a small change in natural frequency the change of the RFC can be shown to follow the changing input levels. Upon examination of a larger frequency change, the PSD does not follow the RFC as illustrated in Fig. 11.

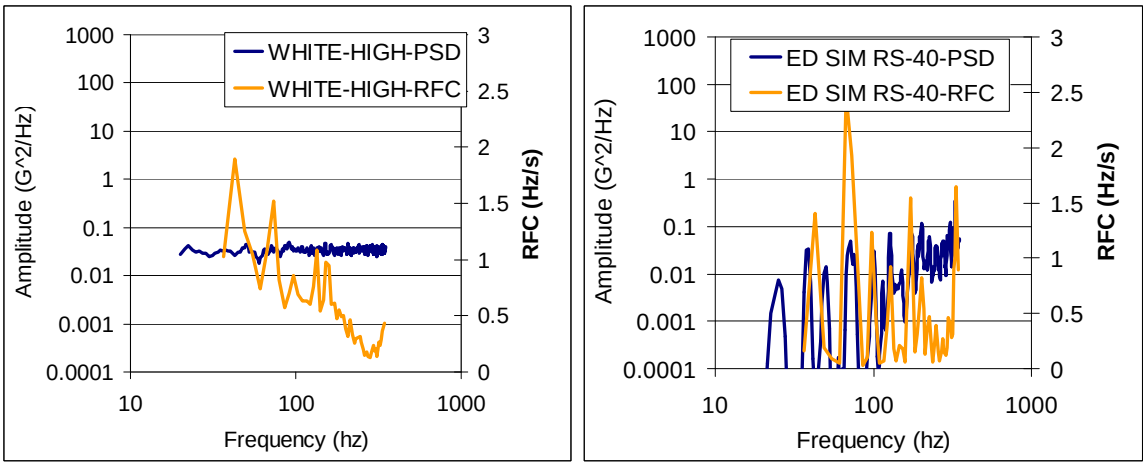

Fig. 11. RFC compared to PSD

It is apparent from the lack of relation between the PSD input and the RFC that the total time to failure would not be well correlated to input PSD or G_{rms}. As the test specimen fails when subjected to WHITE-HIGH, the RFC increases. This is not captured by the input PSD or G_{rms}. The above factors combined with the plasticity near catastrophic failure makes analytical evaluation of the time to failure problematic at best.

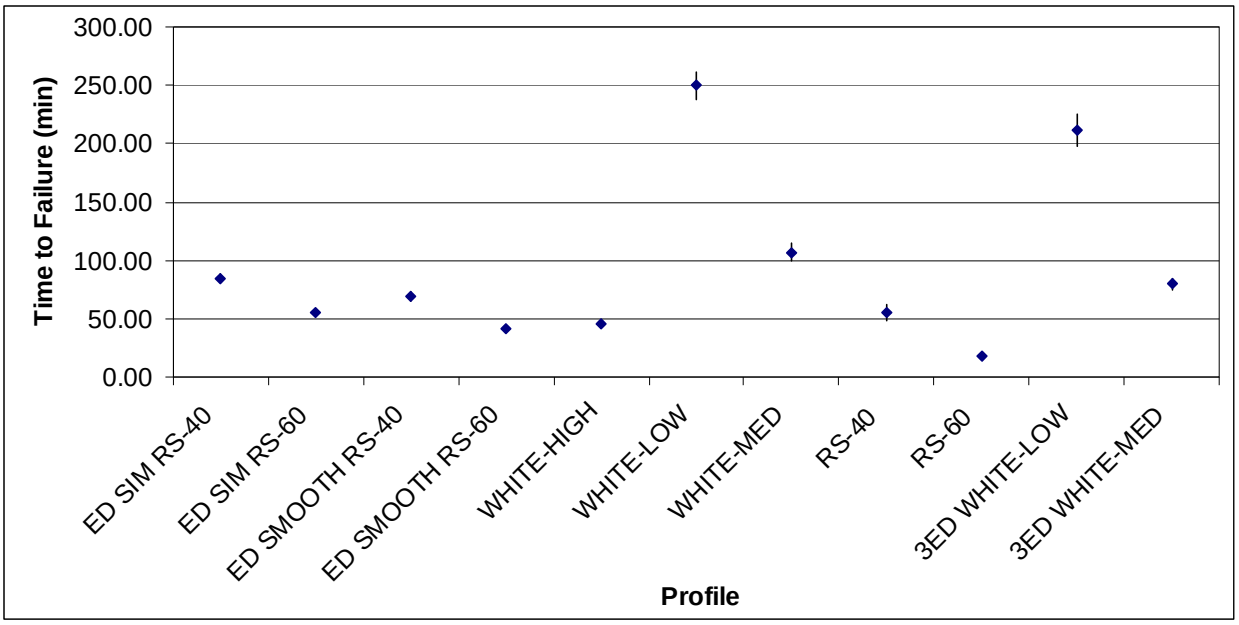

Fig. 12. Beam 1 time to failure with 90% confidence intervals

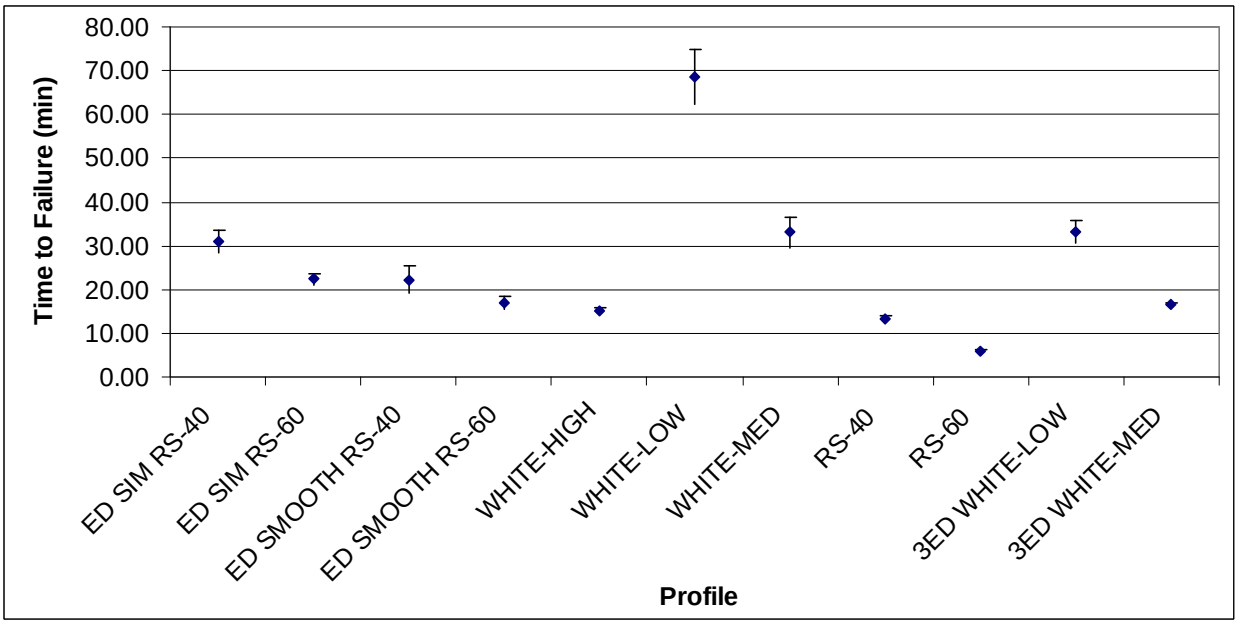

Fig. 13. Beam 2 time to failure with 90% confidence intervals

The ED simulation of the RS-40 profile was ED SIM RS-40, and the ED simulation of the RS-60 profile was ED SIM RS-60. From Fig. 14 the RS system fails the test item faster than the corresponding ED simulation. For both beam configurations the multi-axis test was more severe. Furthermore, when the specimen was sensitive in two directions, the multi-axis case had even more advantage than if the specimen was only

sensitive in one direction. Examination of the single-axis ED and multi-axis ED yields similar results. For Beam 1 and 2 the 3-axis ED system fails the test specimens faster than the single-axis simulation. Once again for both cases the multi-axis test was more severe, although only slightly so for Beam 1. From this it can be concluded that a multi-axis test of the same PSD as the single-axis version will be more severe. It was interesting to note that the multi-axis effect of the RS system was more pronounced than the multi-axis effect of the ED system. The variability between axes of the RS system was believed to account for this difference. These results are depicted graphically in Fig. 14.

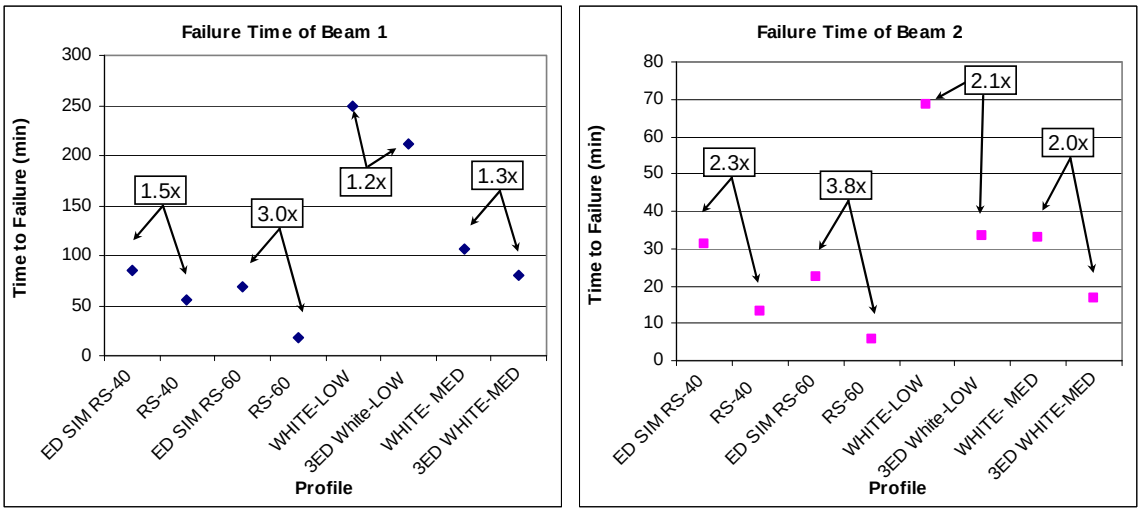

Fig. 14. Multi-axis time to failure

Although a multi-axis test is more severe than the corresponding single-axis test, at the same level, a comparison needs to be made to a profile that exhibits more white-noise characteristics. Note that the RS-40 was used to create WHITE-HIGH based on G_{rms}. It follows from Fig. 15 that the flat line WHITE-HIGH was more severe than the multi-axis RS-40 test. It also follows that WHITE-HIGH was substantially more severe than the ED simulation (ED SIM RS-40) of RS-40. All three of these tests had the same

G_{rms} level from 20-400 Hz. For Beam 2 similar results were also obtained, except that the multi-axis test was slightly more severe than the flat line profile. These observations imply that the G_{rms} is a very poor indicator of the test severity. In addition the low frequency input is very important in the overall time to failure. This is due to the natural frequency shift that happens during failure. It follows that profiles with inadequate low frequency energy should be avoided if full failure is desired.

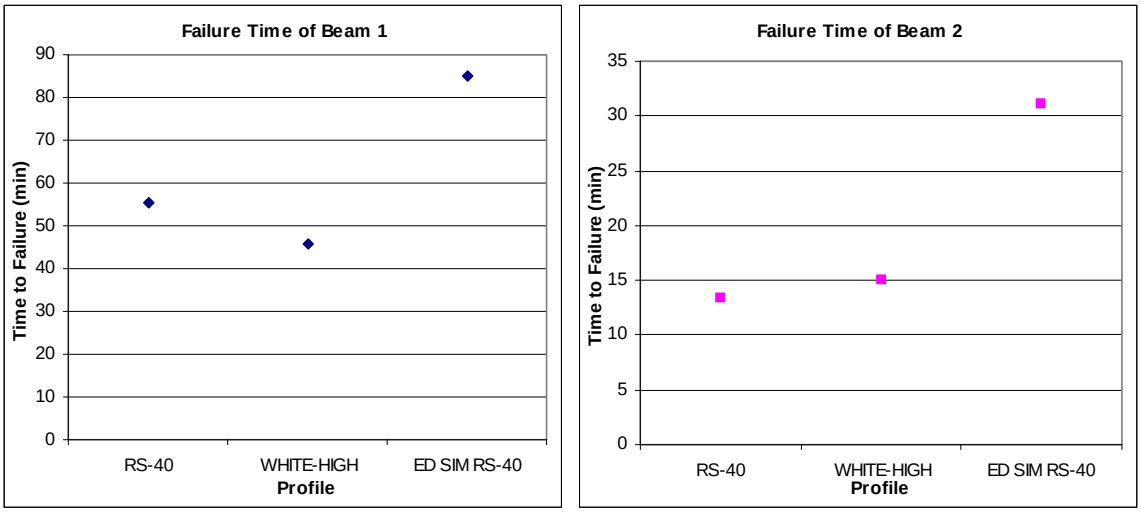

Fig. 15. Comparison of time to failure between WHITE-HIGH and RS system

The effect of smoothing the data was addressed in ED SMOOTH RS-40 and ED SMOOTH RS-60. Although the smoothing technique is not necessarily an advisable method, it does show the effect of smoothing as well as analyzing data with too few lines of resolution. Examination of Fig. 16 shows that by smoothing the profile, the severity of the test was increased. This is particularly important in the lower frequency range, where the difference between the peaks and valleys was more significant.

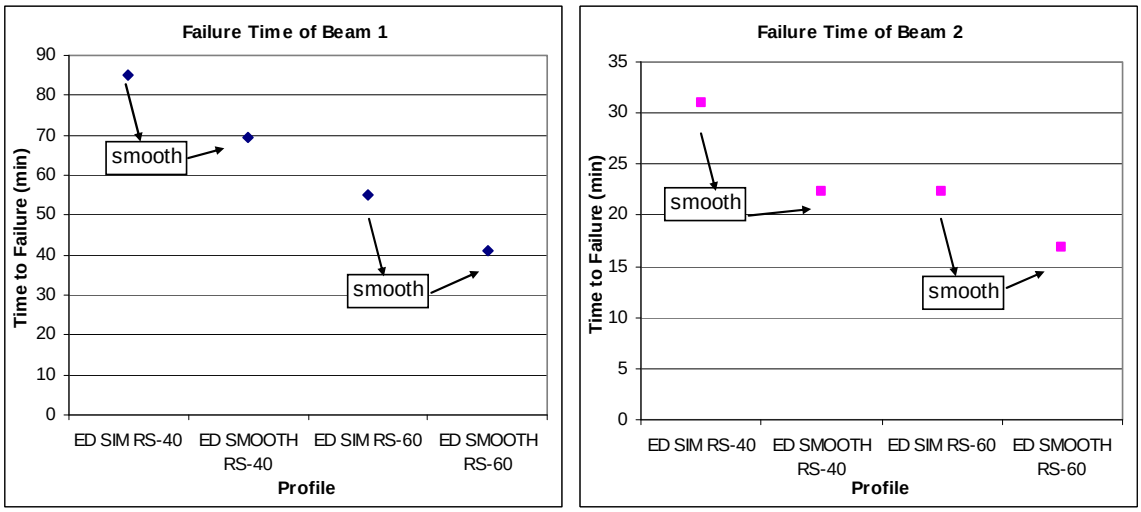

Fig. 16. Examination of data smoothing

3.5 Conclusions

Presented in this work is a set of experimental data comparing repetitive shock (RS) vibration, single-axis ED vibration and multi-axis ED vibration. The multi-axis effect of the RS system was shown to be more pronounced than the multi-axis effect of the ED system. Furthermore, multi-axis testing is more severe than single-axis testing at the same level. This severity is amplified when a component is tested which has sensitivity to vibration in more than 1 axis. In addition weaknesses were found in the RS system at low frequency. A white noise profile of similar G_{rms} was found to be more severe than the RS test. This was due to the lack of input energy below 150 Hz, even if the starting natural frequency was higher. In addition, smoothing of the data or poor line resolution can change the overall severity of a test. A poor correlation was shown between the PSD and the rate of natural frequency change (RFC) over a wide frequency shift. The change in natural frequency caused the initial PSD to not be an effective indicator of test severity. Quantification of the severity of the test profile can be

accomplished through characterization of the RFC. Currently there are no good analytical models available to deal with this in the frequency domain.

3.6 References

[1] M. Paulus and K. Doughty, Effect of resonant frequency shifting on time to failure of a cantilevered beam under vibration, *Journal of the IEST* **53**(1) (2010).

[2] C. Harris and A. Piersol, *Harris' Shock and Vibration Handbook 5th ed*., 2002 New York McGraw-Hill.

[3] D.S. Steinberg, *Preventing Thermal Cycling and Vibration failures in Electronic Equipment,* 2001 Hoboken John Wiley & Sons.

[4] W. C. Fackler, Warren C. *Equivalence techniques for Vibration testing*, 1972 Shock and Vibration Information Center.

[5] N.I. Giannoccaro and A. Messina et al, Fatigue damage evaluation of notched specimens through resonance and anti-resonance data, *Engineering Failure Analysis* **12**(2006), 340-352.

[6] B. Al-Najjar, Accuracy, effectiveness and improvement of vibration-base maintenance in paper mills: case studies, *Journal of Sound and vibration* **229**(2) (2000) 389-410.

[7] K.P. Maynard, M.W. Trethewey et al, Application of torsional vibration measurements to shaft prevention technology, *Proceedings of the 55th meeting of the society for machinery failure prevention technology*, Virginia Beach, VA, April 2-5 (2000), 217-226.

[8] M. Threthewey, J. Friell et al, A spectral simulation approach to evaluate probabilistic measurement precision of a reactor coolant pump torsional vibration shaft crack monitoring system, *Journal of Sound and Vibration* **310** (2008), 1036-1056.

[9] R.J. Wang, D.G. Shang, et al, Fatigue damage model based on the natural frequency changes for spot welded joints, *International Journal of Fatigue* **30** (2008), 1047-1055.

[10] S. Jawaid and P. Rogers, Accelerated reliability test results: Importance of input vibration spectrum and mechanical response of test article, *Proceedings of the Annual Reliability and Maintainability Symposium*, Piscataway, NJ: IEEE. (2000), 248–53

[11] R.M. French, R. Handy and H.L. Cooper, Comparison of simultaneous and sequential single axis durability testing, *Experimental techniques*, **30** (2006) 32-37.

[12] W.E. Whiteman, Inadequacies in uniaxial stress screen vibration testing, *Journal of the IEST*. **44** (2001), 20-23.

[13] H. Himelblau and M.J. Hine, Effects of triaxial and uniaxial random excitation on the vibration response and fatigue damage of typical spacecraft hardware, *Proceedings of the 66th Shock and Vibration Symposium*, Arlington, VA, 1995.

[14] D. Gregory, F. Bitsy and D.O. Smallwood, Comparison of the response of a simple structure to single axis and multiple axis random vibration inputs, *Proceedings of the 79th Shock and Vibration Symposium*, Orlando, FA (2008).

[15] L. Lutes and S. Sarkani, *Random Vibration: Analysis of Structural and Mechanical Systems*, 2004 Elsevier.

Chapter 4 Life Estimation Model of a Cantilevered Beam Subjected to Complex Random Vibration

In the previous chapter a detailed experimental investigation directly compares RS and ED vibration. It was determined that defining the stress state by using only the starting natural frequency was inadequate. A characterization of the rate of frequency change as a function of input vibration profile was necessary. This chapter will develop a model which accounts for the rate of frequency change and uses a frequency domain method to compute the time to failure.

4.1 Introduction

Random vibration testing is common in test labs for assessing high-cycle fatigue durability of structures. Often the relative severity of two different random vibration environments must be assessed. Examples of the need for comparison include comparison of field data to lab data, comparison of two specified vibration environments for equivalence and accelerated testing. One common method for examining equivalence is to look at the fatigue damage accumulation rate for each environment. Numerous articles have been published regarding fatigue models that can be applied to vibration environments [1,2,3]. Many approaches use the power spectral density (PSD) and the G_{rms}, combined with the natural frequency of vibration and S-N curves, to estimate the life of the item [2,4]. Some techniques use equivalent damage models, which were summarized in Ref. 2.

It is widely known that when an item undergoes vibration, a fatigue crack may eventually develop and the natural frequency and mode shapes of the system will change, when the crack becomes appreciably large, compared to the size of the

specimen. This change in natural frequency has been investigated by numerous authors [5-7]. In addition, extensive health assessment work has been done by using the change in natural frequency as an indicator for detecting developing cracks, prior to catastrophic failure [8-10]. In order to make a meaningful life prediction under random vibration, the change in natural frequency must be accounted for.

This paper will present a new analytic method in the frequency domain, which directly takes into account the change in natural frequency and gives reasonably accurate prediction of the time to failure. Strain energy will be used to develop stress equations. The theoretical development, experimental data and finite element analysis (FEA) are presented in this paper.

4.2 Theoretical Development

The fundamental methodology in this paper is general, but the specific implementation details are developed and demonstrated in the context of a uniform cantilevered beam. Other geometries and configurations would follow by analogy. For the cantilevered beam shown in Fig. 1, $w(t)$ is the input displacement of the base, $y(x,t)$ is the relative displacement along the length of the beam (relative to the base) and x is measured from the base to the tip where $x=0$ at the base.

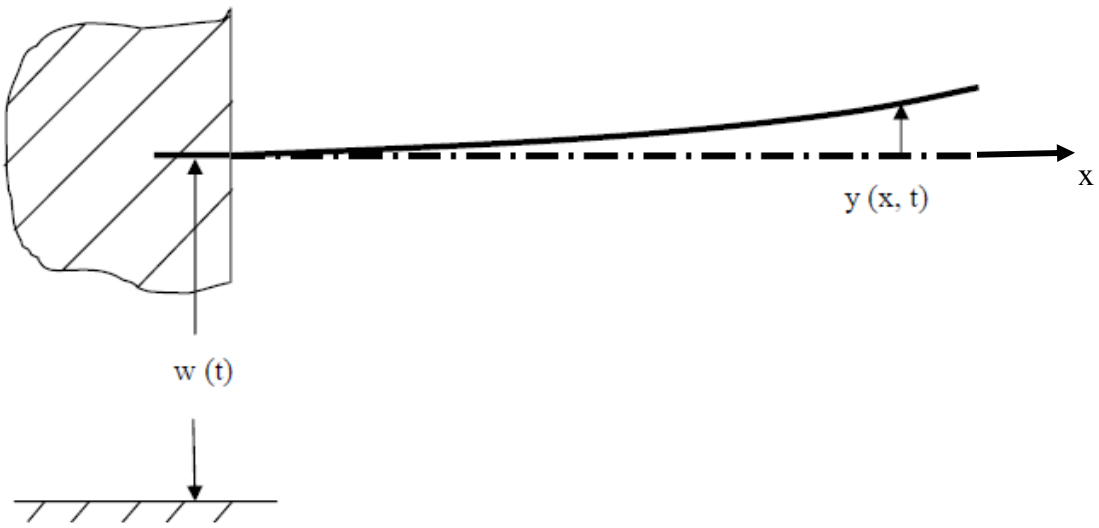

Fig. 1. Cantilever beam [11]

Fatigue crack growth under constant amplitude, completely reversed loading (with zero mean stress) can be modeled using Paris' Law as [12]

$$\frac{da}{dN} = C(\Delta K_I)^m \quad \text{[in/cycle]} \tag{1}$$

where da/dN is the rate of crack growth per cycle, C and m are material constants and ΔK_I is the stress intensity factor for mode I crack growth (K will be used in place of K_I for simplicity). The stress intensity factor can be calculated using

$$\Delta K = \Delta\sigma_r(\pi a)^{1/2} Y \quad \text{[kpsi*in^.5]} \tag{2}$$

where $\Delta\sigma_r$ is the far-field nominal stress range, a is the crack depth and Y is a geometric factor to account for size effects. The geometric factor for simple geometries can be found in handbooks or by FEA [12]. Note that $\Delta\sigma_r$ is the stress range that would have existed at the crack location, but for the initial uncracked beam. Under constant amplitude loading conditions this would stay constant. During vibration the natural frequency and mode shapes and response of the structure will change as the fatigue crack progresses through the material. This change in the response spectrum needs to be

considered as many random vibration inputs have significant peaks and valleys within the range of frequencies of interest. The maximum stress at any cross-section in a beam can be calculated by,

$$\sigma = \frac{Mc}{I} \tag{3}$$

where M is the bending moment at the cross section of interest (at the base $x=0$ of the cantilever beam, in this example), c is the half height of the rectangular cross-section and I is the moment of inertia of the cross-section about the neutral axis. The bending moment can be determined from

$$M(x) = EI(x)\frac{d^2y}{dx^2} \tag{4}$$

Neglecting the higher modes, the deflection of a uniform cantilevered beam can be written in terms of the first mode as [13]

$$y(x) = \frac{Y_t}{A}\frac{\Gamma_1}{\sqrt{\rho L}}\left[\cosh(\beta_1 x) - \cos(\beta_1 x) - \frac{\cos(\beta_1 L) + \cosh(\beta_1 L)}{\sin(\beta_1 L) + \cosh(\beta_1 L)}\left(\sinh(\beta_1 x) - \sin(\beta_1 x)\right)\right] \tag{5}$$

where Y_t is the tip deflection, Γ_1 is the modal participation of the first mode, ρ is the mass density per unit length of the beam, A is a constant to allow $y(x)$ to be expressed in terms of tip displacement, and β_1 for the first mode is represented as

$$\beta_1^4 = \frac{\omega_1^2 \rho}{EI} \tag{6}$$

The 1st eigenvalue for a uniform cantilevered beam is

$$\beta_1 L = 1.8751 \tag{7}$$

The corresponding modal participation factor for the first mode is

$$\Gamma_1 = .7830\sqrt{\rho L} \tag{8}$$

Evaluating the ratio in Eq. 5 for the 1st mode (and dropping subscript 1 for convenience), the following simplification can be made,

$$y(x) = \frac{Y_t}{A}\frac{\Gamma_n}{\sqrt{\rho L}}\left[\cosh(\beta x) - \cos(\beta x) - .73410\left(\sinh(\beta x) - \sin(\beta x)\right)\right] \tag{9}$$

Differentiating Equation 9 twice yields,

$$\frac{d^2 y(x)}{dx^2} = \frac{Y_t}{A}\frac{\Gamma_n}{\sqrt{\rho L}}\beta^2\left[\cos(\beta x) + \cosh(\beta x) - .73410\left(\sinh(\beta x) + \sin(\beta x)\right)\right] \tag{10}$$

where A is defined as,

$$A(L) = \frac{\Gamma_n}{\sqrt{\rho L}}\left[\cosh(\beta L) - \cos(\beta L) - .7341\left(\sinh(\beta L) - \sin(\beta L)\right)\right] = 1.566 \tag{11}$$

Combining Eq. 4, 10 and 11 and evaluating at the base (x=0)

$$M(0) = EIY_t\beta^2 \tag{12}$$

It remains to compute the tip deflection, Y_t. Note that the tip deflection must be for a cantilevered beam, without a crack. The frequency, however, shifts with crack growth and therefore an equivalent uncracked tip displacement is needed. This will be accomplished through use of the strain energy. The strain energy in a uniform uncracked cantilevered beam can be estimated by

$$U = \int_0^L \frac{M(x)^2}{2EI}dx \tag{13}$$

Evaluation of the integral using the above equations and simplifying yields,

$$U = \frac{EI\beta^4}{2A^2}\left(\frac{\Gamma}{\sqrt{\rho L}}\right)^2 Y_t^2 L \tag{14}$$

For a uniform cantilevered beam, noting that the 1st natural frequency is defined as,

$$\omega_n = \beta^2 \sqrt{\frac{EI}{\rho}} \tag{15}$$

solving for *EI*,

$$EI = \left(\frac{\omega_n}{\beta^2} \right)^2 \rho \tag{16}$$

Combining Eq. 14 and 16 yields,

$$U = \frac{1}{2} \frac{\rho L}{A^2} \left(\frac{\Gamma}{\sqrt{\rho L}} \right)^2 {\omega_n}^2 Y_t^2 \tag{17}$$

The energy for the first mode of vibration of this beam can be equated to the energy of an equivalent single degree of freedom (SDOF) lumped-parameter system, where the equivalent lumped mass for this mode shape can be defined as

$$m_e = \frac{\rho L}{A^2} \left(\frac{\Gamma}{\sqrt{\rho L}} \right)^2 = \frac{1}{4} \left(mass\ of\ beam \right) \tag{18}$$

Assuming that the equivalent mass is the same for a cracked beam (i.e. the change in equivalent mass due to change in mode shape is not significant, as the crack grows), the energy in the cracked beam can be represented as

$$U_c = \frac{1}{2} m_e {\omega_{nc}}^2 {Y_{tc}}^2 \tag{19}$$

where the subscript *c* represents the cracked condition. Combining Eq. 17, 18 and 19 and substituting *f* [hz] for ω [rad/s] results in

$$Y_t = \frac{f_{nc} Y_{tc}}{f_n} \tag{20}$$

Substitution into Eq. 12 yields

$$M(0) = EI\frac{f_{nc}Y_{tc}}{f_n}\beta^2 \tag{21}$$

from which the tensile stress can be written as

$$\sigma = E\frac{f_{nc}Y_{tc}}{f_n}\beta^2 c \tag{22}$$

and an equivalent tip load,

$$F = EI\frac{f_{nc}Y_{tc}}{f_n}\frac{\beta^2}{L} \tag{23}$$

where f_{nc} is the cracked natural frequency and f_n is the natural frequency of an uncracked, uniform, cantilevered beam. The equivalent SDOF relative displacement of the cracked beam (Y_{tc}) can be computed using the vibration response spectrum [14]

$$y_{rms}(f) = \sqrt{\int_0^\infty \ddot{w}_{PSD}(f)\left[\frac{1}{(2\pi)^4\left(\left({f_{nc}}^2 - f^2\right)^2 + (2\xi_n f\, f_{nc})^2\right)}\right]df} \tag{24}$$

where f ranges over the frequency of input, and f_n is the input natural frequency in Hz, and $\ddot{w}_{PSD}$ is the base excitation power spectral density (PSD). It follows that the root mean square stress range is.

$$\Delta\sigma_{rms} = E\frac{f_{nc}y_{rms}}{f_n}\beta^2 c \tag{25}$$

Many authors have claimed that Paris' law can be applied to random vibration through the use of an equivalent K [2,3]. For random vibration the equivalent K is generally modeled as C_1K_{rms} where C_1 is an equivalent damage constant. There, however, is not

general agreement in the literature upon specific values of C_1. Rewriting Paris' law with C_1 replaced by C_{ray} yields

$$\frac{da}{dN} = C(C_{ray}\Delta\sigma_{rms}(\pi a)^{1/2}Y)^m \tag{26}$$

The constant C_{ray} represents a correction factor for the statistical distribution of the random vibration response. Steinberg uses a similar approach for crack initiation called the 3 band technique [2]. Determination of C_{ray} will be done using statistical methods that will be discussed in detail later.

During failure the natural frequency and the mode shape will change as the crack grows. The frequency shift is quantified by calculating the rate of natural frequency change (RFC) in accordance with the following,

$$RFC_i = \frac{fn_i - fn_{i-1}}{t_i - t_{i-1}} \text{ [Hz/min]} \tag{27}$$

Eq. 27 allows examination of the RFC at a given natural frequency. The RFC can be combined with the frequency spacing to yield the total time to failure as,

$$TTF = \int_{f_{nc\_fail}}^{f_{nc\_start}} \frac{1}{RFC} df_{nc} \text{ [min]} \tag{28}$$

where f_{nc_start} is the starting cracked natural frequency, f_{nc_fail} is the natural frequency at failure and TTF is total time to failure. Often times this equation is used in discrete form as presented in Appendix A. It is therefore desirable to have Eq. 26 written in terms of the RFC. Realizing that the natural frequency is linearly related to the crack depth over a narrow frequency range [15], and assuming that the response of the item is dominated by its fundamental mode,

$$dN = f_n\delta_T \tag{29}$$

and

$$da = \delta\Delta f_n \frac{a_f}{\Delta f_T} \tag{30}$$

where δ_t is the incremental time, $\delta\Delta f_n$ is the incremental change in natural frequency, a_f is the final crack depth Δf_T is the total change in natural frequency and f_n is the instantaneous fundamental natural frequency. This linearity assumption is verified later, through computational modeling, in Section 4.7. Noting that

$$RFC = \frac{\delta\Delta f}{\delta_T} \tag{31}$$

and combining the above equations yields,

$$RFC = \frac{da}{dN}\frac{\Delta f_T f_{nc}}{a_f} \tag{32}$$

Using Equation 26, the RFC can be written as,

$$RFC(f_n) = \frac{\Delta f_T f_{nc}}{a_f} C(C_{ray}\Delta\sigma_{rms}(\pi a)^{1/2} Y)^m \tag{33}$$

4.3 Statistical Characterization of Response

In the proceeding section, determination of the RFC allowed calculation of the time to failure and degradation for a beam subjected to a random vibration input. The equivalent damage constant C_{ray} was not determined, but left to statistical means. The most common frequency domain method used for fatigue calculations is the Rayleigh fatigue approximation [16]. According to Lutes [16] the distribution of peaks in a narrow band random process has a Rayleigh distribution, with the rate of occurrence of peaks equal to the natural frequency. Using the Rayleigh fatigue approximation for frequency domain calculations approaches the rainflow analysis technique for time

domain analysis in the limit as the process becomes very narrow band [16]. Accuracy of this technique is dependent on the response characteristics of the system. By assuming a SDOF lumped parameter systems, much of the inaccuracy has been removed that can be present in bimodal systems [16]. For systems with a narrowband response, the accuracy of the approximation is a function of the bandwidth. Using WHITE-HIGH and beam 2 the rainflow analysis method and the Rayleigh fatigue approximation method were used to estimate the rate of occurrence of peaks and the mean amplitude of the response. It was determined that there was a maximum difference of 10% on both rate of occurrence of peaks and mean amplitude between the two methods. It was important to note that most of the deviation was present in low amplitude peaks, and would not be expected to effect the fatigue predictions. This comparison did not account for the ability of the rainflow method to account for any mean stress effects. For a complete discussion of the limitations in applying the Rayleigh approximation the reader is referred to Lutes [16].

The use of an equivalent damage constant C_{ray} allows the statistical nature of the stress to be accounted for in one step. This simplifies computation of Eq. 33 since the stress distribution does not need to be maintained throughout the calculation. The equivalent damage value (D_{ray}) can be determined from Eq. 33 as,

$$D_{ray} = (C_{ray}\Delta\sigma_{rms})^m \tag{34}$$

From Lutes [15] the damage of a narrowband process can be written as,

$$D_{ray} = \int_0^\infty x^m \frac{x}{\sigma^2} e^{\frac{-x^2}{2\sigma^2}} dx \tag{35}$$

where m is the Paris Law Exponent, x is the stress amplitude and σ is the shape parameter of a Rayleigh distribution. Note that for a stationary, narrow band, Gaussian

signal, the Rayleigh shape parameter is the same as the standard deviation of the Gaussian signal, therefore $\sigma = \Delta\sigma_{rms}$. Combining Eq. 34 and 35 and simplifying yields,

$$C_{ray} = \left[2^{m/2} \Gamma\left(1 + \frac{m}{2}\right) \right]^{\frac{1}{m}} \tag{36}$$

where $\Gamma(\cdot)$ is the gamma function [16]. As can be seen the equivalent damage constant is only a function of the Paris' law exponent. For this system where *m=3*,

$$C_{ray} = 1.555 \tag{37}$$

4.4 Model Limitations Due to Plastic Deformation

As the fatigue crack progresses through the cross-section of the beam, there will be plastic yielding ahead of the crack tip. After some initial growth there was large scale plastic yielding. LEFM and Paris' Law assumes that the plastic zone size is small at the tip of the crack. In order to ensure that the underlying assumptions of LEFM and Paris' Law are not violated, the plastic zone size must be estimated. According to Stephens [3] the limit of the plastic zone size where Paris' law still applies is

$$r_y' < \frac{t-a}{8} \tag{38}$$

where r_y' is the cyclic plastic zone radius, t is the thickness, and a is the crack length. The cyclic plastic zone size for plane strain can be approximated by,

$$r_y' = \frac{1}{24\pi}\left(\frac{\Delta K_I}{S_y}\right)^2 \tag{39}$$

where S_y is the yield strength. For plane stress,

$$r_y' = \frac{1}{8\pi}\left(\frac{\Delta K_I}{S_y}\right)^2 \tag{40}$$

As discussed later, this limit on the plastic zone size can be used to define a range of validity of the proposed model in terms of a max allowable crack size (and hence, a max allowable frequency shift) for the tested beams.

4.5 Experimental Data

In order to assess the validity of the above model, time to failure data was recorded for two beams subjected to stationary, Gaussian, random vibration inputs [7]. An outline of the data will be provided here. Details of the particular vibration environments will be discussed later. In order to compare the vibration environments, two test specimens were built from cold rolled 1018 steel [7]. The specimens are cantilever beams with specific notches cut into the side walls. The first test specimen had well separated modes and is depicted in Fig. 2. The first bending mode of Beam 1 in the vertical direction was 415 Hz. In the transverse direction the first bending mode was 3520 Hz.

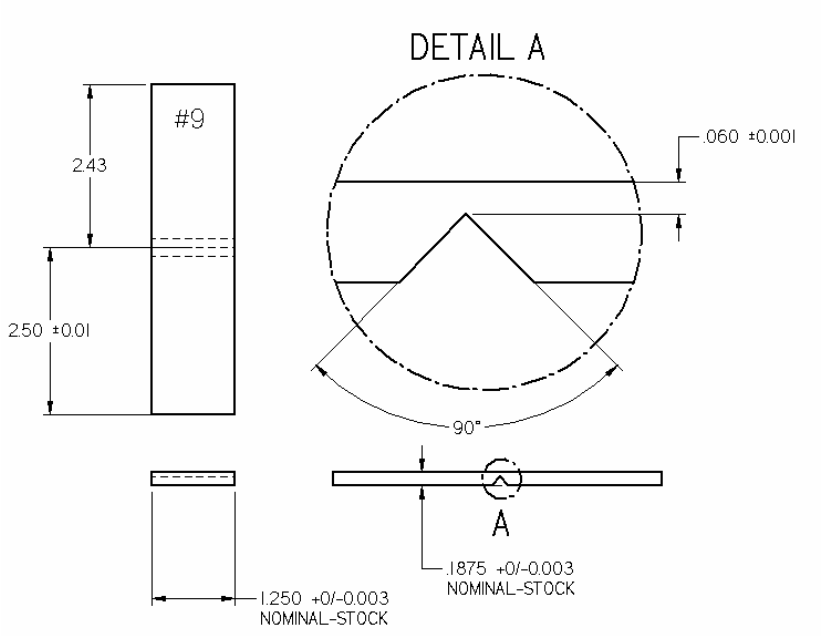

Fig. 2. Test Beam 1

The second test specimen, illustrated in Fig. 3, had first and second modes that were closely spaced, although the stress concentration was higher in the Z-direction. For Beam 2 the first bending mode in the vertical direction was 330 Hz. In the transverse direction the 1st bending mode was also 330 Hz.

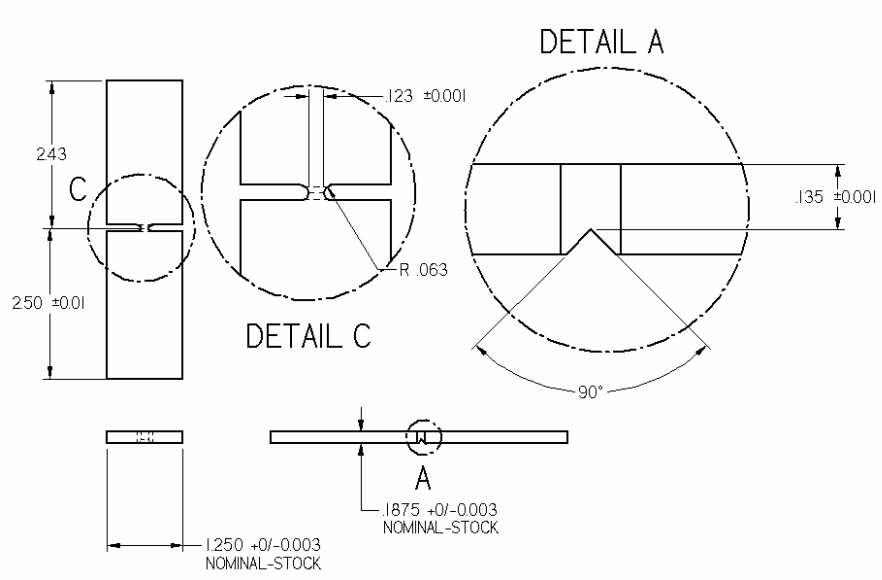

Fig. 3. Test Beam 2

The beam was mounted for vibration testing, as shown in Figure 4

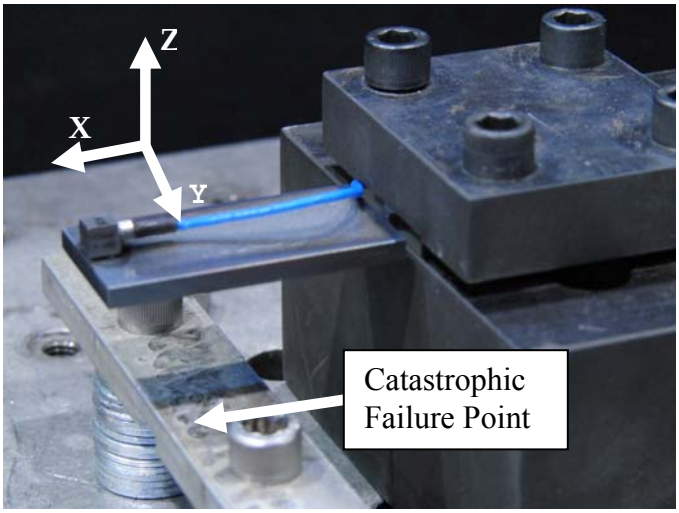

Fig. 4. Beam mounted on shaker

It should be noted that the test was conducted until 'catastrophic failure' of the beam. Catastrophic failure was defined to occur when the test specimen tip made contact with a limit-bar located approximately 1 inch below the tip of the beam, as shown in Figure 4. Details of the test data are presented elsewhere [7] and a brief assessment of the data is provided below. Selected samples of the vibration profiles are displayed in Fig. 5, with a full summary in Table 1. Several of the profiles had large peaks and valleys due to the simulation of the repetitive shock vibration system. These large peaks and valleys drastically alter the response as the natural frequency changes.

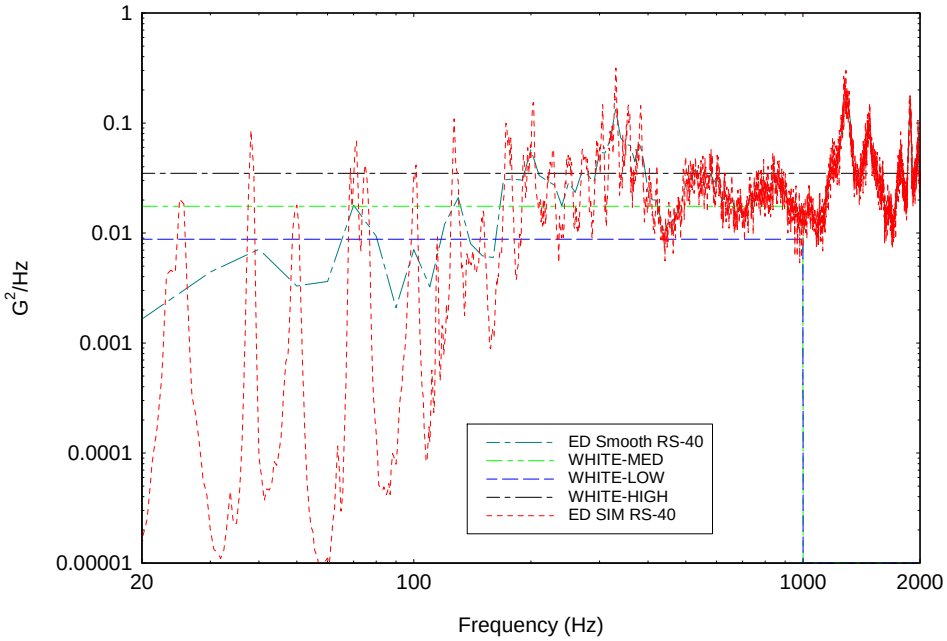

Fig. 5. RS-40 level vibration profiles

Profile Name	Profile Description
RS-40*	Z-axis of repetitive Shock System set to 40 Grms*
RS-60*	Z-axis of repetitive Shock System set to 60 Grms*
ED SIM RS-40	Single-axis ED simulation of RS-40 Z-axis
ED SIM RS-60	Single-axis ED simulation of RS-60 Z-axis
ED SMOOTH RS-40	Smoothed version of ED SIM RS-40
ED SMOOTH RS-60	Smoothed version of ED SIM RS-60
WHITE-HIGH	Match the Grms level of the RS-40 profile from 20-2000 Hz
WHITE-LOW	Single-axis ED -6db of WHITE-HIGH ran from 20-1000 Hz
WHITE-MED	Single-axis ED -3db of WHITE-HIGH ran from 20-1000 Hz

Table 1. Summary description of profiles

*These profiles were not used in this analysis as they are multi-axis profiles

4.6 Experimental Results

The constants used for each beam are as follows,

Cons	Value-Beam 1	Value- Beam 2	Units
C	2.70E-10	2.70E-10	
m	3	3	
S_y	30e3	30e3	psi
L	2.5	2.5	in
b	1.25	1.25	in
h	.1875	.1875	in
E	30E6	30E6	psi
Δf_T	330-37=293	415-40=375	hz
a_f	0.1875-0.022=.1655	.1875-.003=.1845	in
Notch Depth	.0525	.1275	in

Table 2. Constants used for calculation

During fatigue crack growth both plane strain and plane stress will be present along the crack front [12]. Using Eq. 40 for conservativeness, the maximum plastic zone size can be determined. Using the limit of Eq. 38, LEFM should apply at least through a 1 octave frequency shift. Note that the any plastic zone size effect on mode shape was not considered with this limitation.

The geometric factor Y (in Equation 2) is computed from this specimen geometry from Srawley [17] as,

$$Y = \frac{1.99 - \frac{a}{h}\left(1 - \frac{a}{h}\right)\left(2.15 - 3.93\frac{a}{h} + 2.7\left(\frac{a}{h}\right)^2\right)}{\left(1 + 2\frac{a}{h}\right)\left(1 - \frac{a}{h}\right)^{3/2}} \frac{1}{\pi^{1/2}} \tag{41}$$

The damping ratio ζ is computed from the amplification factor by

$$\zeta = \frac{1}{2Q} \tag{42}$$

where Q is computed using the half power points [18, 19] as

$$Q = \frac{f_n}{f_u - f_l} \tag{43}$$

with f_u and f_l being the upper and lower half power points respectively. In order to account for the notch that was machined into the test specimens, the notch depth plus the physical crack depth (Fig. 6) was considered to be the effective crack depth a in accordance with Ref. 20.

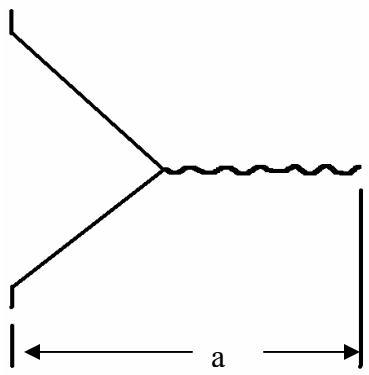

Fig. 6. Effective crack depth

Furthermore for Beam 2 the side notches required the use of a stress concentration factor to determine the far-field stress to be used for stress intensity factor estimation. Using FEA it was determined that the average stress concentration factor from notch root to notch root was 9.7. Using the preceding development, the predicted time for a one octave frequency shift is compared to the measured time for a one octave frequency shift (see Appendix A for more detailed flow chart of calculation method). This is being defined here as the time to failure (TTF).

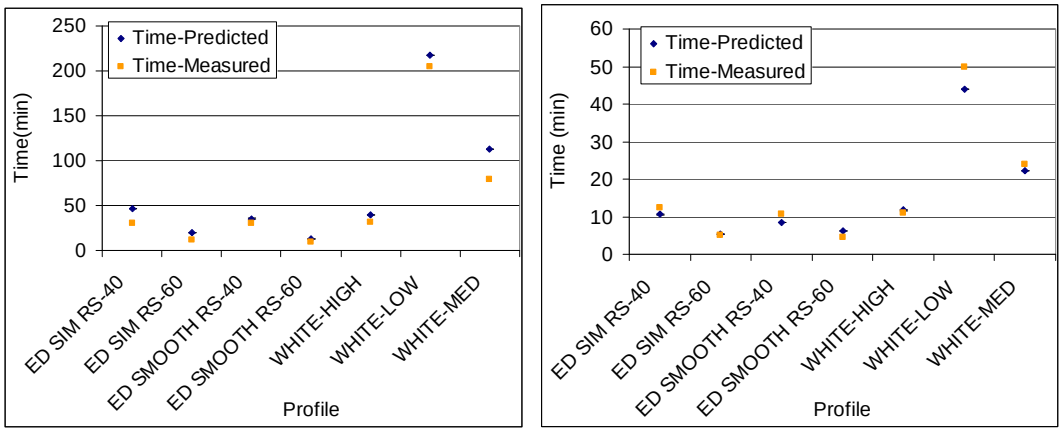

Beam 1 Beam 2

Fig. 7. Comparison of measured and predicted TTF for 1 octave shift

The results are found to be promising for both tested beams. This is particularly good, given the simplicity of the proposed model. The model was also applied to the entire frequency shift including the zone of excessive plasticity. No plastic zone correction was used, with reasonable results.

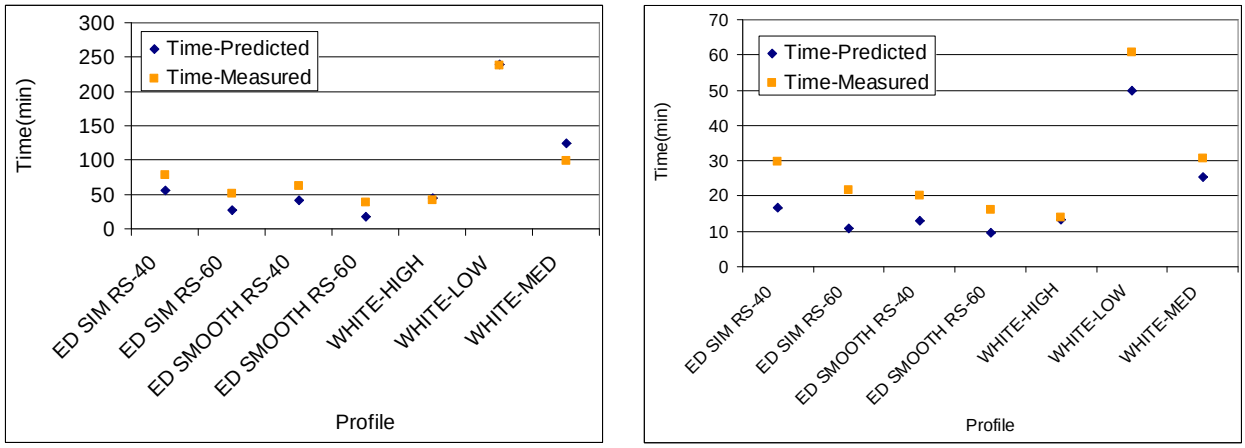

Beam 1 Beam 2

Fig. 8. Comparison of measured and predicted TTF for full frequency shift

Figure 9 shows the Predicted-RFC vs. the Measured-RFC for Beam 2. The prediction is found to be best in this case only between 165-330 Hz, below which, the model fidelity drops off, possibly due to excessive plastic deformation at the crack-tip. As expected,

once the frequency has shifted more than one octave, the prediction and measured RFC begin to diverge. As can be seen the ED-SIM profiles seem to be less susceptible to that divergence. Examination of Fig. 5 shows that the input energy for these two profiles is lower. It is believed that this causes it to be less susceptible to divergence when the plastic zone size is large.

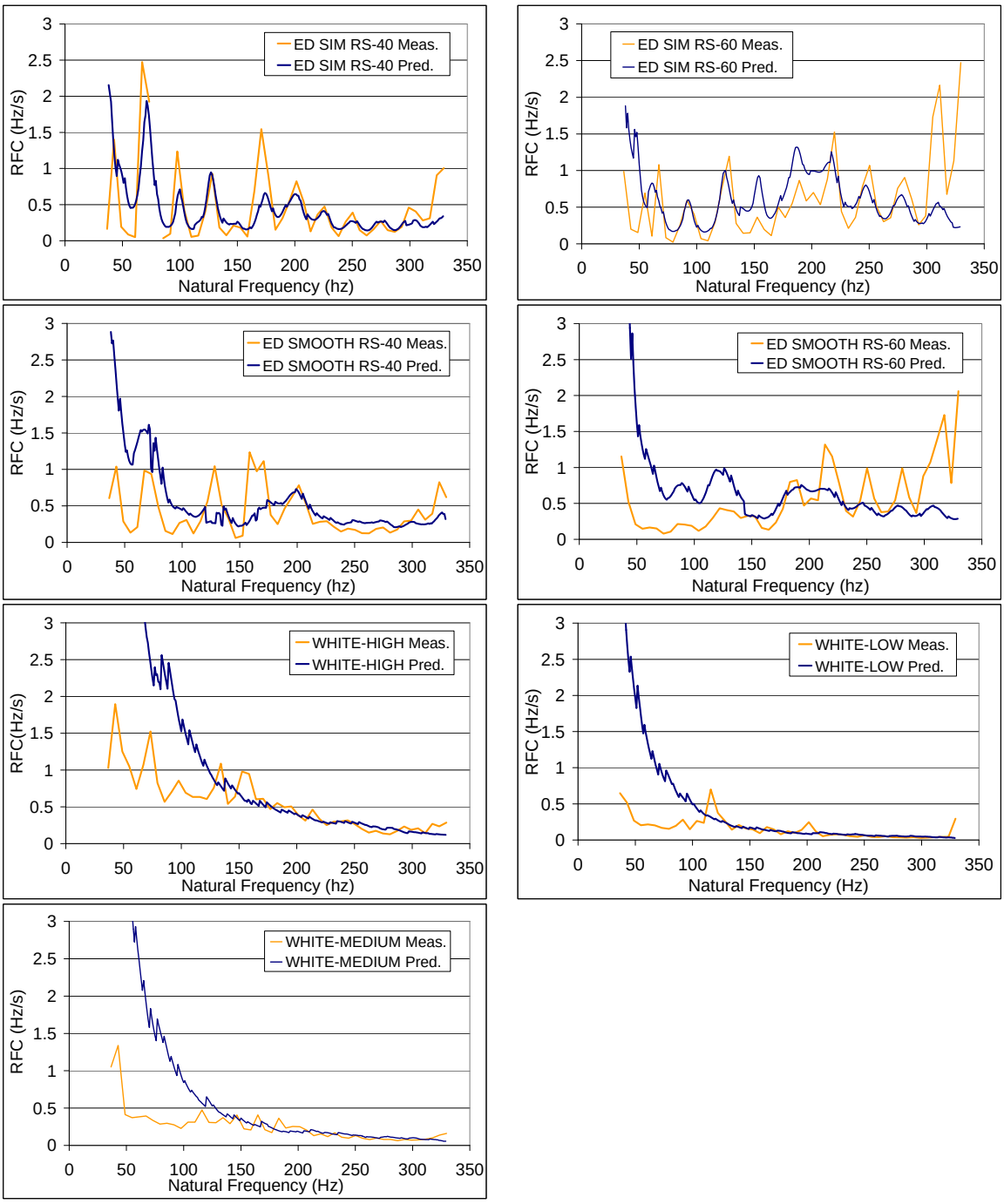

Fig. 9. Beam 2 RFC predicted vs. measured

4.7 FEA Comparison

Computation of the stress intensity factor and natural frequency was performed analytically and by FEA. (A complete discussion of the FEA results presented here is detailed in Ref. 21). A comparison between the two techniques was done using Beam 2 (most complex case). The beam was modeled including the clamping fixture as depicted in Fig. 10.

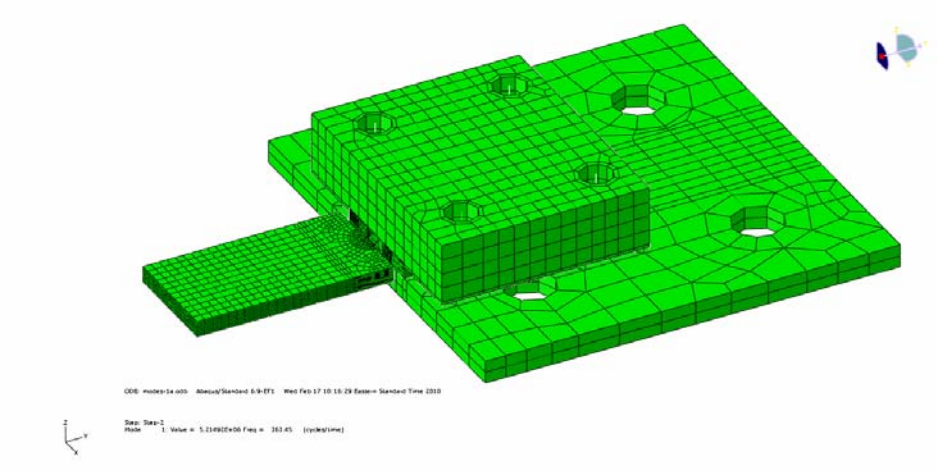

Fig. 10. FEA model

As discussed previously, the natural frequency was assumed to vary linearly as function of crack depth in the analytic model. To verify this assumption, a modal analysis was performed at varying crack depths and compared to the computed natural frequency. Although a slight bias is apparent, the FEA modal analysis showed a linear relationship between natural frequency and crack depth.

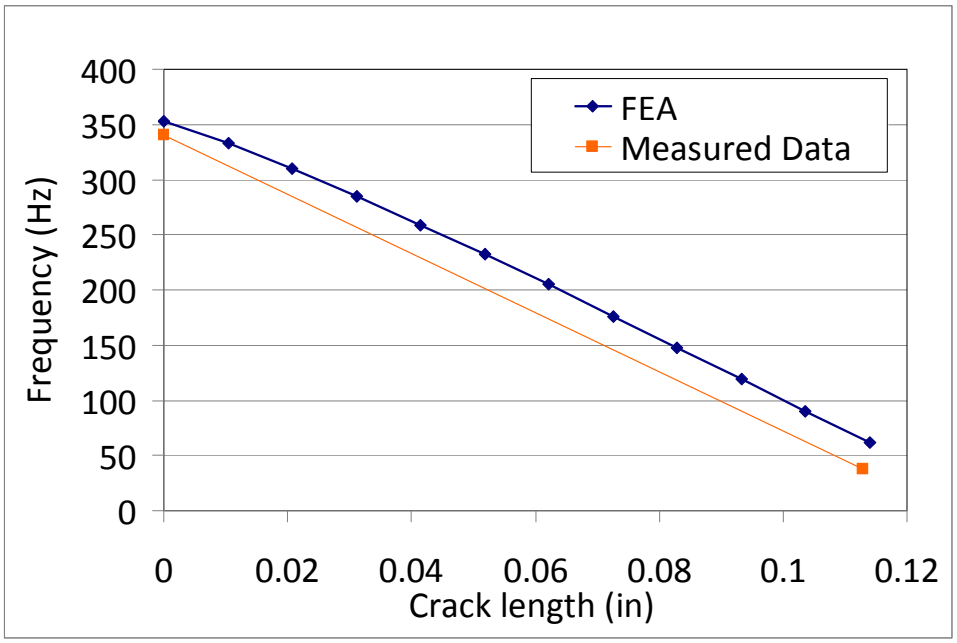

Fig. 11. Comparison of FEA modal analysis to analytic linear model

The mode shapes were also compared for the 0" crack depth case. The static deflection shape and the 1st mode are nearly identical. For this case, however, the mode shape is no longer that of a uniform cantilevered beam, but instead appears to behave like a hinged member as seen in Fig. 12.

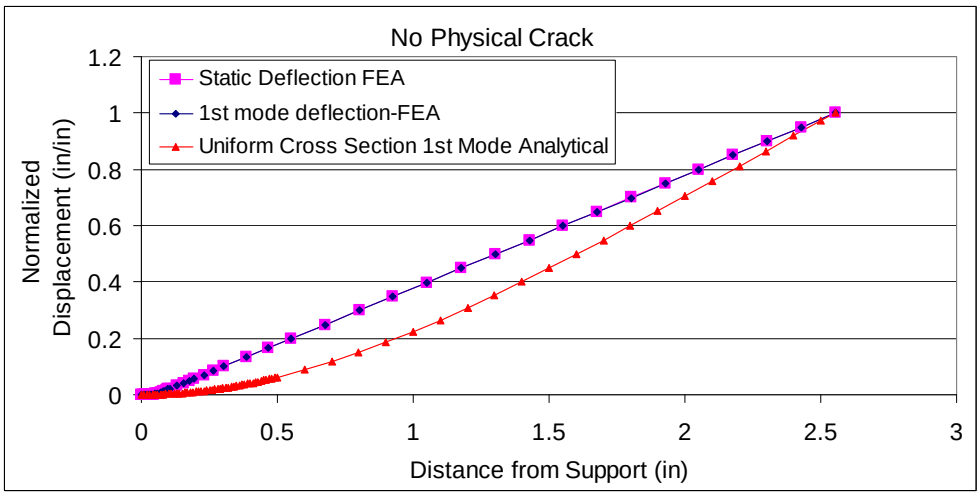

Fig. 12. Comparison of mode shapes

Furthermore the effect of crack growth on mode shape as predicted by FEA can be seen in Fig. 13

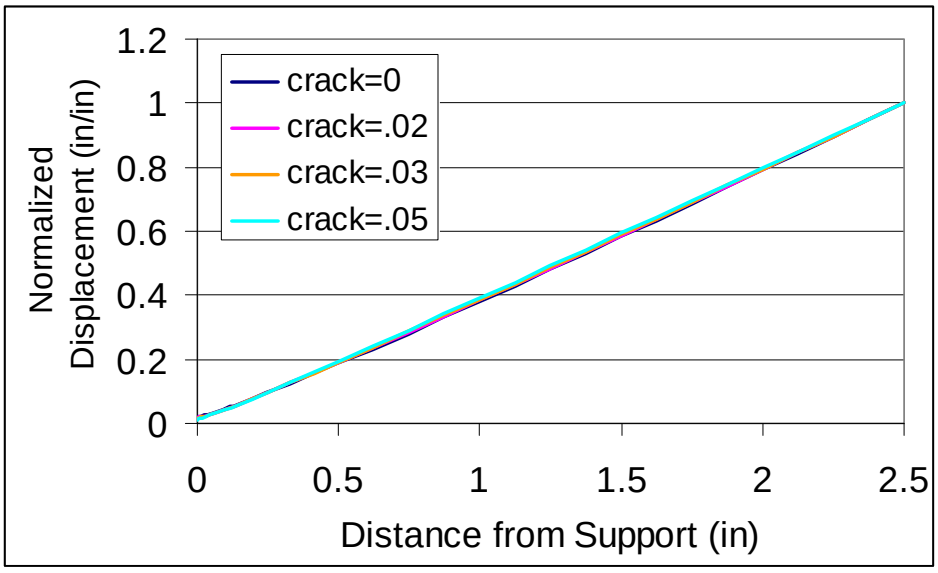

Fig. 13. Comparison of dynamic mode shapes from FEA

Very little change in mode shape was apparent in the range of interest. The RMS stress intensity was calculated by applying a static load at the tip of the beam that was equivalent to the RMS dynamic load. Good agreement was shown as illustrated in Fig. 14

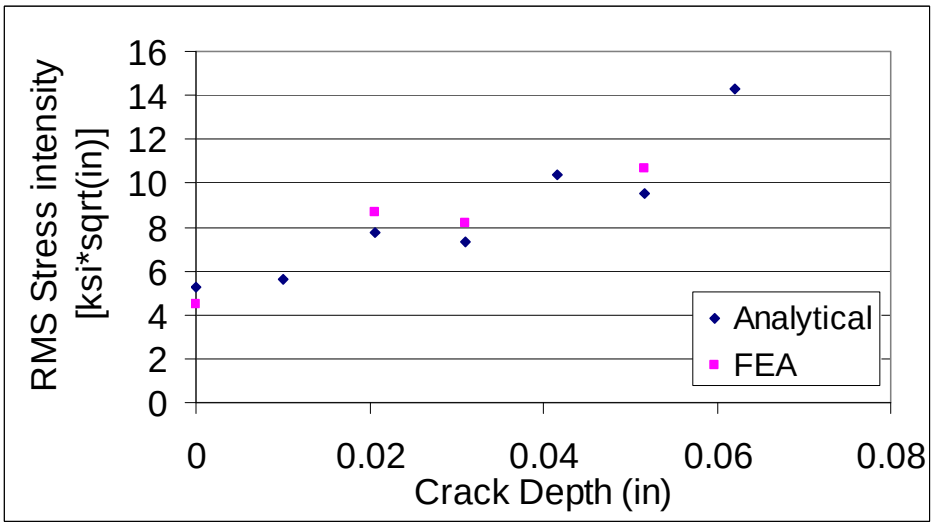

Fig. 14. Stress intensity comparison between analytical and FEA models

4.8 Conclusions

During vibration induced fatigue, the natural frequency shifts due to evolution of structural damage. This natural frequency shift changes the stress state of the structure. This is particularly significant when the input vibration PSD profile has large peaks and valleys as in repetitive shock vibration. Using linear elastic fracture mechanics and equivalent energy, an analytical model was developed which accounts for the natural frequency shifting. Assuming the response is narrowband Gaussian, the time to failure can be directly calculated from the frequency domain input (PSD), without knowledge of the specific time history. For the specific geometries considered in this study, the model was accurate for a frequency shift of about 1 octave. Beyond frequency shifts of 1 octave, excessive plasticity was present at the crack tip, which invalidates the assumptions of LEFM and introduces errors in the assumed mode shapes, leading to less accurate results. A good correlation was found between the experimental data and the model. Two different cantilevered beam geometries were compared with similar results. In addition Beam 2 was analyzed using static FEA. The equivalent static load of the RFC model was used to compute the stress intensity value. Good agreement was seen between the FEA and the analytical models. Furthermore the FEA analysis performed on the simple cantilevered beam demonstrated the ability to compute the stress intensity factors for complex geometries. This technique could be utilized when the geometric correction factor and the subsequent stress intensity cannot be obtained from handbooks as was done in presented model. This model has many applications in accelerated life testing. It can be used as a degradation model, accelerated life model and used to analyze the relative severities of complex vibration environments.

4.9 References

[1] W. C. Fackler, Warren C. *Equivalence techniques for Vibration testing*, 1972 Shock and Vibration Information Center.

[2] D.S. Steinberg, *Preventing Thermal Cycling and Vibration failures in Electronic Equipment,* 2001 Hoboken John Wiley & Sons.

[3] R.I. Stephens, A. Fatemi, R.R. Stephens and H.O. Fuchs, *Metal Fatigue in Engineering 2nd ed*, 2001 John Wiley and Sons.

[4] M. Aykan and M. Celik, Vibration fatigue analysis and multi-axial effect in testing of aerospace structures, *Mechanical Systems and Signal processing*, **23**(2009) 897-907.

[5] R.M. French, R. Handy and H.L. Cooper, Comparison of simultaneous and sequential single axis durability testing, *Experimental techniques*, **30** (2006) 32-37.

[6] W.E. Whiteman, Inadequacies in uniaxial stress screen vibration testing, *Journal of the IEST*, **44** (2001), 20-23.

[7] M. Paulus, Limitations of the power spectral density as an indicator of test severity, submitted to *Journal of Shock and Vibration,* (2010).

[8] B. Al-Najjar, Accuracy, effectiveness and improvement of vibration-base maintenance in paper mills: case studies, *Journal of Sound and vibration* **229**(2) (2000) 389-410.

[9] K.P. Maynard, M.W. Trethewey et al, Application of torsional vibration measurements to shaft prevention technology, *Proceedings of the 55th meeting of the society for machinery failure prevention technology*, Virginia Beach, VA, April 2-5 (2000), 217-226.

[10] M. Threthewey, J. Friell et al, A spectral simulation approach to evaluate probabilistic measurement precision of a reactor coolant pump torsional vibration shaft crack monitoring system, *Journal of Sound and Vibration* **310** (2008), 1036-1056.

[11] T. Irvine, Steady-state vibration response of a cantilever beam subjected to base excitation, www.vibrationdata.com. 2010.

[12] D. Broek, *Elementary engineering fracture mechanics, 4th ed*., 1986 Kluwer Academic Publishers.

[13] L. Meirovitch, *Fundamentals of Vibrations*, 2001 McGraw Hill.

[14] T. Irvine, Optimal use of the vibration response spectrum for enveloping random data, Proceedings *of the Institute of Environmental Sciences and technology*, (1999).

[15] E. Douka and L.J. Hadjileontiadis, Time-frequency analysis of the free vibration response of a beam with a breathing crack, *NDT&E International*, **38** (2005) 3-10.

[16] L. Lutes and S. Sarkani, *Random Vibration: Analysis of Structural and Mechanical Systems*, 2004 Elsevier.

[17] J.E. Srawley, Wide range of stress intensity factor expressions for ASTM #-399 standard fracture toughness specimens, *International Journal of Fracture*, **12** (1976).

[18] B. Balachandran, E.B. Magrab, *Vibrations 2nd ed.,* 2009 Cencage Learning.

[19] J. He and Z.F. Fu, *Modal Analysis*, 2001 Butterworth-Heinemann.

[20] J. Collins, *Failure of Materials in Mechanical Design 2nd ed*., 1993 John Wiley and Sons.

[21] E. Habtour, M. Paulus, A. Dasgupta, Finite element modeling of time to failure using stress intensity, *to be submitted* 2010.

Chapter 5 Rate of Frequency Change Model Uncertainty Analysis

In the previous chapter a frequency domain model was developed to predict the time to failure of a cantilevered beam subject to random vibration. This model was found to agree well with experimental measurements and with FEA results. In this chapter the model sensitivity to uncertainties of the input parameters will be evaluated. Specific error contributions in the measured data will be examined. In addition different damping models will be examined.

5.1 Introduction

Fatigue induced vibration in structural members is a common cause of vibration failures. During vibration induced failures, the natural frequency of the structural member will shift as the crack grows through the material [1-3]. The change in natural frequency leads to a change in the stress state. This is particularly prevalent when the input vibration is random, where the power spectral density (PSD) has large peaks and valleys. Analysis of the instantaneous stress state requires knowledge of the instantaneous response of the cracked member, in view of the changing natural frequency. In Ref. 1, a methodology was developed whereby the natural frequency was used to characterize the stress state in a cantilever beam under random vibration excitation. The methodology allowed characterization of the stress state in the frequency domain without knowledge of the specific time history. This is of particular value as random vibration environments are often reported in the frequency domain. There were many simplifying assumptions that were made during the development of the rate of natural frequency change (RFC) model [1]. One limitation to the new model is the need

for an accurate damping factor, which may require extensive experimental work. This paper will assess the relative importance of the input parameters and assess the accuracy of several damping models.

5.2 Background

A brief summary of the RFC model and data will be presented here in the context of a cantilever beam subjected to random excitation. For a full description see Refs. 1 and 2. The time to failure of the cantilevered beam can be expressed as

$$TTF = \int_{f_{nc\_fail}}^{f_{nc\_start}} \frac{1}{RFC} df_{nc} \text{ [min]} \tag{1}$$

where f_{nc_start} is the starting cracked natural frequency, f_{nc_fail} is the natural frequency at failure and TTF is total time to failure. The RFC can be calculated for each frequency as,

$$RFC(f_{nc}) = \frac{\Delta f_T f_{nc}}{a_f} C(C_{ray} \Delta\sigma_{rms} (\pi a)^{1/2} Y)^m \tag{2}$$

where f_{nc} is the cracked natural frequency in Hz, Δf_T is the total change in natural frequency, a_f is the corresponding final crack depth, C and m are constants of the Paris' Law, C_{ray} is a damage equivalent constant, a is the crack depth, Y is the geometric correction factor and $\Delta\sigma_{rms}$ is root mean square stress amplitude. The stress amplitude is calculated by

$$\Delta\sigma_{rms} = E \frac{f_{nc} y_{rms}}{f_n} \beta^2 c \tag{3}$$

where E is the modulus of elasticity, y_{rms} is the relative displacement in a SDOF representation of the cracked beam, f_n is the uncracked natural frequency $\beta L = 1.8751$ is a

system constant and c is the distance from the neutral axis to the edge of the beam. Furthermore, the uncracked natural frequency is defined as,

$$f_n = \frac{1}{2\pi}\beta^2\sqrt{\frac{Ewh^3/12}{mass/L}} \tag{4}$$

where $I=wh^3/12$ is the moment of inertia, *mass* is the mass of the beam, L is the length of the beam, w is the width of the beam and h is the height of the beam. The SDOF relative displacement can be calculated as,

$$y_{rms}(f) = \sqrt{\int_0^\infty \ddot{w}_{PSD}(f)\left[\frac{1}{(2\pi)^4\left(\left(f_{nc}{}^2 - f^2\right)^2 + (2\xi_n f\, f_{nc})^2\right)}\right]df} \tag{5}$$

where f ranges over the frequency of input, $\ddot{w}_{PSD}$ is the base excitation power spectral density (PSD) and ξ is the damping ratio computed using the half power points [4].

Time to failure data was taken for 2 cantilever beams subjected to stationary random vibration inputs [2]. An outline of the data will be provided here. The details of the vibration environments will be discussed later. In order to compare the vibration environments, two test specimens were built from cold rolled 1018 steel [2]. The specimens are cantilever beams with specific notches cut into the side walls. The first test specimen had well separated modes and is depicted in Fig. 1. The first bending mode of Beam 1 in the vertical direction was 415 Hz. In the transverse direction the first bending mode was 3520 Hz.

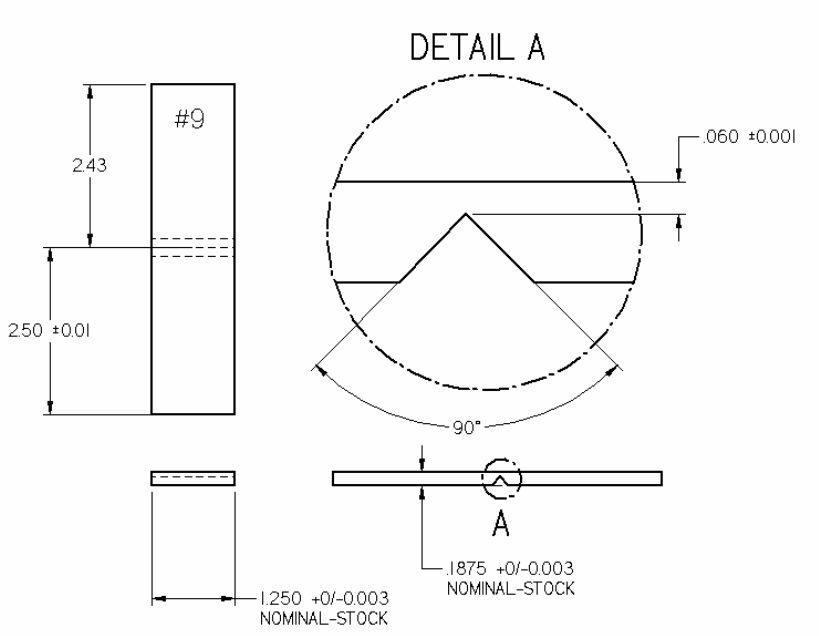

Fig. 1. Test Beam 1.

The second test specimen, illustrated in Fig. 2, had first and second modes that were closely spaced, although the stress concentration was higher in the Z-direction. For Beam 2 the first bending mode in the vertical direction was 330 Hz. In the transverse direction the 1st bending mode was also 330 Hz.

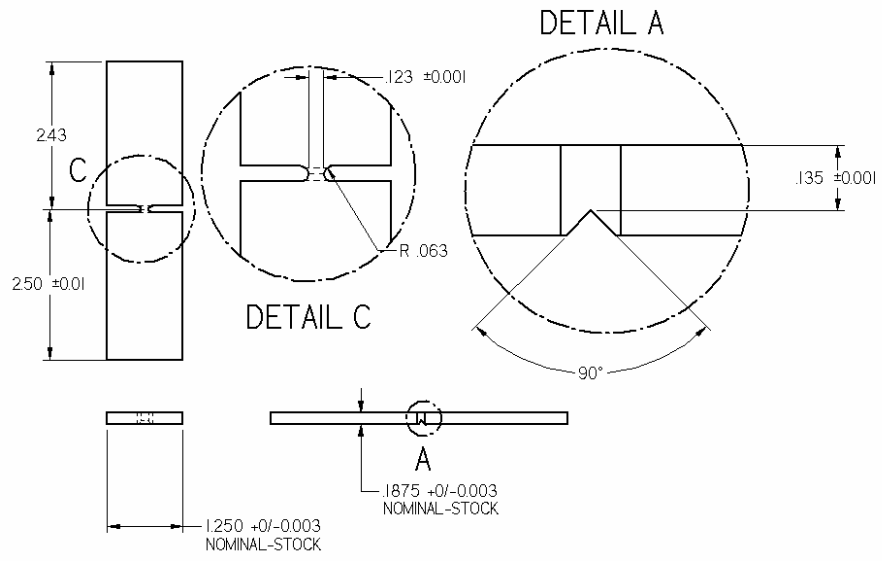

Fig. 2. Test Beam 2

The beam was mounted for vibration testing, as shown in Figure 3

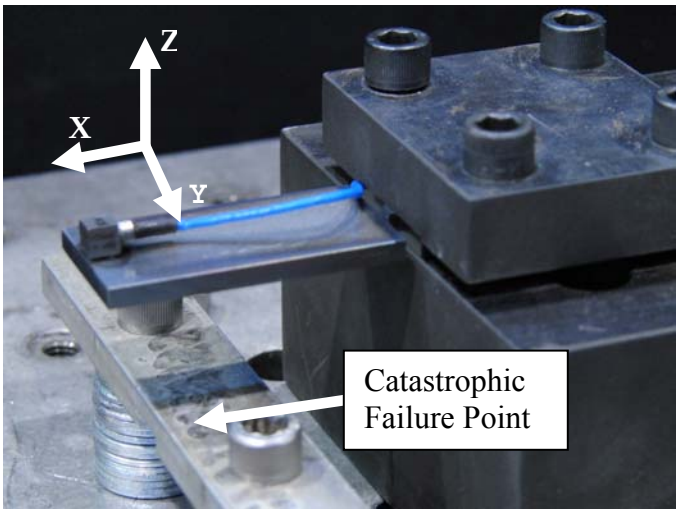

Fig. 3. Beam mounted on shaker

It should be noted that the test was conducted until 'catastrophic failure' of the beam. Catastrophic failure was defined to occur when the test specimen tip made contact with a limit-bar located approximately 1 inch below the tip of the beam, as shown in Figure 4. Details of the test data are presented elsewhere [2] and a brief assessment of the data is provided below. Selected samples of the vibration profiles are displayed in Fig. 4, with a full summary in Table 1. Several of the profiles had large peaks and valleys due to the simulation of the repetitive shock vibration system. These large peaks and valleys drastically alter the response as the natural frequency changes.

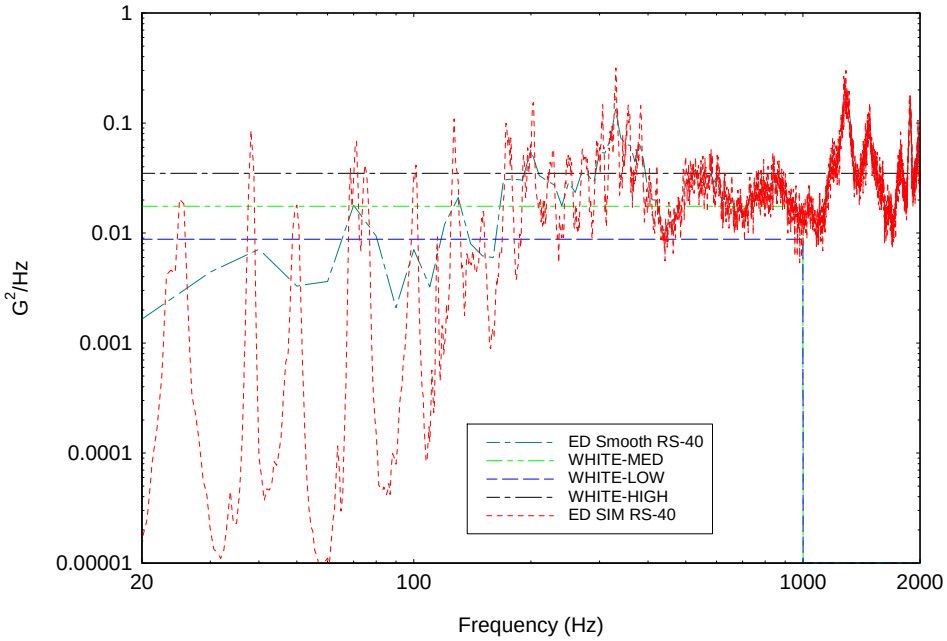

Fig. 4. Example vibration profiles

Profile Name	Profile Description
RS-40*	Z-axis of repetitive Shock System set to 40 Grms*
RS-60*	Z-axis of repetitive Shock System set to 60 Grms*
ED SIM RS-40	Single-axis ED simulation of RS-40 Z-axis
ED SIM RS-60	Single-axis ED simulation of RS-60 Z-axis
ED SMOOTH RS-40	Smoothed version of ED SIM RS-40
ED SMOOTH RS-60	Smoothed version of ED SIM RS-60
WHITE-HIGH	Match the Grms level of the RS-40 profile from 20-2000 Hz
WHITE-LOW	Single-axis ED -6db of WHITE-HIGH ran from 20-1000 Hz
WHITE-MED	Single-axis ED -3db of WHITE-HIGH ran from 20-1000 Hz

Table 1. Summary description of profiles

*These profiles were not used in this analysis as they are multi-axis profiles

5.3 Sensitivity to Parameters

The first comparison performed was the sensitivity of the model to changes in input parameters. Each parameter was varied as described in Table 2 while the remaining parameters were held constant.

Parameter	Lower value	Upper Value
WHITE-LOW PSD [G^2/Hz]	0.00726	0.00803
WHITE_MEDIUM PSD [G^2/Hz]	.0144	.0159
WHITE_HIGH PSD [G^2/Hz]	.0327	.0362
Damping Factor	$.9\xi^{*}$	$1.1\xi^{*}$
Length of Beam [in]	2.49	2.51
Modulus of Elasticity [psi]	29000000	30000000
Width of Beam [in]	1.246	1.254
Height of Beam [in]	0.1845	0.1905
Mass of Beam [slugs]	0.004980745	0.005081366
Final Crack Length [in]	0.103	0.123
Initial Crack Length [in]	0.0515	0.0535
C [Paris Law Constant]	3.60E-10	1.80E-10
M [Paris Law Exponent]	2.85	3.15
Stress Concentration []	9.215	10.185

Table 2. Monte Carlo input parameters

* The equivalent viscous damping factor ξ is a measured value and varies as a function of frequency

The resulting variations in the time to failure values for Beam 2 are illustrated in Fig. 5.

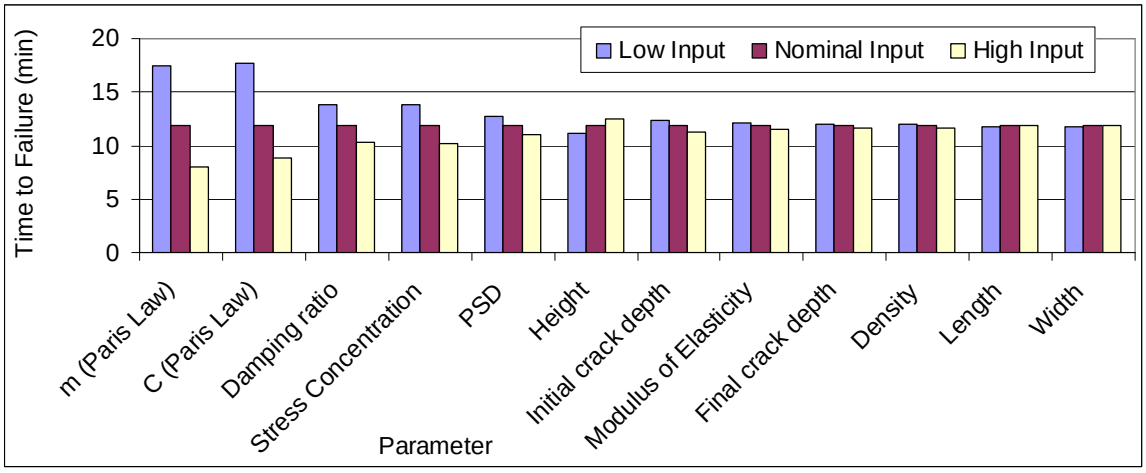

Fig. 5. Effect on time to failure with of parameter uncertainty

As can be seen the Paris' Law exponent *m* and constant *C* have the largest effect. The damping ratio is also a significant contributor. This analysis, however, does not take into account the variation of the damping factor with frequency. This variation with frequency will be discussed in detail in Section 5.4. If simplifying models are used for

the damping factor the time to failure would be more significantly effected than depicted by Fig. 5.

To further understand the model uncertainties, a Monte Carlo simulation was carried out with 1000 combinations of input values [5]. This furthered the understanding of the specific effect of each parameter on the predicted time to failure. The ranges of the input parameters were based on the measured data [2] defined in Table 2. The input parameters were assumed to have uniform distributions of uncertainty within these limits.

Due to approximations introduced by plastic deformations at the crack tip, the modeling results are limited to a 1 octave frequency shift. For Beam 2 the starting natural frequency was 330 Hz, and the ending natural frequency was 165 Hz. The time to failure data was analyzed using maximum likelihood estimate (MLE) with Kaplan-Meier ranking method, and the results were expressed with lognormal distributions. The PDFs of the measured TTF are compared to the Monte Carlo simulations in Figure 6. The failure data PDF was computed using 5 samples for each input level profile for a total of 15 samples.

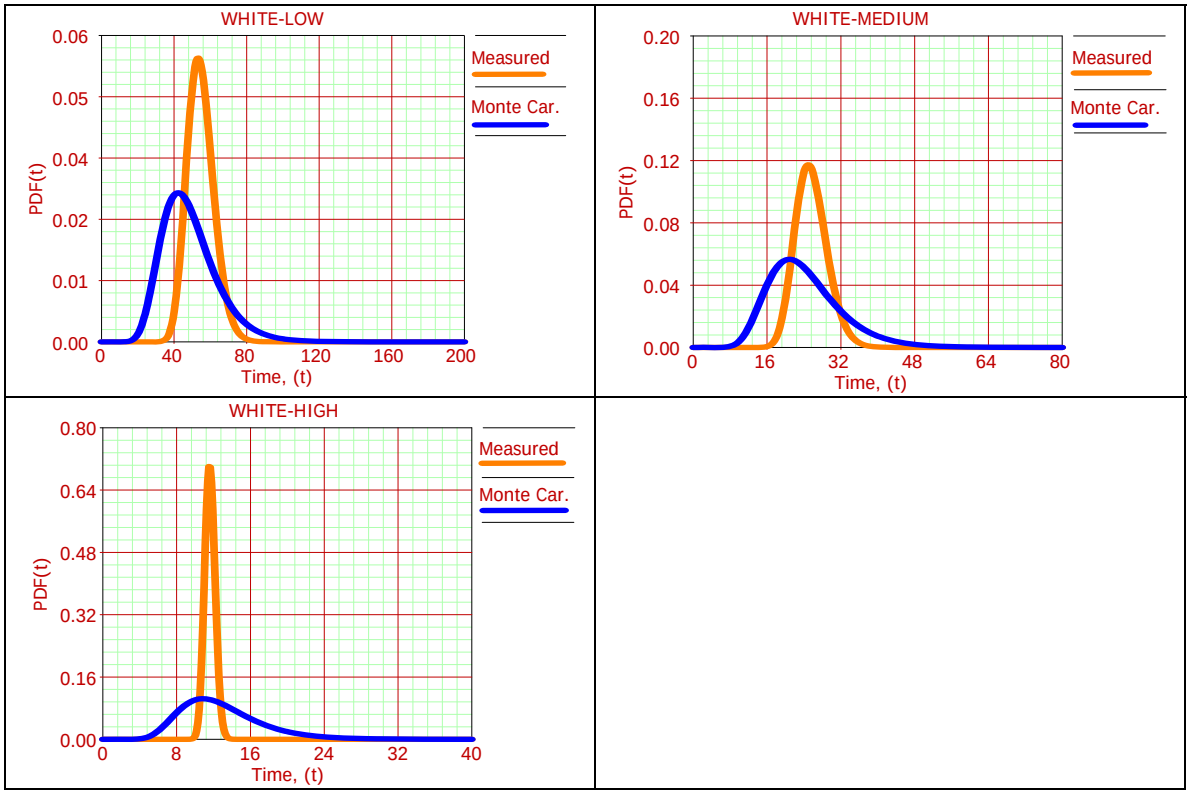

Fig. 6. PDF of Monte Carlo prediction and measured data for TTF of Beam 2

As can be seen above, the predicted time to failure (TTF) distribution using the Monte Carlo Simulation was wider than the measured TTF distribution. This illustrates the sensitivity of the model to uncertainties of input parameters. Examination of 20^{th} and 80^{th} TTF failure percentile in the Monte Carlo simulations shows that with the given uncertainties, the resulting difference between the 20^{th} and 80^{th} percentile is a factor of 1.7. This can be seen in the Figure 7.

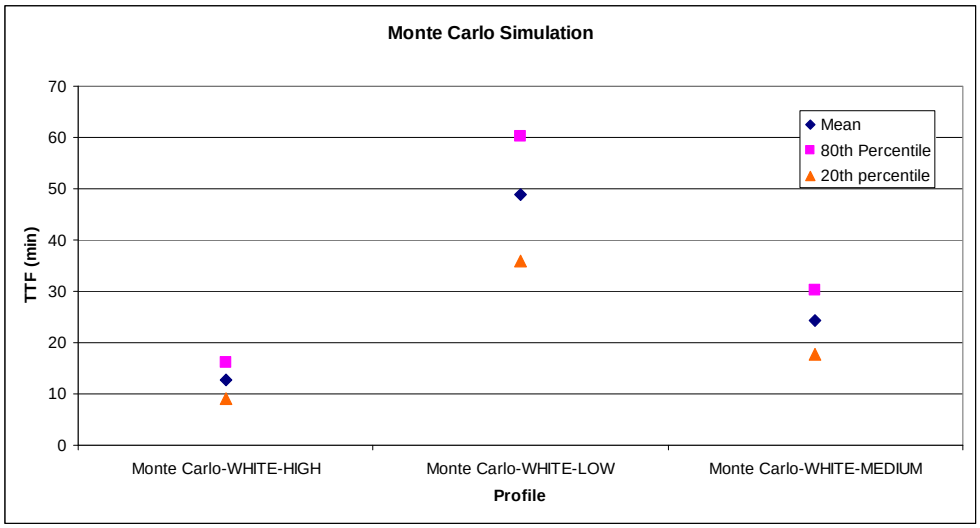

Fig. 7. TTF distribution of Monte Carlo

This implies that even with relatively well known input parameters the model would be expected to have an uncertainty of about a factor of 2.

5.4 Uncertainty of Damping Factor

Up to this point the uncertainty associated with the damping factor has been associated with the overall accuracy of the damping factor independent of natural frequency. For this study it will be assumed that the viscous damping ratio is sufficiently small that the following relationship holds,

$$\zeta = \frac{1}{2Q} \tag{6}$$

where Q is the quality factor. Three methods for estimating the quality factor will be compared. Method 1 will be to measure the response PSD at each natural frequency and computing Q using the half power points [1]. The second method will be to allow Q to vary as a function of natural frequency as suggested by Steinberg [6],

$$Q = 2\sqrt{f_n} \tag{7}$$

The third method will be to assume that Q decreases linearly from the starting Q value of an uncracked beam, to the ending values of Q=0 at f_n=0.

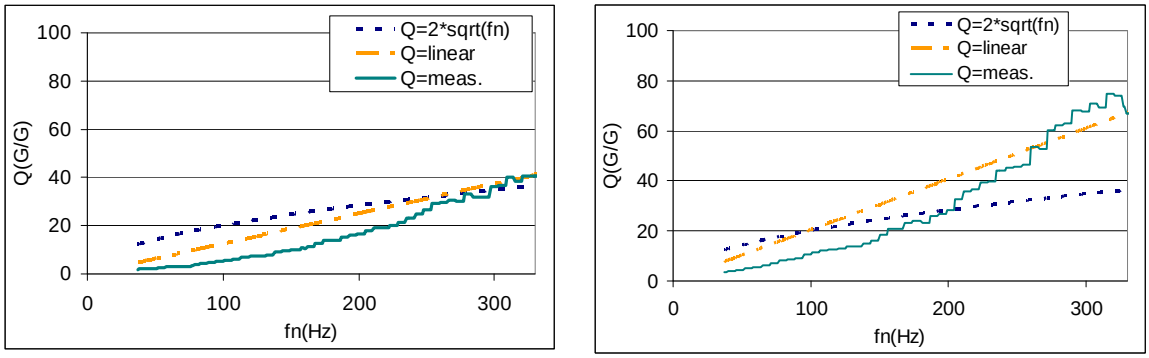

WHITE-HIGH WHITE-LOW

Fig. 8. Amplification factor for Beam 2

From the proceeding figure it is immediately obvious that Steinberg's relationship $Q = 2\sqrt{f_n}$ is not representative of the measured Q values. In particular it can be seen that Q is a function of both the input amplitude and the natural frequency. In addition, it can be seen that the effect of the crack causing a change in natural frequency causes the shape of the Q curve to be different. Obtaining values for Q at all the cracked natural frequencies requires that a component be tested through full failure. This is often time and cost prohibitive. If a linear relationship is assumed between Q and f_n for a given input profile, only the uncracked Q needs to be measured. Using the different Q values, time to failure estimates were made using Eqs. 1-5 and compared against the experimental data. These results are included below.

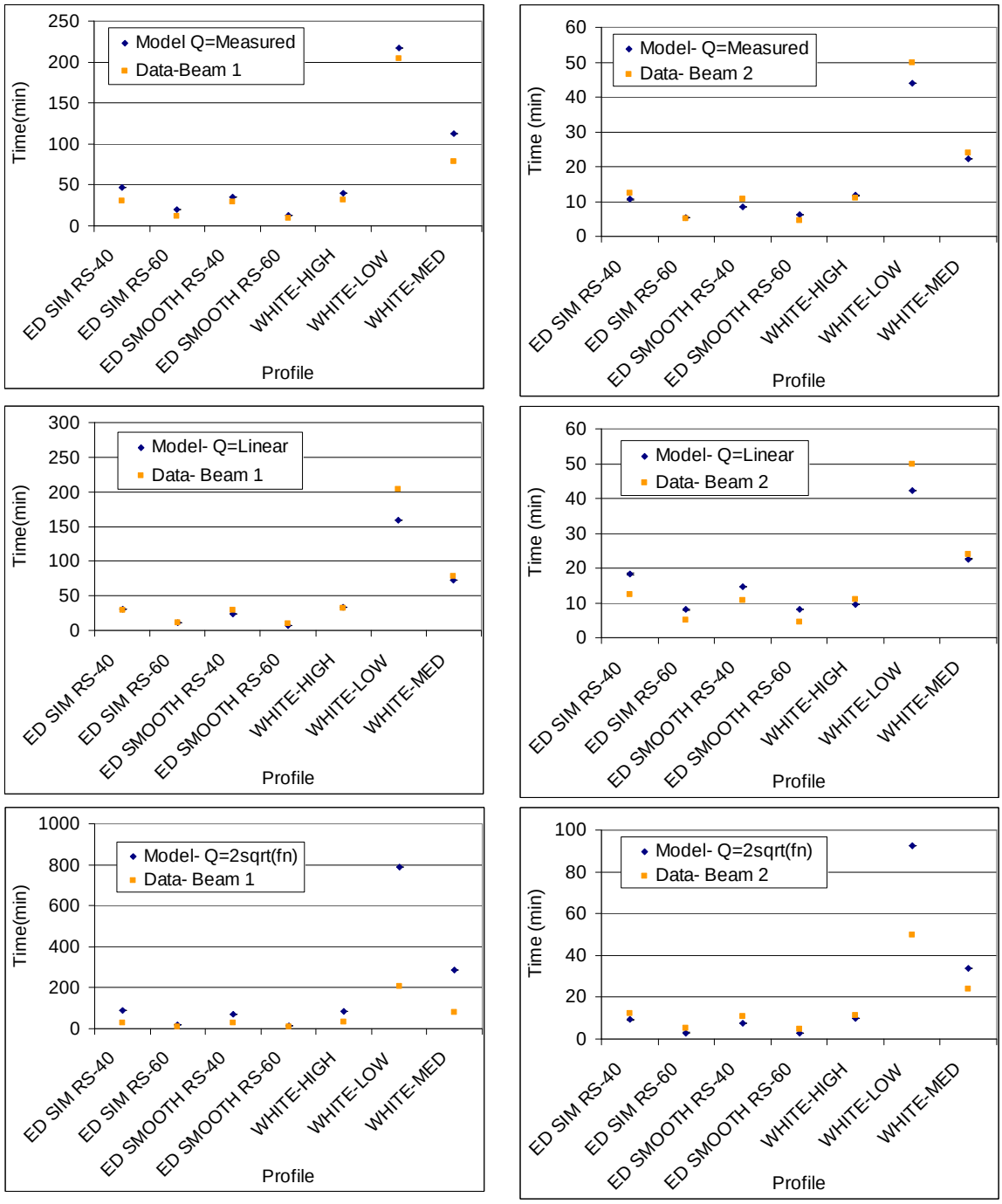

Fig. 9. Comparison of *Q* formulations

In order to evaluate the inaccuracy of each *Q* model, a linear least squares regression (LLSQ) was performed between the predicted TTF and the measured TTF. It was assumed that the constant coefficient (y intercept) was zero. The results for the 3 formulations for *Q* are presented for each beam in Fig. 10

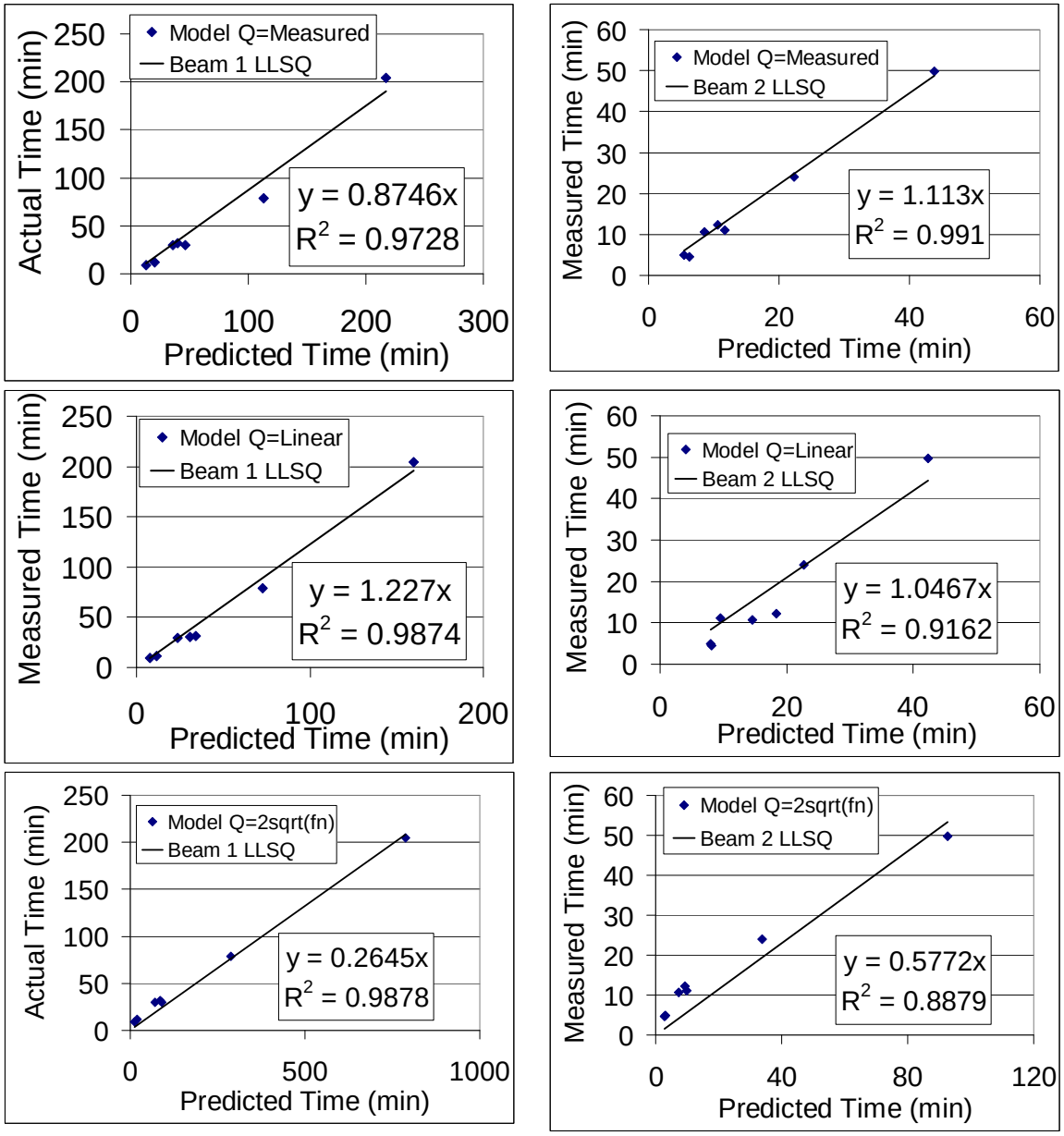

Fig. 10. Comparison of fit for Q models

The R^2 value represents how good the fit is for the determined β_1 coefficient where the LLSQ is defined as

$$Actual\ TTF = \beta_1 * \ Predicted\ TTF \tag{8}$$

If the model perfectly predicted the TTF, β_1 would be 1. Defining the offset error as

$$offset = |1 - \beta_1| \tag{9}$$

a summary of results is presented in Table 3.

	Beam 1		Beam 2	
Q model	R^2	offset	R^2	offset
Measured	.9728	0.1254	.991	0.113
Linear	.9874	0.227	.9162	0.0467
2*sqrt(fn)	.9878	0.7355	.8879	0.4228

Table 3. Summary of comparison of fit

From Table 3 and Fig. 10 important conclusions can be drawn. Changing from the measured Q values to a linear model for Q the offset of the predicted time to failure is primarily effected. Even when Steinberg's formulation for Q is used, the residual remains reasonable while the offset becomes very large. This is particularly important when trying to compute acceleration factors, as an offset will be canceled out during the calculation of acceleration factor

A Chi-Square test was performed for the various formulations to asses the overall goodness of fit for different Q values. The χ^2 statistic is defined as [5],

$$W = \chi^2 = \sum_{i=1}^{k} \frac{(o_i - e_i)^2}{e_i} \tag{10}$$

where o_i is the ith measured data and e_i is the i^{th} prediction using the RFC model. A summary of the results is included in the following table.

Q model	W-Beam 1	W-Beam 2
Measured	191	53
Linear	180	79
2*sqrt(fn)	2988	141

Table 4. Chi-Squared statistic for various Q formulations

From Table 4, use of a linear function for Q results in a slight improvement of the goodness of fit for Beam 1 and a slight decrease for Beam 2. Despite these errors, the

error associated with using a linear function for Q is much less than the geometric and material uncertainty that was demonstrated by the Monte-Carlo (factor of 2).

5.5 Uncertainty When Used as an Acceleration Factor

When using the RFC model to predict the acceleration factor (AF) between vibration environments several simplifications can be made. Let the subscript 1 represent vibration input 1 and the subscript 2 represent vibration input 2. The AF factor can be represented by

$$AF = \frac{Time_2}{Time_1} = \frac{\int_{fnc\_fail}^{fnc\_start} \frac{1}{RFC_2} df_{nc}}{\int_{fnc\_fail}^{fnc\_start} \frac{1}{RFC_1} df_{nc}} \tag{11}$$

Simplify yields

$$AF = \frac{Time_2}{Time_1} = \int_{fnc\_fail}^{fnc\_start} \frac{RFC_1}{RFC_2} df_{nc} \tag{12}$$

where,

$$\frac{RFC_1(f_{nc})}{RFC_2(f_{nc})} = \frac{\frac{\Delta f_T f_{nc}}{a_f} C(C_{ray} E \frac{f_{nc} y_{rms1}}{f_n} \beta^2 c(\pi a)^{1/2} Y)^m}{\frac{\Delta f_T f_{nc}}{a_f} C(C_{ray} E \frac{f_{nc} y_{rms2}}{f_n} \beta^2 c(\pi a)^{1/2} Y)^m} \tag{13}$$

Simplification of Eq. 13

$$\frac{RFC_1(f_{nc})}{RFC2(f_{nc})} = \left(\frac{y_{rms1}}{y_{rms2}} \right)^m \tag{14}$$

where y_{rms} depends only on the damping factor. Combining Eq. 12 and Eq. 14 yields

$$AF = \frac{Time_2}{Time_1} = \int_{f_{nc\_fail}}^{f_{nc\_start}} \left(\frac{y_{rms_1}}{y_{rms_2}} \right)^m df_{nc} \tag{15}$$

From Eq. 15 the AF prediction between two vibration profiles is a function of equivalent viscous damping and *m* only. This increases the importance of accurately knowing these values. The coefficient of variation can be calculated by

$$V_x = \frac{S}{\bar{U}} \tag{16}$$

where S is the standard deviation and $\bar{U}$ is the mean value. The uncertainty on AF between WHITE-HIGH and WHITE-LOW was determined using a Monte Carlo simulation with the inputs presented in Table 2. The resulting coefficient of variation for Beam 2 is tabulated for the failure data, the Monte Carlo simulation and the AF.

Description	Coefficient of Variation
Failure Data WHITE-HIGH	0.020
AF Monte Carlo WHITE-HIGH to WHITE-LOW	0.029
Failure Data WHITE-LOW	0.033
Monte-Carlo WHITE-LOW	0.080
Monte-Carlo WHITE-HIGH	0.134

Table 5. Comparison of coefficient of variation

From table 5 the lower the coefficient of variation the less uncertainty is present. The AF Monte Carlo shows less uncertainty that the prediction of either WHITE-HIGH or WHITE-LOW. This is accounted for by alleviating offset errors.

5.6 Conclusions

Use of the RFC model has uncertainties associated with it. The primary contributors to error are the Paris' Law constants *m* and *C*. Particular attention should be

paid to these two values when performing analysis. Given uncertainties detailed previously, the Monte Carlo simulation predicts a total error of a factor of 2. Further analysis of the uncertainty shows that using a linear function for Q provides sufficient accuracy for many engineering situations. By utilizing a linear Q, a minimal amount of experimental data is needed to characterize the components time to failure. In particular a component does not need to be taken to full failure to predict life for any vibration environment. This is particularly advantageous where expensive or hard to get components are tested. Finally it was shown that the relative severity of two vibration environments can be characterized given the equivalent viscous damping ratio, the Paris' law exponent and the starting natural frequency are known.

References

[1] M.E. Paulus, A. Dasgupta and E. Habtour, *Life Estimation Model of a Cantilevered Beam Subjected to Random Vibration*, to be published (2010).

[2] M. Paulus, Limitations of the power spectral density as an indicator of test severity, submitted to *Journal of Shock and Vibration,* (2010).

[3] M. Paulus and K. Doughty, Effect of resonant frequency shifting on time to failure of a cantilevered beam under vibration, *Journal of the IEST* **53**(1) (2010).

[4] B. Balachandran, E.B. Magrab, *Vibrations 2nd ed.,* 2009 Cencage Learning.

[5] M. Modarres, M. Kaminskiy and V. Krivtsov, *Reliability Engineering and Risk Analysis 2nd ed.,* 2010 CRC Press.

[6] D.S. Steinberg, *Preventing Thermal Cycling and Vibration failures in Electronic Equipment,* 2001 Hoboken John Wiley & Sons.

[7] D.C. Montgomery, *Design and analysis of experiments 4th ed.,* 1997 John Wiley and Sons.

Chapter 6 Semi-Empirical Life and Degradation Model of a Cantilevered Beam Subject to Random Vibration

In the previous two chapters the RFC model was developed. This was a physics of failure based model that allowed prediction of the time to failure of a structural member when subjected to a random vibration environment. This chapter will develop a semi-empirical approach where 1-3 parameters can be determined experimentally.

6.1 Introduction

Development of accelerated life testing models is important within the structural and defense community. Vibration life tests for qualifying new designs must be accelerated within the lab due to cost and time constraints. Reference 1 describes a life model based on the power spectral density (PSD) inputs. Many models, including the methods in Refs, 1 and 2, rely on fatigue S-N curves. More advanced models have been developed, but without a large increase in widespread accuracy [3]. These models generally evaluate the severity of the vibration environment at the initial natural frequency. It is widely known and the subject of much investigation that as structural components begin to fail their fundamental frequency will decrease due to accumulated damage. This has been reported by many investigators in machinery monitoring as well as in multi-axis vibration testing [4-7]. Many structures can withstand some change in natural frequency before failure. Furthermore, during testing cracks may not be detectable until full failure has occurred. The shift of natural frequency can sometimes cause the damage progression to be arrested despite having high initial natural frequencies [4,7]. To this end a model was developed by Paulus et. al. [8] where the

natural frequency shift was taken into account. A frequency domain calculation allowed prediction of time to failure. This method required knowledge of the damping and input PSD. This paper will build on this model by eliminating the need for a detailed stress analysis in favor of an empirical approach.

6.2 Test Specimen

In order to assess the validity of the subsequent model, time to failure data was recorded for two beams subjected to stationary, Gaussian, random vibration inputs [4]. An outline of the data will be provided here. Details of the particular vibration environments will be discussed later. In order to compare the vibration environments, two test specimens were built from cold rolled 1018 steel [4]. The specimens are cantilever beams with specific notches cut into the side walls. The first test specimen had well separated modes and is depicted in Fig. 1. The first bending mode of Beam 1 in the vertical direction was 415 Hz. In the transverse direction the first bending mode was 3520 Hz.

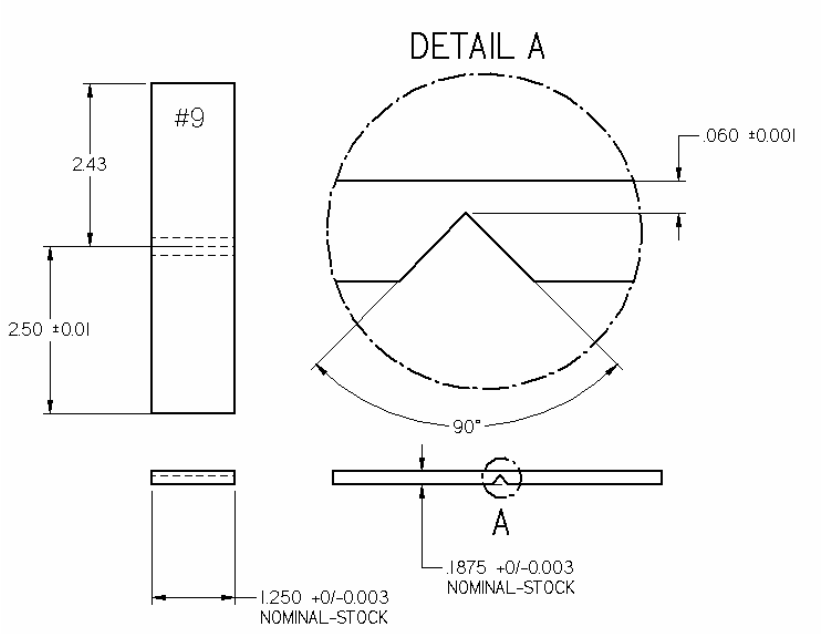

Fig. 1. Test Beam 1.

The second test specimen, illustrated in Fig. 2, had first and second modes that were closely spaced, although the stress concentration was higher in the Z-direction. For Beam 2 the first bending mode in the vertical direction was 330 Hz. In the transverse direction the 1st bending mode was also 330 Hz.

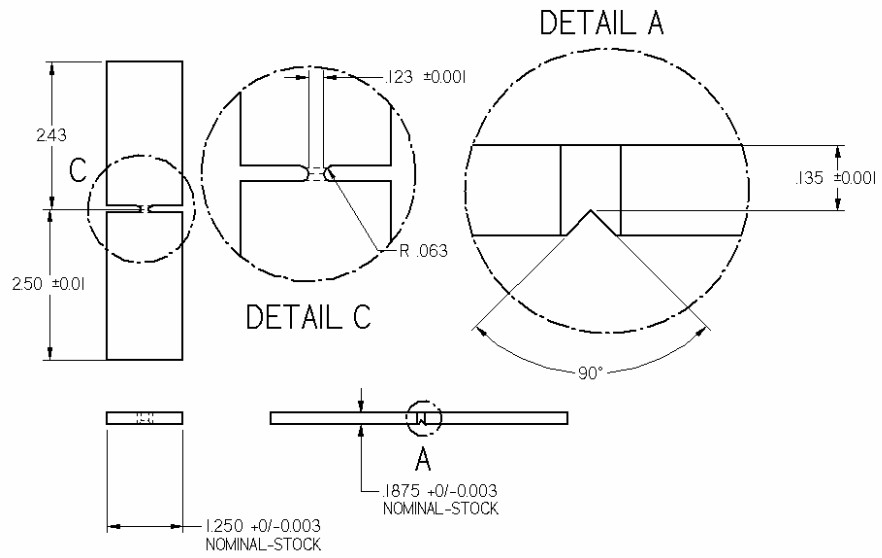

Fig. 2. Test Beam 2

The beam was mounted for vibration testing, as shown in Fig. 3.

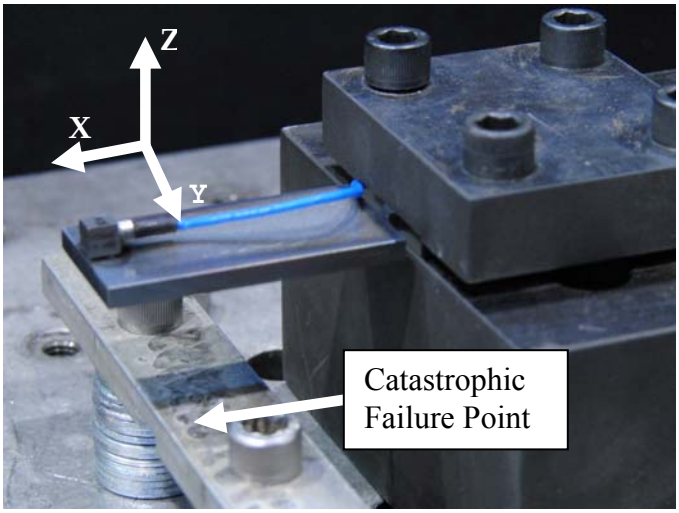

Fig. 3. Beam 2 mounted on shaker

It should be noted that the test was conducted until 'catastrophic failure' of the beam. Catastrophic failure was defined to occur when the test specimen tip made contact with a limit-bar located approximately 1 inch below the tip of the beam, as shown in Fig. 3. Details of the test data are presented elsewhere [4] and a brief assessment of the data is provided below. Selected samples of the vibration profiles are displayed in Fig. 4, with a full summary in Table 1. Several of the profiles had large peaks and valleys due to the simulation of the repetitive shock vibration system. These large peaks and valleys drastically alter the response as the natural frequency changes.

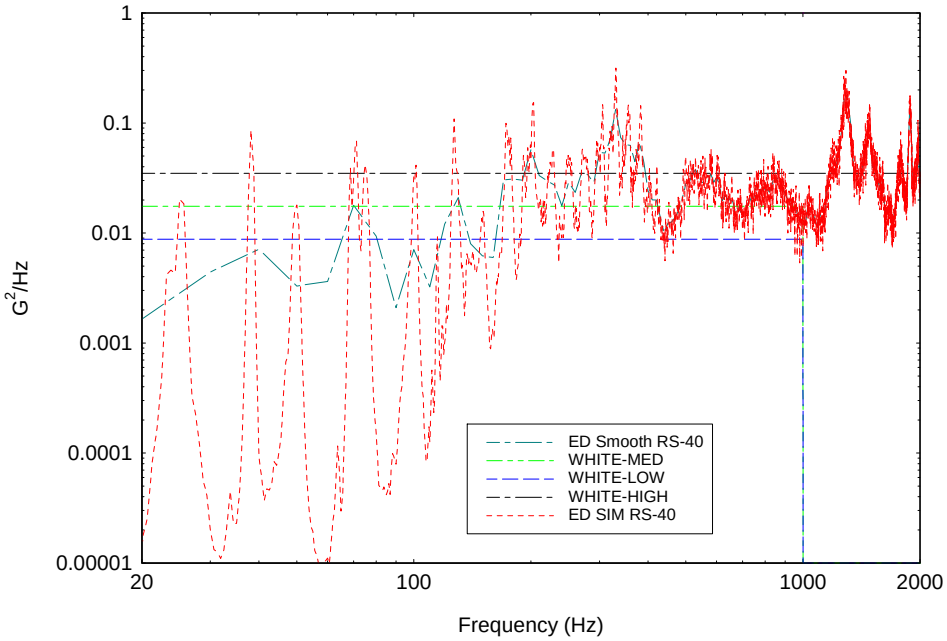

Fig. 4. RS-40 Level vibration profiles

Profile Name	Profile Description
RS-40*	Z-axis of repetitive Shock System set to 40 Grms*
RS-60*	Z-axis of repetitive Shock System set to 60 Grms*
ED SIM RS-40	Single-axis ED simulation of RS-40 Z-axis
ED SIM RS-60	Single-axis ED simulation of RS-60 Z-axis
ED SMOOTH RS-40	Smoothed version of ED SIM RS-40
ED SMOOTH RS-60	Smoothed version of ED SIM RS-60
WHITE-HIGH	Match the Grms level of the RS-40 profile from 20-2000 Hz
WHITE-LOW	Single-axis ED -6db of WHITE-HIGH ran from 20-1000 Hz
WHITE-MED	Single-axis ED -3db of WHITE-HIGH ran from 20-1000 Hz

Table 1. Summary description of profiles

*These profiles were not used in this analysis as they are multi-axis profiles

6.3 Theory

During random vibration, Ungar and others [8,9] have proposed that the pseudo velocity is proportional to stress. This applies to cantilevered beams as well as other geometries. From Ref. 9, it can be concluded that stress in a cantilevered beam can be determined by,

$$\sigma = C_1 * PV \tag{1}$$

where C_1 is a constant and PV is the pseudo velocity. The pseudo velocity can be written as

$$PV = z\omega_n \tag{2}$$

where z is the relative displacement and ω_n is the first natural frequency. Computation of the relative displacement can be accomplished by use of the vibration response spectrum (VRS) [10]. Relative displacement throughout this paper will be computed by assuming an equivalent single degree of freedom (SDOF) system. Fatigue crack growth under constant amplitude loading in the elastic regime can be modeled using the Paris Law as [11],

$$\frac{da}{dN} = C(\Delta K_I)^m \quad \text{[in/cycle]} \tag{3}$$

where da/dN is the rate of crack growth per cycle, C and m are material constants and ΔK_I is the stress intensity factor for mode I crack growth. The stress intensity factor can be calculated using

$$\Delta K_I = \Delta\sigma_r (a)^{1/2} Y \quad \text{[ksi*in^.5]} \tag{4}$$

where $\Delta\sigma_r$ is the stress range, a is the crack depth and Y is a geometric factor. Many authors have claimed that the Paris law can be applied to random vibration through the use of an equivalent K [2,11]. For random vibration the equivalent K is generally modeled as $C_1 K_{rms}$ where C_1 is an equivalent damage constant. There, however, is not general agreement in the literature upon specific values of C_1. Equation 3 can be rewritten as,

$$\frac{da}{dN} = C_2 (z_{rms}\omega_n (a)^{1/2} Y)^m \tag{5}$$

where C_2 is a constant that includes C and C_1. The equivalent SDOF lumped parameter system relative displacement of the cracked beam (z_{rms}) can be computed using the vibration response spectrum [10]

$$z_{rms}(f) = \sqrt{\int_0^{\infty} \ddot{w}_{PSD}(f) \left[\frac{1}{(2\pi)^4 \left(\left({f_{nc}}^2 - f^2 \right)^2 + (2\xi_n f \, f_{nc})^2 \right)} \right] df} \tag{6}$$

where f ranges over the frequency of input, and f_n is the input natural frequency in Hz, and $\ddot{w}_{PSD}$ is the base excitation power spectral density (PSD). Over a limited frequency shift the following relationship holds [12]

$$a \propto \omega_n \tag{7}$$

Assuming that the geometric factor Y can be approximated by a power law relationship,

$$Y \propto {\omega_n}^r \tag{8}$$

where r is the power law exponent. It follows that Eq. 5 may be rewritten as

$$\frac{da}{dN} = C_3 {z_{rms}}^p {\omega_n}^n \tag{9}$$

where C_3 is a proportionality constant and p and n are experimentally determined exponents. As discussed earlier, during fatigue damage evolution the natural frequency shifts. A more thorough discussion is presented in Ref. 8. The rate of natural frequency change (RFC) can be expressed as

$$RFC_i = \frac{fn_i - fn_{i-1}}{t_i - t_{i-1}} \text{ [Hz/min]} \tag{10}$$

Equation 10 allows examination of the RFC at a given natural frequency. The total time to failure (TTF) can be computed as,

$$TTF = \int_{f_{nc\_fail}}^{f_{nc\_start}} \frac{1}{RFC} df_{nc} \quad [\text{min}] \tag{11}$$

where f_{nc_start} is the starting cracked natural frequency and f_{nc_fail} is the natural frequency at failure. It is desirable to have Eq. 9 expressed in terms of RFC so that Eq. 11 could be used to calculate the total time to failure. Assuming that the response of the item is dominated by its fundamental mode,

$$dN = f_n \delta_T \tag{12}$$

and

$$da = \delta \Delta f_n \frac{a_f}{\Delta f_T} \tag{13}$$

where δ_T is the incremental time $\delta\Delta f_n$ is the incremental change in natural frequency, a_f is the final crack depth Δf_T is the total change in natural frequency at failure and f_n is the fundamental natural frequency. Noting that

$$RFC = \frac{\delta \Delta f}{\delta_T} \tag{14}$$

and substituting Eq.12 & 13 into Eq. 14 it follows that

$$RFC = \frac{da}{dN} \frac{\Delta f_T f_n}{a_f} \tag{15}$$

Combing Eq. 15 and Eq. 9 noting that Δf_T and a_f are constants yields

$$RFC = C_4 {z_{rms}}^p {\omega_n}^n \tag{16}$$

Equation 16 now represents a model that can be used to fit experimental data. The purpose of this model will be to fit a minimal number of data points. To this end n will

be set to equal 1. This reduces flexibility in the model but allows fewer data points to be used in the fitting process. As will be seen later, there exists a strong correlation between z_{rms} and ω_n. The following set of equations will be used to predict time to failure.

$$RFC = C{z_{rms}}^{p}\omega_n \text{ [Hz/s]} \tag{17}$$

$$TTF = \int_{f_{nc\_fail}}^{f_{nc\_start}} \frac{1}{RFC} df_{nc} \text{ [min]} \tag{18}$$

where z_{rms} is determined from equation 6. Use of the model is based on the following key assumptions:

1) The model was developed for an elastic system. The data presented here is from test data that contain both plastic and elastic deformations, but the theory assumes strictly elastic deformations only. The applicability to plastic deformations during crack propagation is believed to be indirectly accounted for by the change in damping factor.

2) Fatigue crack propagation is the primary means of failure. This model should only be used when the dominant failure mode is crack propagation. If the crack initiation time is large relative to the crack propagation time, errors will result. Input amplitude is accounted for through the VRS.

3) It is assumed that the applied load will generate a stress intensity factor that is above the stress intensity threshold.

6.4 Model Assessment

Statistical analysis of the model will be done on 1/RFC at each natural frequency. This will allow various frequency shift intervals to be evaluated. Furthermore the experimental parameters (C and p) will be determined using data from a single profile (WHITE-HIGH) and then evaluated at other profiles. Note that experimental measurements of the RFC and equivalent viscous damping as a function of natural frequency are required. The input PSD is specified by the analyst. This methodology would simulate a single test in the lab, and prediction of failure in other vibration environments. It was assumed that 1/RFC would follow a lognormal distribution. This assumption was based on the fact that the RFC should always be positive and would have a larger scatter at larger time to failures. A comparison was made between the Weibull, Exponential and Lognormal distribution using a maximum likelihood estimation (MLE). The results showed that Lognormal provided the best fit to the data. Fig. 5 is a plot of the failure probability for WHITE-HIGH for frequencies between 36 and 330 Hz.

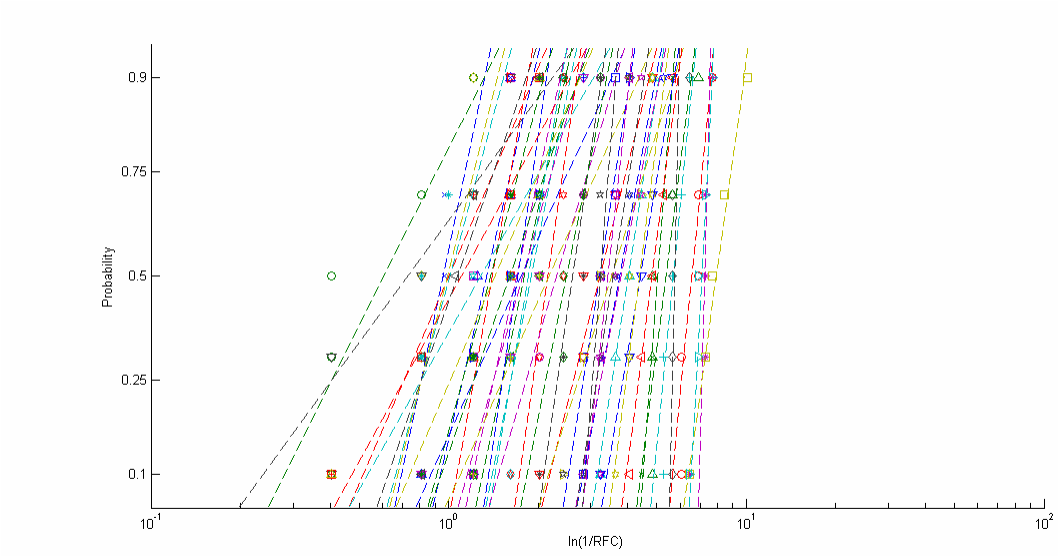

Fig. 5. Lognormal probability plot of WHITE-HIGH for all frequencies

Using the data of WHITE-HIGH a MLE was performed on the LN likelihood function,

$$f(t) = \frac{1}{\sigma_t t\sqrt{2\pi}} \exp\left[-\frac{1}{2\sigma_t^{\,2}} \left(\ln(t) - \mu_t\right)^2 \right] \tag{19}$$

$$\mu_t = \ln\left(\frac{1}{RFC}\right) = -\ln(C) - \ln(\omega_n) - p\ln(z_{rms}) \tag{20}$$

resulting in σ_t=.5091, p=2.8331, C=3789. The resulting Covariance matrix is

$$\text{Cov} = \begin{pmatrix} 5.4\times 10^{-4} & -3.247\times 10^{-13} & -6.987\times 10^{-9} \\ -3.247\times 10^{-13} & 7.045\times 10^{-3} & 150.867 \\ -6.987\times 10^{-9} & 150.867 & 3.246\times 10^{6} \end{pmatrix}. \tag{21}$$

The large values of the off diagonal of the covariance matrix suggest a strong dependence between the relative displacement and the natural frequency. The uncertainties of the parameters are contained in Table 2.

Parameter	mean	90% Confidence LL	90% confidence UL
σ_t	.509	.471	.547
p	2.833	2.695	2.972
C	3789	816	6762

Table 2. MLE of parameters based on WHITE-HIGH data

The uncertainty on the natural log (LN) mean is defined as

$$S_{\mu_t} = \sqrt{H^T Cov\ H} \tag{22}$$

where,

$$H = \begin{bmatrix} \dfrac{d}{d\sigma_t}\left(\ln\left(\dfrac{1}{RFC}\right)\right) \\ \dfrac{d}{dp}\left(\ln\left(\dfrac{1}{RFC}\right)\right) \\ \dfrac{d}{dC}\left(\ln\left(\dfrac{1}{RFC}\right)\right) \end{bmatrix} \tag{23}$$

Defining the mean time at each frequency as [13]

$$\mu_y = \exp\left(\mu_t + \frac{\sigma_t^{\,2}}{2}\right) \tag{24}$$

The confidence limits can be expressed as, [14]

$$UCL_{\mu_y} = \mu_y \exp\left(K_\gamma S_{\mu_t}\right)$$

$$LCL_{\mu_y} = \mu_y \exp\left(-K_\gamma S_{\mu_t}\right) \tag{25}$$

where K_γ is the 2 sided z estimate at the appropriate confidence. For this study a 90% confidence will be used where K_γ =1.65. A comparison of the mean RFC of the measured data verse the prediction of Eq. 17 for WHITE-HIGH are plotted as follows,

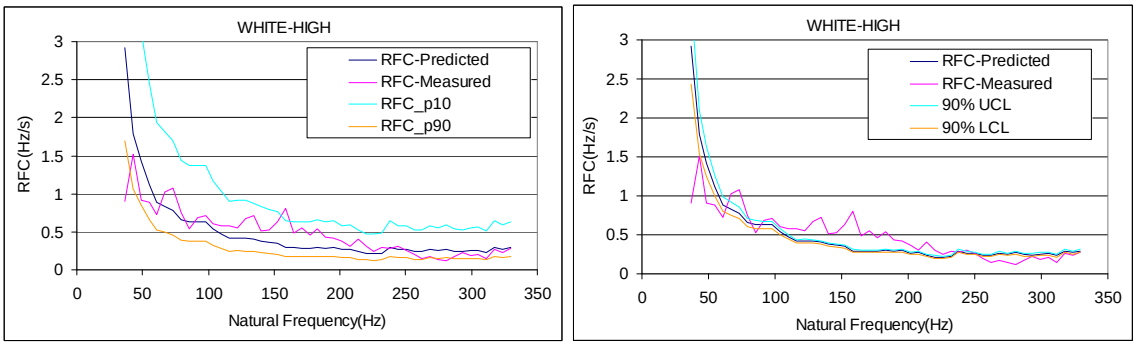

Fig. 6. Predicted RFC verse the measured RFC for WHITE-HIGH Beam 2

The predicted RFC follows the measured RFC quite well. Although there is some discrepancy at individual natural frequencies, the overall trend is quite good. From the RFC the lognormally distributed mean time to failure (MTTF) can be calculated using Eq. 18. This model has been developed where the input stress is the PSD. The prediction of model should, therefore be accurate over a wide range of PSD shapes and amplitudes for a given test specimen. The independence of the model parameters from the PSD amplitude and shape is what makes the model useful as life estimation model. In order to asses the accuracy of the model, the parameters from the MLE of WHITE-HIGH were used to evaluate the time to failure (TTF) of the remaining profiles. It was

assumed that the input PSD and equivalent viscous damping ratio are available. In particular the damping ratio must be known as function of frequency and input amplitude. Effects of different damping ratio formulations were explored in Ref. 15. For these profiles the specified input PSD and measured Q values were used. This allowed conclusions to be drawn on the ability to extrapolate the model to different input PSDs, without making measurements at that particular input PSD. In order to estimate the accuracy of the MTTF, Eq. 18 was also applied to the 90% confidence levels on μ_y and plotted as error bars in Fig. 7.

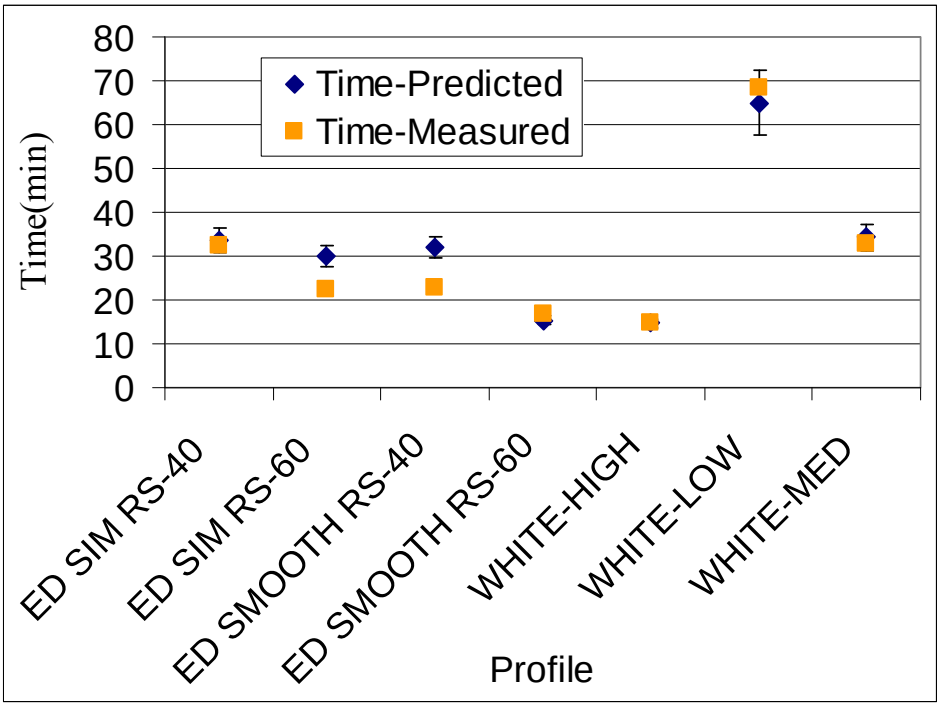

Fig. 7. MTTF using WHITE-HIGH MLE parameters for Beam 2

The measured MTTF generally falls within the estimated confidence levels of the predicted MTTF. Given the inherently large scatter of fatigue and the vastly different PSDs, this is reasonable. In addition the model should also predict partial frequency shift. For the most accurate results the model should be developed for the frequency

shift that dictates failure, but a partial frequency shift should still yield good predictions of time. The following figure illustrates a one octave natural frequency shift.

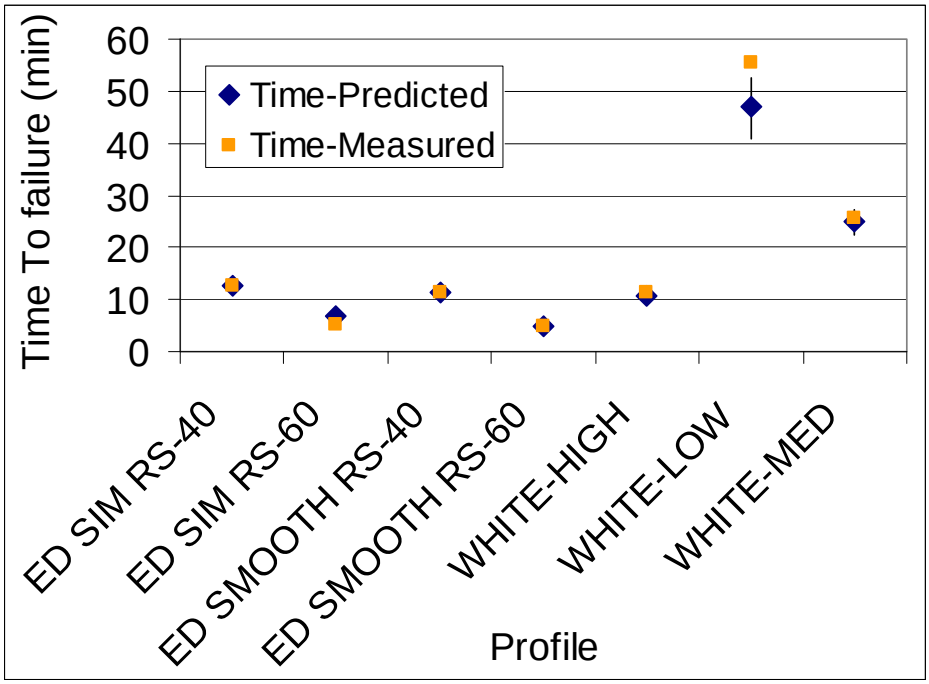

Fig. 8. MTTF using WHITE-HIGH MLE parameters for Beam 2 (1 octave frequency shift)

Although good results are still obtained the effect of the predicted mean and measured mean being different at various frequencies (Fig. 6) becomes evident. Meaningful results can still be obtained with this simple model. In the following figure the RFC is plotted vs. the natural frequency for all profiles. Good results are seen for all profiles.

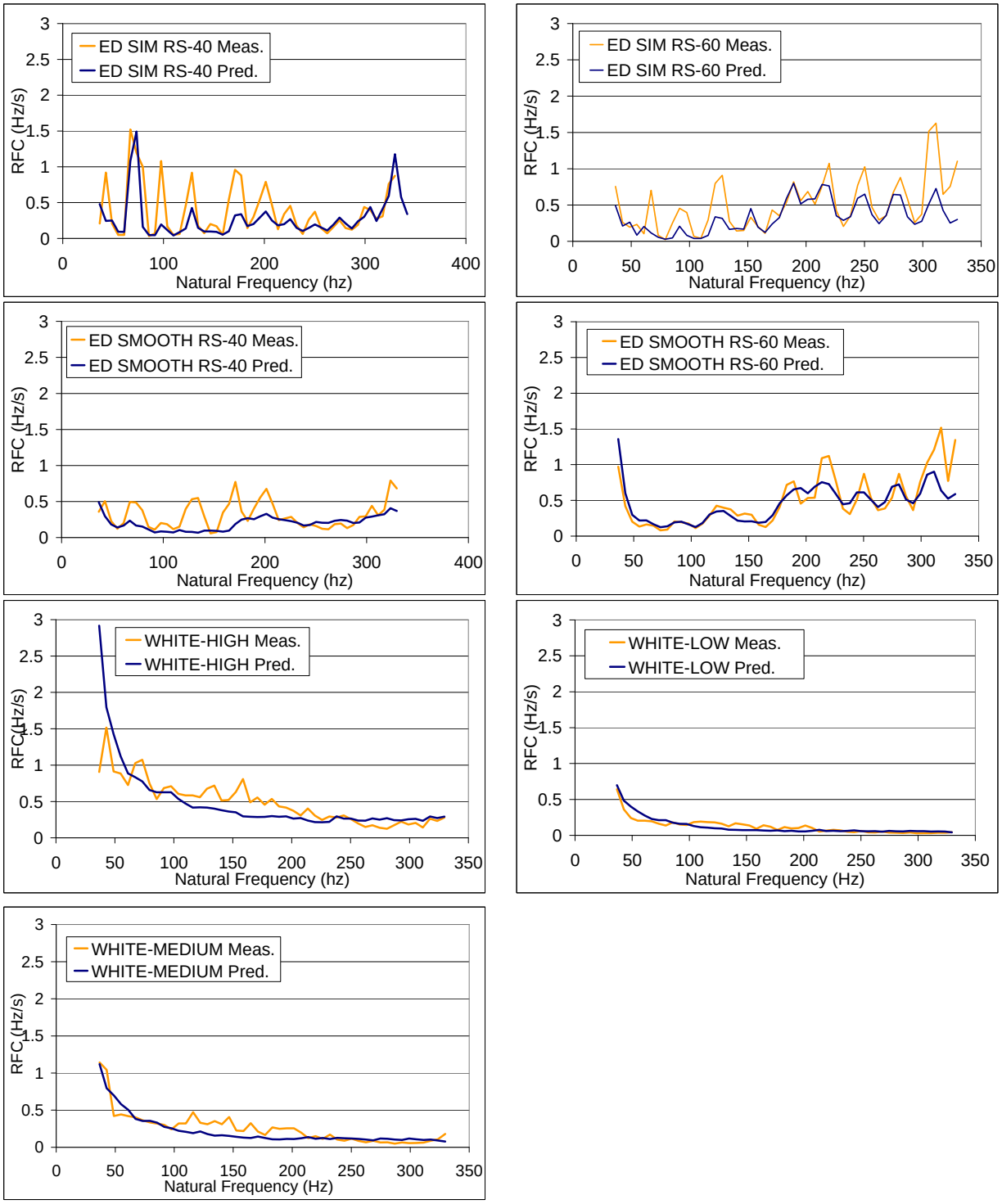

Fig. 9. RFC vs. natural frequency for Beam 2

From previous work detailed in Ref. 8 the plastic zone size is sufficiently large that the LEFM assumptions begin to breakdown after about a 1 octave frequency shift. As can

be seen in Fig. 9 even when the plastic zone size is large (40-165 Hz range) the prediction of RFC is still accurate. This is believed to be accounted for by experimentally determining p and C. These experimental parameters account for the inaccuracies in generalized Paris' law constants as well as the limitations in handbook calculations of the geometric correction factor Y. Furthermore measured data was used for the equivalent viscous damping term, which indirectly accounts for some of the plasticity effects. An additional beam (Beam 1) was also used to validate the model. Beam 1 was subjected to the same profiles as Beam 2. The empirical parameters σ_t=.5973, p=2.9274 and C=2536 were computed by performing a MLE on WHITE-HIGH data for Beam 1. Using the parameters, the time to failure was calculated for the remaining profiles. Good results were obtained as indicated below.

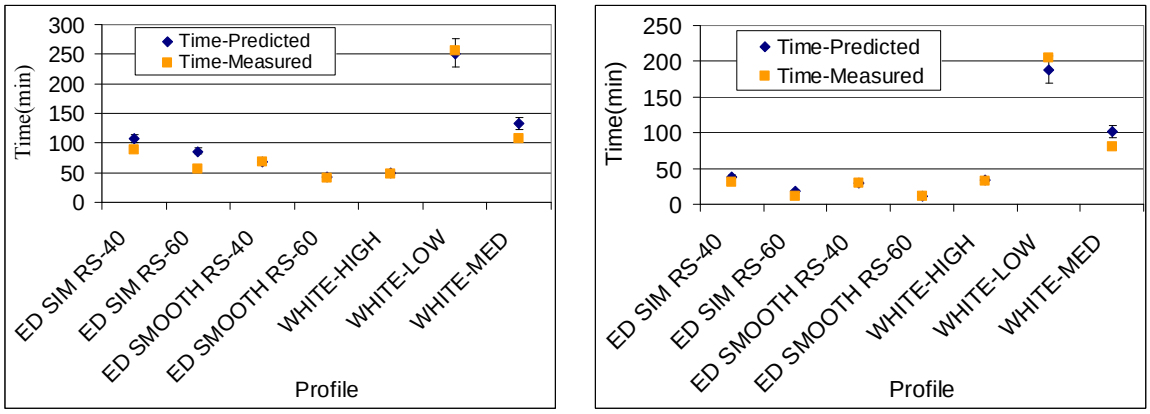

Full Frequency Shift MTTF One Octave Frequency Shift MTTF

Fig. 10. Beam 1 MTTF using WHIITE-HIGH to compute the MLE values

6.5 Comparison to existing methods

To illustrate the differences between MIL-STD 810 and the proposed model a comparison of WHITE-HIGH and WHITE-LOW was performed. WHITE-HIGH will simulate a laboratory environment while WHITE-LOW will simulate the use level. Predictions of field life are made using MIL-STD-810 as follows.

$$T_2 / T_1 = W_1 / W_2^{\,4} \tag{26}$$

where T is the time to failure and W is the power spectral density in G^2/Hz. The exponent 4 is the suggested exponent of MIL-STD 810. It can be determined more exactly by using actual S-N data. Table 3 gives the comparison between MIL-STD-810 and the proposed model.

Lab Level PSD [G^2/Hz]	Field Level PSD [G^2/Hz]	Lab Time to Failure [min]	Actual Field Time To failure [min]	Predicted Field Life in Accordance with MIL-STD 810 [min]	Predicted Field Life of Current Model [min]
.0349	.0088	13	69	3340	66
			Error➔	48x	0.96x

Table 3. Predicted field life vs. lab test data

As can be seen the lab failure time was 13 minutes. Using MIL-STD 810, the prediction of field time to failure was over 3300 min vs. the actual field time of 69 minutes. This is an overestimate of life of 48 times. In contrast using the current model, a slightly conservative field life was arrived at. Although typical calculations of fatigue using S-N data assume that a crack has initiated when the crack is 1mm long, the models do not account for any frequency change during the initial phase.

Further improvements over Mil-Std 810 can be realized by using the inverse power law and experimental data. The inverse power law is expressed as [13, 14]

$$TTF(G_{rms}) = \frac{1}{kG_{rms}^{\;n}} \tag{27}$$

or

$$TTF(PSD) = \frac{1}{kPSD^n} \tag{28}$$

where TTF is the time to failure, k and n are determined from experimental data, G_{rms} is the RMS acceleration of the input and PSD is the power spectral density at the starting natural frequency. Using the data from WHITE-HIGH and WHITE-LOW an MLE was performed to determine k and n for Beam 1 and Beam 2. The resulting coefficients are included in table 4.

Beam	Stress characterization	k	n
Beam 1	G_{rms}	.0009	1.5315
Beam 1	PSD	.9182	1.1135
Beam 2	G_{rms}	.0037	1.3628
Beam 2	PSD	1.8468	.9909

Table 4. Resulting exponent and coefficient using power law

A comparison between the measured data and the predicted data was done for all the profiles previously discussed. This comparison was done using the new model and the semi-empirical life (SEL) model of Eqs. 27 and 28.

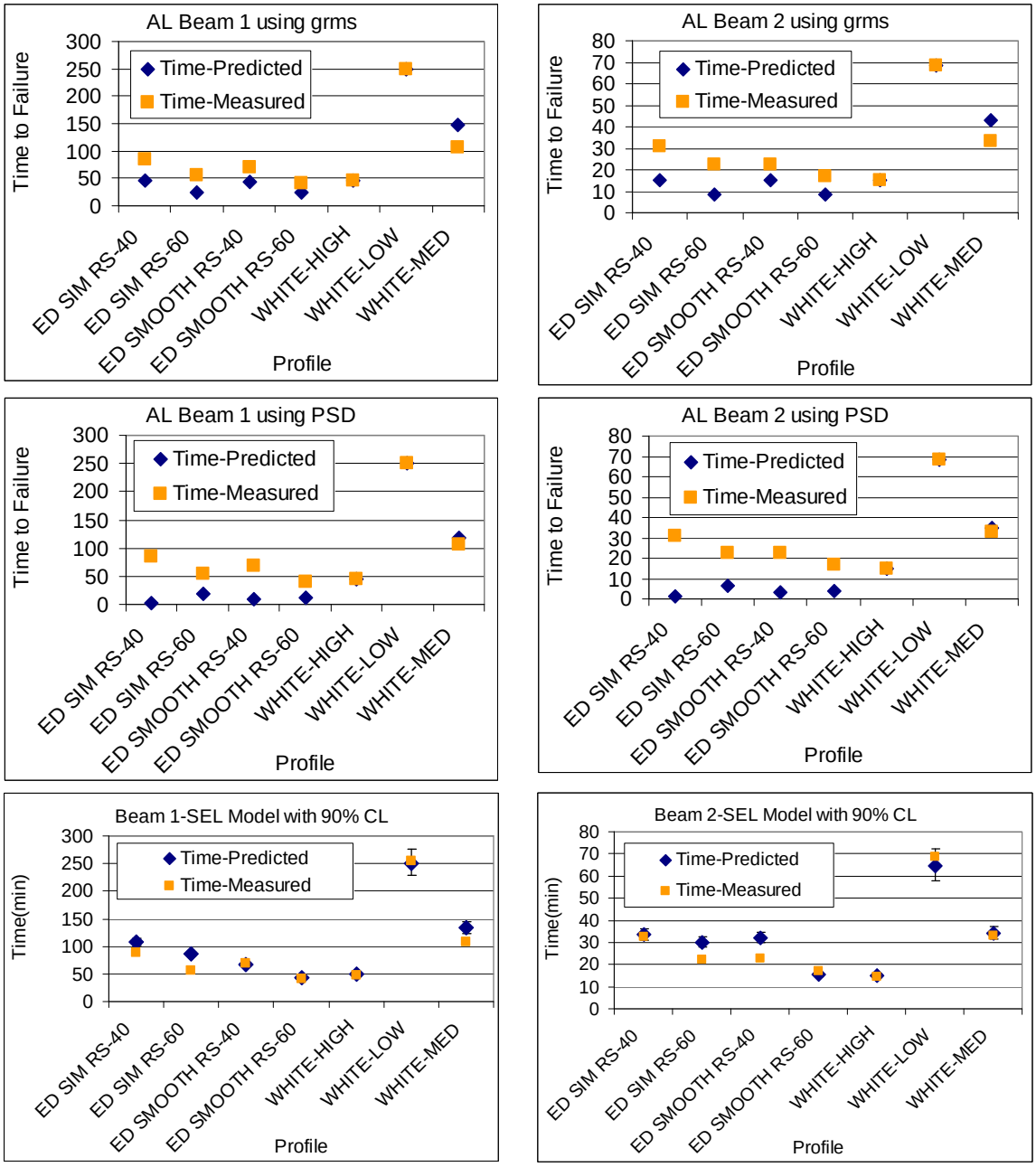

Fig. 11. Comparison of SEL model and existing life models to predict MTTF

In Fig. 11, some data points lie directly on top of each other, and can't be seen (i.e. AL Beam 1 WHITE-HIGH). An improvement is realized when using the SEL model over existing life models as depicted in Fig. 8. In particular The ED SIM and ED SMOOTH profiles realize the greatest improvement. This is due to the fact that the SEL model

accounts for the change of input spectrum shape that is present in ED SMOOTH and ED SIM. The white noise profiles are adequately modeled using existing methods. It appears from the profiles used here that G_{rms} was a slightly better indicator of stress than the PSD level. This was surprising as the input G_{rms} doesn't reflect the starting initial stress. It is believed that due to the frequency change, the G_{rms} allowed the lower levels at lower frequency to be loosely accounted for through averaging. It is conceivable however, to have a profile where this effect would not be present (large amount of high frequency energy). It is important to note that for the existing life models, two input vibration profiles must be measured to develop the constants. For the semi-empirical life model only 1 input vibration profile needs to be used.

6.6 Conclusions

A model has been developed to represent the rate of natural frequency change (RFC) as a function of natural frequency (ω_n) and relative displacement (z_{rms}). This function can be integrated between the initial and final natural frequency to determine the time to failure. It was found that the RFC and the total time to failure were lognormally distributed. Using the maximum likelihood estimation (MLE) technique the experimental constant and exponents can be determined if the single degree of freedom (SDOF) lumped parameter relative displacement, cracked natural frequency and rate of natural frequency change are known. An estimate of the relative displacement can be obtained directly from the input power spectral density (PSD) by using the vibration response spectrum (VRS) and equivalent viscous damping ratio. Only one input PSD shape and amplitude is required to predict the failure time for a PSD of any shape or amplitude. In this study up to 4 decades of variation were evaluated. Comparison to

existing techniques (use of excitation G_{rms} or initial PSD) showed that the accuracy was significantly improved over existing models when comparing PSDs of different shape. In this work the failure had both elastic and highly plastic failure modes. The mode of failure did not affect the prediction of the model. It is important to note that when using the VRS to predict relative displacement, accurate values of the damping factor must be used. Using this method many properties of the material that would affect typical handbook calculations (e.g. Mil-Std 810 [1] or RFC model [8]) can be incorporated into the empirical portion of the formulation.

6.7 References

[1] MIL-STD-810G. "Environmental Engineering Considerations and Laboratory Tests"

[2] D.S. Steinberg, *Preventing Thermal Cycling and Vibration failures in Electronic Equipment,* 2001 Hoboken John Wiley & Sons.

[3] W. C. Fackler, Warren C. *Equivalence techniques for Vibration testing*, 1972 Shock and Vibration Information Center.

[4] M. Paulus, Limitations of the power spectral density as an indicator of test severity, submitted to *Journal of Shock and Vibration,* (2010).

[5] R.M. French, R. Handy and H.L. Cooper, Comparison of simultaneous and sequential single axis durability testing, *Experimental techniques*, **30** (2006) 32-37.

[6] W.E. Whiteman, Inadequacies in uniaxial stress screen vibration testing, *Journal of the IEST*, **44** (2001), 20-23.

[7] M. Paulus and K. Doughty, Effect of resonant frequency shifting on time to failure of a cantilevered beam under vibration, *Journal of the IEST* **53**(1) (2010).

[8] M.E. Paulus, A. Dasgupta and E. Habtour, Life estimation model of a cantilevered beam subjected to random vibration, *to be published* (2010).

[9] E.E. Ungar, Maximum stresses in beams and plates vibrating at resonance, *Journal of Engineering for Industry*, **84** (1962) 149-155.

[10] T. Irvine, Optimal use of the vibration response spectrum for enveloping random data, *Proceedings of the Institute of Environmental Sciences and technology*, (1999).

[11] R.I. Stephens, A. Fatemi, R.R. Stephens and H.O. Fuchs, *Metal Fatigue in Engineering 2nd ed*, 2001 John Wiley and Sons.

[12] E. Douka and L.J. Hadjileontiadis, Time-frequency analysis of the free vibration response of a beam with a breathing crack, *NDT&E International*, **38** (2005) 3-10.

[13] M. Modarres, M. Kaminskiy and V. Krivtsov, *Reliability Engineering and Risk Analysis 2nd ed.,* 2010 CRC Press.

[14] W. Nelson, *Accelerated testing: statistical models, test plans, and data analysis*, 2004 John Wiley and Sons.

[15] M.E. Paulus, A. Dasgupta and E. Habtour, *Rate of frequency change model uncertainty analysis*, to be published (2010).

Chapter 7 Summary

This chapter will summarize the results contained in previous chapters, list the major contributions of this dissertation, discuss the limitations of this study and recommend relevant future work

7.1 Major Conclusions

Experimental data clearly shows that notching of the excitation PSD at frequencies below the initial resonant frequency of a vibrating structure can lead to reduction (or even complete arrest) of the fatigue damage accumulation. During vibration induced fatigue failure, the natural frequency drops due to accumulating fatigue damage, causing the response and stress state to change. If the input PSD has peaks and valleys like in a RS vibration system, this frequency drop is very important since the instantaneous natural frequency of the structure may coincide with a valley, thus reducing the response amplitude and fatigue damage accumulation rate.

Further experimental comparison show multi-axis testing at the same PSD as a single-axis test is more severe. For RS vibration systems this effect was more pronounced than ED vibration. Despite the increased effectiveness of multi-axis testing, a single-axis white noise profile was shown to be more severe than a multi-axis RS test of the same excitation G_{rms}. This demonstrates the effect of low frequency notching in test severity. Furthermore it calls into question the validity of sine dwells. If the natural frequency were to change, a sine dwell test could cease to excite the test item.

As a result, the traditional approach of considering the PSD level at the initial natural frequency or the excitation G_{rms} does not sufficiently characterize the severity of

a vibration environment. Defining the stress state using only the starting natural frequency was shown to lead to large errors with heavily notched PSDs. This error was reduced when examining smooth PSDs such as white noise. Furthermore, in the case of heavily notched PSDs, it was shown that smoothing of the input profile can drastically alter time to failure results.

In response to these shortfalls in traditional approaches for assessing vibration durability, the rate of natural frequency change (RFC) model was developed. This model allowed prediction of the time to failure using analysis in the frequency domain. Use of the frequency domain means that an explicit time history is not needed. This is advantageous when working with many of the military specifications as the vibration environment is often provided as a PSD. In addition, the frequency-domain approach is computationally much more efficient than a time-domain approach. Using a cantilevered beam subject to single-axis vibration, the RFC model was compared to both FEA and experimental data with good results.

The RFC model was determined to be heavily dependent on the Paris' law exponent, the height of the beam cross section and the damping factor for accurate predictions. It was, however, demonstrated that use of a linear function for Q would provide sufficient accuracy in many cases. Furthermore, a geometric correction factor was needed which requires the use of FEA, except in simple cases. In addition, computation of stress intensity using FEA requires large amounts of computing time for even simple structures. For this reason, a semi-empirical model was developed. This model allows determination of 2 parameters whereby the RFC could be calculated for arbitrary input PSDs. The semi-empirical model accounts for complex geometries,

unknown material properties and plasticity through a life test. This model was compared to experimental results with good success. In addition, comparison with MIL-STD-810, and S-N fatigue life models showed a marked improvement, especially with complex PSDs.

7.2 Contributions of this work

The contributions of this dissertation are as follows:

- Although there are isolated reports in the literature comparing the effectiveness of RS and ED vibration, a comprehensive and direct experimental comparison was still lacking. This work expands the knowledge base by providing one of the most detailed experimental comparisons to date of the fatigue damage accumulation rates between RS, single-axis ED and 3-axis ED vibration. The experimental work presents qualitative differences between these three types of vibration, in regards to fatigue durability. Design engineers will be able to make informed decisions on the type of testing to use and the suitability of G_{rms} and input PSD for defining relative severity of proposed testing programs.
- The analytic and semi-empirical frequency domain models developed in this work allow the quantification of the damage accumulation rates due to complex, single-axis, random vibration environments. These models are a substantial improvement over existing models by accounting for the change in natural frequency and the corresponding change in damage accumulation rates. Furthermore, the characteristic peaks and valleys in the frequency domain of the RS system are able to be accounted for in 1DOF. This work is the first step towards developing a more general 6DOF model.

- An alternative method of quantify the damping factor in complex vibration environments was presented. The new method was shown to introduce an acceptable amount of error for many engineering applications.

7.3 Limitations and future work

- The multi-axis effect of RS vibration was more significant than ED vibration. It is suspected that it had to do with the rotational motion, the high frequency energy exciting the 2^{nd} mode, or uneven input in the orthogonal axes. A systematic experimental investigation of these factors would be advantageous.
- The RS vibration system used in this study produced Gaussian excitation with a kurtosis of 3. It would be valuable to pursue the effect of higher kurtosis inputs on time to failure.
- This study demonstrated that the simple analytic RFC model worked reasonably well for elastic response but the accuracy of the model progressively diminished as the effect of plasticity increased with increasing fatigue crack length. This needs more detailed investigation in the future, with a goal of developing possible correction factors that could be introduced in the analytic model.
- Generalized values of the Paris' law constants from the literature were used in this study. However, these values should be experimentally verified in the future since a lot of fatigue scatter is present in the data. Uncertainty analysis clearly shows these parameters to be very influential in the accuracy of the life prediction. Values specific to the material used would increase the confidence in the model.

- Damping has been clearly shown to affect the accuracy of the model predictions. The methodology for determining and accounting for damping in the model should be further investigated. Employing an instantaneous frequency measurement technique may improve the results. It is also suggested to change analysis bandwidth and the number of averages.
- During crack closure and opening, the natural frequency should vary. This was not accounted for in the RFC model. Furthermore natural frequency was not measured as a function of crack depth. This relationship was developed in the context of FEA and an analytic model. Experimental verification of the linearity of the relationship between crack depth and natural frequency should be performed.
- The Rayleigh Approximation for fatigue analysis in the frequency domain is not sufficiently accurate for broadband or bimodal responses. Investigation into improved frequency domain peak approximations would improve the results.
- During the entire natural frequency shift it was assumed that the notch depth plus the physical crack could be used as an equivalent crack depth. This is not strictly true. During crack initiation, a stress concentration value should be used. Alternate methods to address this complicating factor should be explored.
- The model predictions were found to work well for the excitation levels that were used in this study. Larger acceleration factors should be explored in future to examine the range of validity of the model over larger ranges of time to failure.

- The RFC model is currently restricted to a 1DOF vibration environment. The analytical and semi-empirical RFC model should be extrapolated to a 3DOF vibration environment
- This model was tested for simple structural beams. It would be advantageous to assess its validity for use in more complex structures, e.g. electronic assemblies or complex mechanical systems. In particular, use of the model for vibration durability of solder interconnects, where large amounts of plasticity would be present, may prove difficult. Furthermore use in complex structures where multiple cracks may be growing would also be difficult.

7.4 References

[1] Jawaid, Shams. 2000. Accelerated Reliability Test results: Importance of Input Vibration Spectrum and Mechanical Response of test Article. *2000 Proceedings*

[2] Harris, Cyril, Piersol, Allan. 2002. *Harris' Shock and Vibration Handbook*. 5th Ed. New York. McGraw-Hill.

[3] Steinberg, Dave S. Preventing Thermal Cycling and Vibration failures in Electronic Equipment. 2001. Hoboken. John Wiley & sons.

[4] Fackler, Warren C. *Equivalence techniques for Vibration testing*. Shock and Vibration Information Center. 1972.

[5] Giannoccaro, N.I., Messina, A. et al. 2006. Fatigue damage evaluation of notched specimens through resonance and anti-resonance data. *Engineering Failure Analysis* 12. 340-352.

[6] Al-Najjar, B. 2000. Accuracy, effectiveness and improvement of vibration-base maintenance in paper mills: case studies. *Journal of Sound and vibration* 229(2):389-410

[7] Maynard, K.P., Trethewey, M.W. et al. Application of torsional vibration measurements to shaft prevention technology, Proceedings of the 55th meeting of the society for machinery failure prevention technology, Virginia Beach, VA, April 2-5 pp. 217-226.

[8] Threthewey, Martin, Friell, Joshua et al . 2008. A spectral simulation approach to evaluate probabilistic measurement precision of a reactor coolant pump torsional vibration shaft crack monitoring system. *Journal of Sound and Vibration* 310:1036-1056.

[9] Wang, Rui-Jie, Shang, De-Guang et al. 2008. Fatigue damage model based on the natural frequency changes for spot welded joints. *International Journal of Fatigue* 30. 1047-1055.

Appendix A

In order to facilitate use of the model presented in chapter 4, a flow chart of the calculation steps will be presented below.

Step	Description	Eq. #	Equation	Variable Description
1	Compute Equivalent Viscous Damping	42 & 43	$\xi_n = \frac{f_u - f_l}{2 f_{nc}}$	$f_{nc} = Natural\ Frequency\ cracked\ beam$ $f_u = Upper\ 1/2\ \ power\ frequency\ [hz]$ $f_l = Lower\ 1/2\ \ power\ frequency\ [hz]$
2	SDOF relative displacement	24	$y_{rms}(f_{nc}) = \sqrt{\int_0^\infty \ddot{w}_{PSD}(f) \frac{1}{(2\pi)^4 \left(\left({f_{nc}}^2 - f^2 \right)^2 + (2\xi_n f\ f_{nc})^2 \right)} df}$	$\ddot{w}_{PSD} = input\ \ PSD$ $f_{nc} = Natural\ Frequency\ cracked\ beam$ $f = frequency\ [hz]$ $\xi_n = Equivalent\ viscous\ damping$
3	Use equivalent energy to calculate Stress Range	25	$\Delta\sigma_{rms} = E \frac{f_{nc} y_{rms}}{f_n} \beta^2 c$	$f_{nc} = Natural\ Frequency\ cracked\ beam$ $f_n = Natural\ Frequency\ uniform\ beam$ $E = Modulus\ of\ Elasticity$ $\beta = 1.8751/L$ $L = Length\ of\ beam$ $c = dis\tan ce\ \ from\ \ neutral\ \ axis$

4	Equivalent Damage Constant	36	$C_{ray} = \left[2^{m/2} \Gamma\left(1 + \frac{m}{2}\right) \right]^{\frac{1}{m}}$	$m = Paris\ \ Law\ \ \text{exp}onent$ $\Gamma(\bullet) = Gamma\ \ function$
5	Calculate crack depth-integrate equation 30	30	$a = \Delta f_n \frac{a_f}{\Delta f_T} + a_i$	$a\ \ = initial\ \ crack\ \ length$ $\Delta f_n = f_{nc}\_start - f_{nc}$ $f_{nc} = natural\ \ frequency\ \ cracked\ \ beam$ $f_n\_start = Starting\ \ natural\ \ frequency$ $a_f\ = final\ \ crack\ \ length$ $\Delta f_T\ = total\ \ change\ \ in\ \ Natural\ \ frequency$
6	Geometric Correction Factor	41	$Y = \frac{1.99 - \frac{a}{h}(1 - \frac{a}{h})\left(2.15 - 3.93\frac{a}{h} + 2.7\left(\frac{a}{h}\right)^2\right)}{\left(1 + 2\frac{a}{h}\right)\left(1 - \frac{a}{h}\right)^{3/2}} \frac{1}{\pi^{1/2}}$	$a = crack\ \ length$ $h = thickness\ \ of\ \ beam$
7	Use LEFM and natural frequency to compute RFC	33	$RFC(f_{nc}) = \frac{\Delta f_T f_{nc}}{a_f} C(C_{ray} \Delta\sigma_{rms} (\pi a)^{1/2} Y)^m$	$f_{nc} = Natural\ \ Frequency\ \ cracked\ \ beam$ $\Delta f_T\ = total\ \ change\ \ in\ \ natural\ \ frequency$ $a_f\ = final\ \ crack\ \ length$ $C = Paris\ \ law\ \ constnat$ $a = crack\ \ length$ $m = Paris\ \ law\ \ \text{exp}onent$

8	Calculate total time to failure. Discrete case with uniform natural frequency analysis is also presented	28	$TTF = \int_{f_{nc\_fail}}^{f_{nc\_start}} \frac{1}{RFC} df_{nc}$ or *discrete version* $TTF = \sum_{i=1}^{N} \frac{\Delta f_{nc\,i}}{RFC(f_{nc\,i})}$ $\Delta f_{nc} = \frac{f_{nc\_start} - f_{nc\_fail}}{N}$ $f_{nc\,i} = f_{nc\_start} + \Delta f_{nc}(i-1)$	f_{nc} = *Natural Frequency cracked beam* f_{nc_start} = *Starting Natural Frequency cracked beam* f_{nc_fail} = *failure Natural Frequency cracked beam*
9	Calculate Stress intensity to verify plastic zone size	Step 7	$\Delta K_I = \Delta\sigma_{rms}(\pi a)^{1/2} Y$	a = *crack length*
10	Calculate Plastic zone size to verify application of LEFM	40	$r_y' = \frac{1}{8\pi}\left(\frac{\Delta K_I}{S_y}\right)^2$	S_y = *Yield Strength*

References

References presented here are in the order used. As each chapter is meant to be a standalone paper, the references for each chapter are contained within that chapter.

Jawaid, S. and P. Rogers. 2000. Accelerated reliability test results: Importance of input vibration spectrum and mechanical response of test article. *Proceedings of the Annual Reliability and Maintainability Symposium*, 248–53. Piscataway, NJ: IEEE.

Harris, Cyril and Allan Piersol. 2002. *Harris' shock and vibration handbook,* 5th ed. New York: McGraw-Hill.

Steinberg, Dave S. 2001. *Preventing thermal cycling and vibration failures in electronic equipment*. Hoboken, NJ: John Wiley & Sons.

Fackler, Warren C. 1972. *Equivalence techniques for vibration testing*. Shock and Vibration Information Center. Washington, DC: US Department of Defense.

Giannoccaro, N. I., A. Messina, et al. 2006. Fatigue damage evaluation of notched specimens through resonance and anti-resonance data. *Engineering Failure Analysis* 12:340–52.

Al-Najjar, B. 2000. Accuracy, effectiveness and improvement of vibration-base maintenance in paper mills: case studies. *Journal of Sound and Vibration* 229 (2): 389–410.

Maynard, K. P., M. W. Trethewey, et al. 2001. Application of torsional vibration measurements to shaft prevention technology. *Proceedings of the 55th Meeting of the Society for Machinery Failure Prevention Technology* 55:217–26.

Trethewey, Martin, Joshua Friell, et al. 2008. A spectral simulation approach to evaluate probabilistic measurement precision of a reactor coolant pump torsional vibration shaft crack monitoring system. *Journal of Sound and Vibration* 310:1036–56.

Wang, Rui-Jie, De-Guang Shang, et al. 2008. Fatigue damage model based on the natural frequency changes for spot welded joints. *International Journal of Fatigue* 30:1047–55.

Mfoumou, Etienne, Oleg V. Rudenko, et al. 2006. Acoustical measurement accompanying tensile test: New modality for nondestructive testing and characterization of sheet materials. Paper presented at the 13th International Congress on Sound and Vibration, Vienna, Austria.

Henderson, G. and Piersol, A. G. 1995. Fatigue damage related descriptor for random vibration test environments. Special dynamic testing reference issue, *Shock and Vibration*, 20–24.

M. Paulus and K. Doughty, Effect of resonant frequency shifting on time to failure of a cantilevered beam under vibration, *Journal of the IEST* **53**(1) (2010).

R.M. French, R. Handy and H.L. Cooper, Comparison of simultaneous and sequential single axis durability testing, *Experimental techniques*, **30** (2006) 32-37.

W.E. Whiteman, Inadequacies in uniaxial stress screen vibration testing, *Journal of the IEST*. **44** (2001), 20-23.

H. Himelblau and M.J. Hine, Effects of triaxial and uniaxial random excitation on the vibration response and fatigue damage of typical spacecraft hardware, *Proceedings of the 66th Shock and Vibration Symposium*, Arlington, VA, 1995.

D. Gregory, F. Bitsy and D.O. Smallwood, Comparison of the response of a simple structure to single axis and multiple axis random vibration inputs, *Proceedings of the 79th Shock and Vibration Symposium*, Orlando, FA (2008).

L. Lutes and S. Sarkani, *Random Vibration: Analysis of Structural and Mechanical Systems*, 2004 Elsevier.

R.I. Stephens, A. Fatemi, R.R. Stephens and H.O. Fuchs, *Metal Fatigue in Engineering 2nd ed*, 2001 John Wiley and Sons.

M. Aykan and M. Celik, Vibration fatigue analysis and multi-axial effect in testing of aerospace structures, *Mechanical Systems and Signal processing*, **23**(2009) 897-907.

M. Paulus, Limitations of the power spectral density as an indicator of test severity, submitted to *Journal of Shock and Vibration,* (2010).

T. Irvine, Steady-state vibration response of a cantilever beam subjected to base excitation, www.vibrationdata.com. 2010.

D. Broek, *Elementary engineering fracture mechanics, 4th ed*., 1986 Kluwer Academic Publishers.

L. Meirovitch, *Fundamentals of Vibrations*, 2001 McGraw Hill.

T. Irvine, Optimal use of the vibration response spectrum for enveloping random data, Proceedings *of the Institute of Environmental Sciences and technology*, (1999).

E. Douka and L.J. Hadjileontiadis, Time-frequency analysis of the free vibration response of a beam with a breathing crack, *NDT&E International*, **38** (2005) 3-10.

J.E. Srawley, Wide range of stress intensity factor expressions for ASTM #-399 standard fracture toughness specimens, *International Journal of Fracture*, **12** (1976).

B. Balachandran, E.B. Magrab, *Vibrations 2nd ed.,* 2009 Cencage Learning.

J. He and Z.F. Fu, *Modal Analysis*, 2001 Butterworth-Heinemann.

J. Collins, *Failure of Materials in Mechanical Design 2nd ed*., 1993 John Wiley and Sons.

E. Habtour, M. Paulus, A. Dasgupta, Finite element modeling of time to failure using stress intensity, *to be submitted* 2010.

M.E. Paulus, A. Dasgupta and E. Habtour, *Life Estimation Model of a Cantilevered Beam Subjected to Random Vibration*, to be published (2010).

M. Modarres, M. Kaminskiy and V. Krivtsov, *Reliability Engineering and Risk Analysis 2nd ed.,* 2010 CRC Press.

D.C. Montgomery, *Design and analysis of experiments 4th ed.,* 1997 John Wiley and Sons.

MIL-STD-810G. "Environmental Engineering Considerations and Laboratory Tests"

E.E. Ungar, Maximum stresses in beams and plates vibrating at resonance, *Journal of Engineering for Industry*, **84** (1962) 149-155.

W. Nelson, *Accelerated testing: statistical models, test plans, and data analysis*, 2004 John Wiley and Sons.

M.E. Paulus, A. Dasgupta and E. Habtour, *Rate of frequency change model uncertainty analysis*, to be published (2010).